Université de Montréal

# Développement et caractérisation d'une méthode photonique pour créer des distributions spatiales de protéines

par
Jonathan Bélisle

Institut de Génie Biomédical
Faculté de Médecine

Thèse présentée à la Faculté de Médecine
en vue de l'obtention du grade de Philosophiae Doctor (Ph.D)
en Génie Biomédical

Décembre 2011

Université de Montréal

Faculté des études supérieures et postdoctorales

Cette thèse intitulée :

Développement et caractérisation d'une méthode photonique pour créer des distributions spatiales de protéines

présentée par :

Jonathan Bélisle

a été évaluée par un jury composé des personnes suivantes :

Rikard Blunck, président-rapporteur
Santiago Costantino, directeur de recherche
Frédéric Lesage, membre du jury
Albert Folch, examinateur externe
Paul Cisek, représentant du doyen de la FES

# Résumé

Les cellules sont capables de détecter les distributions spatiales de protéines et ainsi de migrer ou s'étendre dans la direction appropriée. Une compréhension de la réponse cellulaire aux modifications de ces distributions spatiales de protéines est essentielle pour l'avancement des connaissances dans plusieurs domaines de recherches tels que le développement, l'immunologie ou l'oncologie. Un exemple particulièrement complexe est le guidage d'axones se déroulant pendant le développement du système nerveux. Ce dernier nécessite la présence de plusieurs distributions de molécules de guidages étant attractives ou répulsives pour connecter correctement ce réseau complexe qu'est le système nerveux. Puisque plusieurs indices de guidage collaborent, il est particulièrement difficile d'identifier la contribution individuelle ou la voie de signalisation qui est déclenchée *in vivo*, il est donc nécessaire d'utiliser des méthodes pour reproduire ces distributions de protéines *in vitro*. Plusieurs méthodes existent pour produire des gradients de protéines solubles ou liées aux substrats. Quelques méthodes pour produire des gradients solubles sont déjà couramment utilisées dans plusieurs laboratoires, mais elles limitent l'étude aux distributions de protéines qui sont normalement sécrétées *in vivo*. Les méthodes permettant de produire des distributions liées au substrat sont particulièrement complexes, ce qui restreint leur utilisation à quelques laboratoires.

Premièrement, nous présentons une méthode simple qui exploite le photoblanchiment de molécules fluorescentes pour créer des motifs de protéines liées au

substrat : *Laser-assisted protein adsorption by photobleaching (LAPAP)*. Cette méthode permet de produire des motifs de protéines complexes d'une résolution micrométrique et d'une grande portée dynamique. Une caractérisation de la technique a été faite et en tant que preuve de fonctionnalité, des axones de neurones du ganglion spinal ont été guidés sur des gradients d'un peptide provenant de la laminine.

Deuxièmement, LAPAP a été amélioré de manière à pouvoir fabriquer des motifs avec plusieurs composantes grâce à l'utilisation de lasers à différentes longueurs d'onde et d'anticorps conjugués à des fluorophores correspondants à ces longueurs d'onde. De plus, pour accélérer et simplifier le processus de fabrication, nous avons développé LAPAP à illumination à champ large qui utilise un modulateur spatial de lumière, une diode électroluminescente et un microscope standard pour imprimer directement un motif de protéines. Cette méthode est particulièrement simple comparativement à la version originale de LAPAP puisqu'elle n'implique pas le contrôle de la puissance laser et de platines motorisées, mais seulement d'envoyer l'image du motif désiré au modulateur spatial.

Finalement, nous avons utilisé LAPAP pour démontrer que notre technique peut être utilisée dans des analyses de haut contenu pour quantifier les changements morphologiques résultant de la croissance neuronale sur des gradients de protéines de guidage. Nous avons produit des milliers de gradients de laminin-1 ayant différentes pentes et analysé les variations au niveau du guidage de neurites provenant d'une lignée cellulaire neuronale (RGC-5). Un algorithme pour analyser les images des cellules sur les gradients a

été développé pour détecter chaque cellule et quantifier la position du centroïde du soma ainsi que les angles d'initiation, final et de braquage de chaque neurite. Ces données ont démontré que les gradients de laminine influencent l'angle d'initiation des neurites des RGC-5, mais n'influencent pas leur braquage.

Nous croyons que les résultats présentés dans cette thèse faciliteront l'utilisation de motifs de protéines liées au substrat dans les laboratoires des sciences de la vie, puisque LAPAP peut être effectué à l'aide d'un microscope confocal ou d'un microscope standard légèrement modifié. Cela pourrait contribuer à l'augmentation du nombre de laboratoires travaillant sur le guidage avec des gradients liés au substrat afin d'atteindre la masse critique nécessaire à des percées majeures en neuroscience.

**Mots-clés** : motifs de protéines, guidage d'axones, photoblanchiment

# Abstract

Cells are able to sense spatial distribution of proteins and accordingly migrate or extend in the appropriate direction. Understanding cellular responses to modifications in molecular spatial distributions is essential for advances in several fields such as development, immunology and oncology. A particularly complex example is axonal guidance that occurs during the development of the nervous system, which relies on distributions of attractive and repulsive guidance molecules to correctly wire this intricate network. Since several guidance cues collaborate to development of the nervous system, it is particularly difficult to assess the individual contribution of each cue and the signaling cascade each trigger *in vivo*; therefore methods to reproduce those distributions individually *in vitro* are necessary to study in detail the effect of each guidance cue. Several methods exist to produce graded distributions of protein that are either soluble or substrate-bound. A few methods making solution gradients are already widely used in several laboratories to perform experiments with the guidance cues that are normally diffusing *in vivo*. However, current methods allowing the fabrication of substrate-bound gradients are quite complex, which restrict their use to a few laboratories.

First, we present a straightforward method exploiting photobleaching of a fluorescently tagged molecule using a visible laser to generating substrate-bound protein patterns: Laser-assisted protein adsorption by photobleaching (LAPAP). This method allows producing complex patterns of protein with micron spatial resolution and high

dynamic range. An extensive characterization of the technique was performed and as proof of functionality, axons from dorsal root ganglions cells were guided on laminin peptide gradients.

Secondly, LAPAP was improved in order to produce multicomponent patterns by using lasers at different wavelengths and antibodies conjugated to fluorophores corresponding to these wavelengths. Moreover, to speed-up the fabrication process and simplify the device, we developed widefield illumination LAPAP which uses a spatial light modulator, a light emitting diode and a standard microscope to directly print patterns. This patterning method is relatively simple compared to the original LAPAP setup, since it does not involve controlling the laser power or a motorized stage, but only sends an image of the desired pattern to a spatial light modulator.

Finally, we used LAPAP to show how it could be used in automated high-content screening assays to quantify the morphological changes resulting from axon growth on gradients of guidance proteins. We produced thousands of laminin-1 gradients of different slopes and analyzed the variations in neurite guidance of neuron-like cells (RGC-5). An image analysis algorithm was developed to process bright field microscopy images, detecting each cell and quantifying the soma centroid and the initiation, terminal and turning angles of the maximal neurite. This data showed that laminin gradients influence the initiation angle of neurite extension of RGC-5, but does not contribute to its turning.

We believe that the results presented in this thesis will facilitate the use of substrate-bound protein patterning in typical life science laboratories, since a confocal microscope or a slightly modified standard microscope is the only specialized equipment needed to fabricate patterns by LAPAP. This could increase the number of laboratories working with substrate-bound protein patterns in order to reach the critical mass necessary for major advances in neuroscience.

**Keywords** : protein patterning, axon guidance, photobleaching

# Table of contents

# List of figures

# List of abbreviations and symbols

| | |
|---|---|
| +TIP | plus-end-tracking protein |
| ° | degree |
| °C | degree Celsius |
| µCP | microcontact printing |
| µg | microgram |
| µm | micrometer |
| µVCD | microvalve chemotaxis device |
| 2D | two-dimensional |
| 3D | three-dimensional |
| AOM | acousto-optical modulator |
| AOTF | acousto-optical tunable filter |
| B4F | biotin-4-fluorescein |
| BDNF | brain-derived neurotrophic factor |
| BMP | bone morphogenetic protein |
| BSA | bovine serum albumine |
| $Ca^{2+}$ | calcium ion |
| cAMP | cyclic adenosine monophosphate |
| CCD | charge-coupled device |
| cGMP | cyclic guanosine monophosphate |

| | |
|---|---|
| CNS | central nervous system |
| $CO_2$ | carbon dioxide |
| Comm | commissureless |
| Cy5 | cyanine-5 |
| DCC | deleted in colorectal carcinoma |
| DMEM | Dulbecco's modified Eagle medium |
| DMS | dimethyldichlorosilane |
| DNA | deoxyribonucleic acid |
| Dpp | decapentaplegic |
| DRG | dorsal root ganglion |
| EDS | 3-[(2-aminoethyl)amino]propyltrimethoxysilane |
| EGF | epidermal growth factor |
| F-actin | filamentous actin |
| FAD | flavin adenine dinucleotide |
| FITC | fluorescein isothiocyanate |
| GF | growth factor |
| GPI | glycosylphosphatidylinositol |
| Hh | hedgehog |
| HRP | horseradish peroxidase |
| ICAM-1 | intercellular adhesion molecule-1 |
| IFN-γ | interferon-gamma |

| | |
|---|---|
| IgG | immunoglobulin G |
| IL-2 | interleukin-2 |
| IL-8 | interleukin-8 |
| kDa | kilodalton |
| LAPAP | laser-assisted protein adsorption by photobleaching |
| LCD | liquid crystal display |
| LED | light-emitting diode |
| MAP | microtubule stabilizing proteins |
| min | minute |
| mL | milliliter |
| mM | millimolar |
| mW | milliwatt |
| NA | numerical aperture |
| NGF | nerve growth factor |
| nm | nanometer |
| nM | nanomolar |
| NrCAM | neural cell adhesion molecule |
| NSC | neural stem cells |
| NVOC | nitroveratryloxycarbonyl |
| ONH | optic nerve head |
| PBS | phosphate buffered saline |

| | |
|---|---|
| PC | polycarbonate |
| PDL | poly-D-lysine |
| PDMS | polydimethylsiloxane |
| PEG | polyethylene glycol |
| PI-PLC | phosphatidylinositol-specific phospholipase |
| PLL | poly-L-lysine |
| PLL-g-PEG | poly-L-lysine-grafted-polyethylene glycol |
| PMMA | polymethylmethacrylate |
| PNS | peripheral nervous system |
| RAGS | repulsive axon guidance signal |
| RGC | retinal ganglion cells |
| Robo | roundabout |
| SAM | self assembled monolayer |
| s | seconds |
| Shh | sonic hedgehog |
| SC | superior colliculus |
| SVGA | super video graphics array |
| TGF-β | transforming growth factor-β |
| TRITC | tetramethylrhodamine isothiocyanate |
| USAF | United States Air Force |
| UV | ultraviolet |

| | |
|---|---|
| VEGFA | vascular endothelial growth factor A |
| Wnt | wingless integration |

*À Laurence, Édouard et Victor*

# Remerciements

Je voudrais tout d'abord remercier mon superviseur le Dr Santiago Costantino de m'avoir fait confiance pour être son premier étudiant gradué et de m'avoir confié ce projet qui est au centre de ses intérêts de recherche. Je lui suis reconnaissant pour l'encadrement stimulant, sa grande disponibilité ainsi que le jugement critique qu'il a su me transmettre au cours de ces quatre années. Je voudrais également remercier Dr Dario Kunik et Dr Javier Mazzaferri, deux chercheurs postdoctoraux du laboratoire qui m'ont aidé au cours de mon projet de recherche et qui ont contribué à créer une excellente ambiance de travail. Un merci aussi à tous les étudiants du laboratoire : Carolyne Dion, Kanwarpal Singh, Mikhaela Anca Marian, Samuel Boutin, Charles-André Couture, Dominique Matte, Sarah Power et Faezeh Lorghaba. Je voudrais également remercier Dr Timothy Kennedy et James Correia d'avoir contribué à mon projet de doctorat. Je voudrais également remercier Dr Elliot Drobetsky ainsi que ses étudiants Raphaël Rouget et Yannick Auclair de m'avoir initié à la réparation de l'ADN par excision de nucléotides dans le cadre d'un projet connexe. Un autre remerciement au Dr Stephane Lefrançois et ainsi qu'à ses étudiants Dr Aline Mamo, Felix Jules, Karine Dumaresq-Doiron et Andreanne Goyette de m'avoir permis d'en apprendre davantage sur le transport des protéines aux lysosomes. Je voudrais également en profiter pour exprimer ma gratitude au Dr Leonard Levin et les membres de son laboratoire Rachel Beaubien, Wesley Chan, Maria-Magdalena Catrinescu et Dr Akiyasu Kanamori de m'avoir appris la culture des cellules ganglionnaires de la rétine et de m'avoir permis de

mettre à contribution mon expertise en optique pour collaborer à un projet portant sur la dégénération des axones suite à un dommage à la rétine. Je remercie aussi Alan Vlautin pour sa lecture attentive permettant d'améliorer la qualité de la langue de cette thèse.

Finalement, je voudrais remercier ma famille, mes parents Johanne et Michel et ma sœur Ève qui m'ont toujours encouragé à persévérer dans mes études. Un merci très spécial à ma conjointe Laurence qui m'a toujours supporté lors des bons et moins bons moments de mon doctorat ainsi qu'à mes deux fils Édouard et Victor qui ont vu le jour au cours des travaux qui ont mené à cette thèse et m'ont fait comprendre le véritable miracle qu'est le développement d'un être vivant.

# 1 Introduction

The nervous system has fascinated mankind for a long time. The earliest evidence coming from a papyrus dated from approximately 1700 BC reveals that Egyptians studied brain injury [1]. During antiquity, Plato correctly believed that the brain was directly responsible for reasoning, however his views on the subject were not accepted among fellow philosophers. Leonardo da Vinci undertook research in order to show how the brain perceived exterior stimulus; concentrating mostly on vision and olfaction [2]. In *Traité de l'homme*, René Descartes proposed that the visual world as perceived by the eye is projected in a Cartesian manner to the brain forming an accurate map of the outside world in the brain (Figure 1.1).

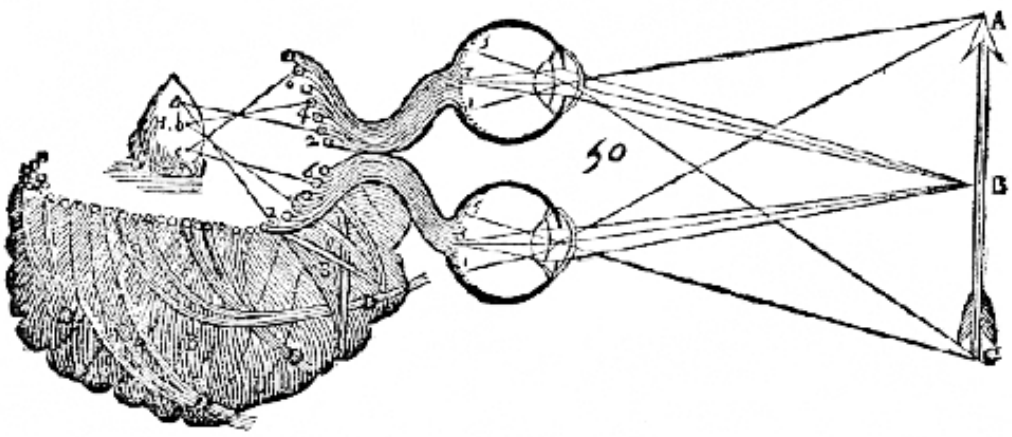


Figure 1.1: A diagram from *Traité de l'homme* by René Descartes showing that a map of the external world is first formed on the retina, which is later reproduced in the brain. This mapping will later become one major research field for axonal guidance.

By the end of the 19th century, the field of neuroscience made a major step forward due to improvements in staining made by Camillo Golgi and its use by Santiago Ramon y Cajal to visualize neurons. Since the late 1950s, the development of techniques in molecular biology allowed to better understand how neurons correctly extend their axons and dendrites to form an intricate network. Several guidance cues that showed graded distributions at various stages of development helped to explain how the axon correctly navigates to its destination. However, several questions about the shape of the gradients or their combinations still remain unanswered. For example, how minute changes in protein distributions would influence guidance? How small discontinuities or variations in protein gradients would be perceived? Is there a noise limit in a gradient for growth cones or cells to correctly sense direction? However, most of the techniques already existing to mimic *in vitro* the protein distributions that are found *in vivo* are not precise enough, and when they are, most of the time their complexity limits their usage in typical life science laboratories.

This thesis presents a novel technique to fabricate substrate-bound protein patterns, laser-assisted protein adsorption by photobleaching (LAPAP). This technique can fabricate protein patterns with micrometer resolution, 2D control on protein distributions and great dynamic range in terms of concentration. This introduction will provide a basic background of the nervous system, axonal guidance and the various families of cues, as well as a description of commonly used protein patterning techniques.

## 1.1 The nervous system

During development, cells of living organisms orchestrate an amazing process during which they divide and differentiate in various cell types required for a functional system. Early in the embryogenesis of complex animals, the embryo forms three germ layers: mesoderm, endoderm and ectoderm. At the midline of the embryo, the ectoderm forms the neural plate, which folds on itself to form the neural tube that will later give rise to the central nervous system (CNS). The CNS is composed of the brain, spinal cord and retina. The peripheral nervous system (PNS) is composed of sensory and motor neurons, ganglia (mass of nerve cell bodies) and the nerves that connect them to muscle, tissue and CNS. Two categories of cells form most on the nervous system: glial cells and neurons. Glial cells main function is to provide structural support and bring nutrient to neurons as well as to form myelin in order to electrically insulate axons. Neurons, the most fundamental component of the nervous system, have the property of being able to communicate with other neurons via electrical or chemical synapses (Figure 1.2). To communicate, neurons receive signals via their dendrites, which are arborized processes extending away from the soma, the cell body of the neuron. If sufficient synapses receive signals in a coordinated manner, the sum of electrical signals directed towards the soma by the dendrites will reach the threshold required for an action potential to be formed and travel along the axon to communicate with other neurons or specific cells. The axon is a tube-like structure that can extend over long distances with particularly high accuracy

during development; this phenomenon called axon guidance has been investigated for more than hundred years and several questions still remain elusive [3-6].

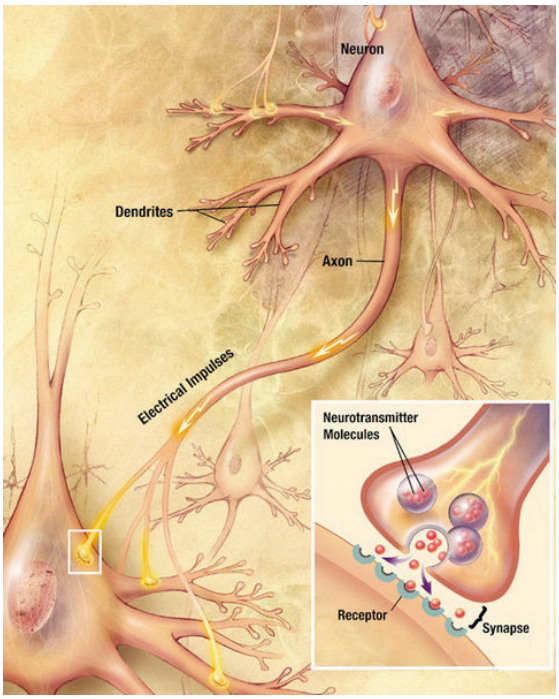


Figure 1.2: Representation of a neuron showing its different components: cell body (soma), dendrites, axon and synapse. Electrical signals are directed towards the soma via the dendrites and induce an action potential that will travel along the axon to induce the release of neurotransmitters at the synapse to communicate with another neuron (Reproduced from the brochure ‘‘Alzheimer's Disease: Unraveling the Mystery’’ from the National Institute of Aging).

## 1.2 Axon guidance

More than a century ago, Ramon y Cajal showed that the nervous system was composed of individual cells, the neurons, and not from a continuous network as it was

previously thought. Moreover, he made observations of a club-shaped structure at the end of axons that he named ‘growth cones’. Even though, he was observing growth cones in static images, he correctly hypothesized that these structures were responsible for guiding the axon to their appropriate target. In 1907, Ross G. Harrison developed a new tissue culture technique that allowed seeing, for the first time, the motility of the growth cone [7]. One fundamental question still remained: How was the growth cone at the tip of the axon guided? During the 30’s and the 40’s, it was widely believed that axons were guided in a restrictive mechanical manner [8]. However, work from Roger W. Sperry showed that axonal guidance was most probably due to distributions of chemical cues [9]. In this work, he severed the optic nerve linking the retina to the optical tectum of *Xenopus* and then rotated the position of the eye 180 degrees in its socket, before he allowed the nerve to regenerate. The position of retinal ganglion cells (RGC) in the retina was inverted compared to their original location. If axons were to regenerate in restrictive mechanical manner, the axons would extend to the optical tectum and connect to target corresponding to their new position, resulting in accurate vision for the frog. However, axons of RGCs were able to reconnect to their original target in the optical tectum and the frog saw an inverted world. From these findings, Sperry suggested the presence of at least two different perpendicular molecular gradients that would be responsible for the retino-tectal mapping. The search for these molecular cues led to the discovery of one of the family of guidance proteins: the ephrins.

In this section we will cover the four principal families of guidance cues: ephrins, semaphorins, netrins and Slits, and other guidance cues such as morphogens, extracellular matrix, growth factors and neurotransmitters, as well as their effect on the cytoskeleton to induce growth cone turning.

### 1.2.1 Ephrins

The group of Bonhoeffer developed an *in vitro* technique named the 'stripe assay' that allowed testing the preference of RGCs axonal growth between membrane fragments originating from different locations [10]. It is worth noting that this 'stripe assay' was the first PDMS microfluidic device used for patterning. Alternating stripes of membranes from the anterior or posterior regions of the tectum were used as a substrate to grow axons from retinal explants. Nasal axons grew on the stripes showing no preference for anterior or posterior tectum. However, temporal axons showed a marked preference for extending on the anterior tectum, which is their natural target (Fig. 1.3). In a subsequent study, heat treatment helped elucidating that temporal axons most probably recognized a repulsive protein that did not affect nasal axons [11]. Years later it was found, by incubating tectal membrane with phosphatidylinositol-specific phospholipase (PI-PLC), that the repulsive protein was anchored to cell membrane by glycosylphosphatidylinositol (GPI) [12]. This 25 kDa protein (first called RAGS for repulsive axon guidance signal, but now known has ephrinA5) was later isolated and comparison of its amino acid sequence showed significant

homology with ligands for Eph receptor tyrosine kinases [13]. The same year, it was also shown that ephrinA2 (ELF-1) and its receptor EphA3 (Mek4) were expressed in complementary gradients in the retina and the tectum, respectively [14]. Further evidence showed that EphA receptor and ephrinA interaction was necessary for RGCs axon guidance [15]. Moreover, experiments performed on mice shows that the retinal mapping in the superior colliculus (SC), was dependent on the relative levels of EphAs compared to neighboring cells [16], not the absolute value [17].

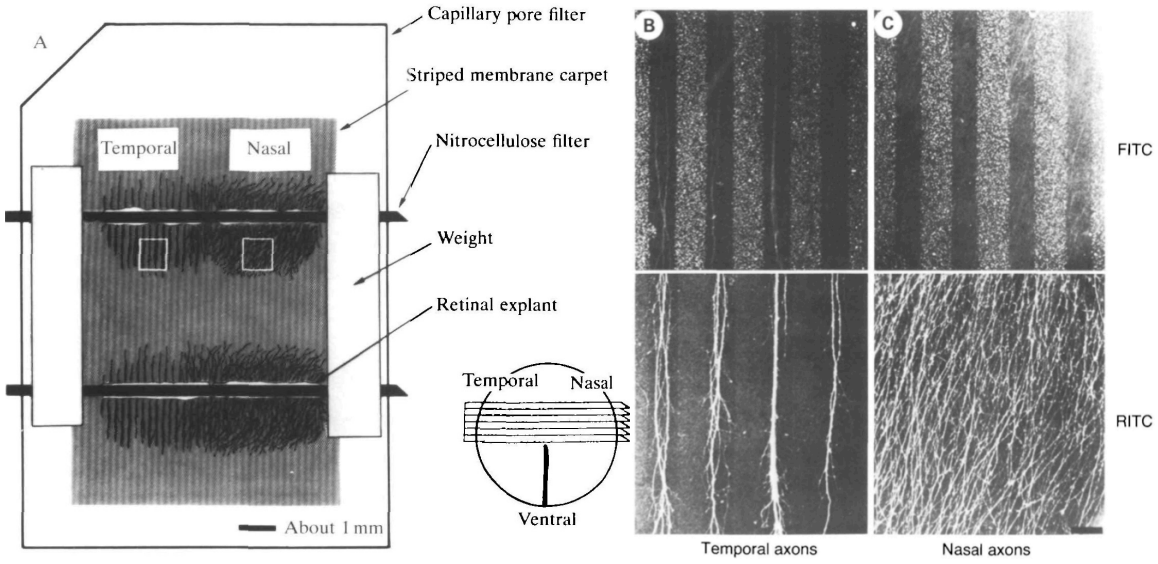


Figure 1.3: Stripes assay showing preference of temporal axons for growth on the anterior tectum instead of the posterior, but no difference for nasal axons. (a) Two retinal explants cultured on alternating stripes of membrane fragments from cells of the anterior (dark stripes) and posterior (FITC labeled stripes) part of the optical tectum. (b and c) Temporal axons preferably grow on anterior membrane stripes while nasal axons show no preference (reproduced from [10]).

Even though EphA receptor family interaction with ephrinA ligands family explained the retino-tectal mapping along the nasotemporal (anteroposterior) axis, this mapping was still not understood for the dorso-ventral (lateral-midline) axis. This was however explained by the discovery of ephrinB, a trans-membrane protein that binds to the EphB receptor [18-20]. EphrinB1 has been shown to attract branches of axons that express EphB receptor [20]. Since the initial axon overshoots its final destination, the portion of axon that travelled too far is eliminated later on and the branching is then responsible for mapping on the lateral-midline axis. Even though the retino-tectal mapping can be explained by two gradients, one of ephrinA and the other of ephrinB in the optical tectum (superior colliculus in mammals) and graded level of their respective receptors, Eph A and B, on the axons of RGCs (Fig. 1.4), this is an overly simplistic model and several protein distributions are necessary for accurate guidance [21].

Ephrins and Eph receptors also play other roles apart from retino-tectal mapping, for example, EphrinB2 and EphB1 have also shown to mediate the axonal divergence at the optic chiasm, which is necessary to establish binocular vision [22]. Even if ephrins are usually the ligands and Ephs the receptors, this can be inverted with Ephs acting as ligands and ephrins as receptors [21]. For example, axons from commissural neurons express high levels of ephrinB1 (acting as receptor) that are guided by EphB receptor (acting as ligand) [23]. The bidirectional signaling of ephrins is also present for GPI-anchored EphrinA [24]

and has been shown to contribute to retino-tectal mapping [25] and topographic targeting of vomeronasal axons to the olfactory bulb [26].

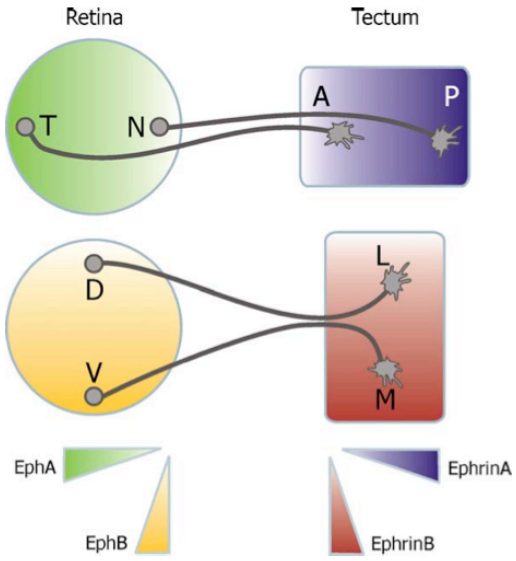


Figure 1.4: Schematic distributions of EphA and EphB receptors of axons from cells in the retina and the distributions of ephrin A and B in the optical tectum. The level EphA receptor on growth cones from RGCs is graded (green) as a function of position, with highest concentration from temporal neurons and lowest from nasal neurons. Its ligand, ephrinA, found on the membrane of cells in the optical tectum also forms a gradient (purple) with increasing concentration from anterior to posterior regions. EphB receptors on RGCs also form a gradient (yellow) that increases from dorsal to ventral neurons as well as their ligand, ephrinB, that is graded (red) with increasing concentration from the lateral to the midline region of the optical tectum (reproduced from [5]).

### 1.2.2 Semaphorins

Semaphorins are a family of signalling proteins that are implicated in the development of the nervous system and other organs [27]. The first semaphorin was identified in grasshoppers [28] and axonal repulsion was demonstrated *in vitro* by the growth cone collapsing of neurons from chick embryos [29] which led to the discovery of the semaphorin family [30]. Semaphorins are divided into 8 classes (1-7 and V), classes 1 and 2 are found in invertebrates, classes 3-7 in vertebrates and class V in viruses [4]. Semaphorins can either be transmembrane, GPI-anchored or secreted proteins. Class 3 semaphorins (semaphorin-3A-3G), which effect on axonal guidance is the most widely studied, is a secreted protein. The main receptor of class 3 semaphorins receptors that have been identified are the Neuropilins and the Plexins [31]. Neuropilin-1 [32, 33] and Neuropilin-2 [33, 34] can either form homodimers or heterodimers to bind with a dimerized form of semaphorin-3 to either induce axon repulsion (semaphoring-3A) or block that repulsion via competitive binding (semaphoring-3B and -3C) [31]. In *Drosophila*, Neuropilins are not present, Plexin A [35] and the tyrosine kinase OTK [36] acts together as a receptor complex of semaphorin-1s. In vertebrates, Plexins form protein complexes with Neuropilins to transduce the signal from secreted semaphorin-3s or it can also directly bind other semaphorins [37-40]. Other proteins can also take part in complexes such as the neural cell adhesion molecule (NrCAM) and the tyrosine kinase Met [41-43], as well as β1-integrin [44]. Most of the time, semaphorins act as short-range repellant cues [27]; for

example, it repels axons from RGCs once they have reached the midline of the optical chiasm [45] or repels them at the tectum to contribute to the dorsoventral axis mapping [46]. Semaphorins have been repulsive for other neuron types such as commisurals [47], dorsal root ganglion [48], olfactory [49], thalamocortical [50]. It has also been demonstrated that semaphorins can act as an attractive cue [43, 51, 52], moreover repulsion can be converted into attraction by the presence of cyclic nucleotides (cGMP) [53].

### 1.2.3 Netrins

Netrins genes were first discovered in *C. elegans* and named *unc-6* where they were involved with *unc-5* and *unc-40* in guiding pioneering axons [54]. DNA sequencing later showed that the protein coded by *unc-6*, UNC-6, was closely related to the structural protein, laminin [55]. In parallel to these finding, the group of Tessier-Lavigne was looking for a guidance cue for commisural axons attraction from the roof to the floor plate of the spinal cord [56]. This intriguing guidance cue was found to be the vertebrate homologue of UNC-6 [57-59] and named 'netrin' based on the Sanskrit word *netr* meaning 'to guide'. Floor plate and neural epithelial cells in the spinal cord respectively secrete netrin-1 and netrin-2. Clear turning from commissural neurons *in vitro* was observed when they were in the presence of a netrin-1 source in co-cultures in biological hydrogel [57, 60]. Direct observation of netrin-1 gradient in the spinal cord later confirmed that it works as a long-range guidance cue [61] (Fig. 1.5). It must be mentioned that netrin-1 is a secreted protein

with high affinity for cell membranes and it is not well understood how far it can diffuse *in vivo* [4, 57, 58]. It was also demonstrated that netrin-4 was able to bind laminin-111 by interacting with its $\gamma$1 arms [62]. As it was the case for ephrins and semaphorins, netrins can act both as attractive and repulsive cues [63-65]. Moreover, the concentrations of cytosolic cyclic nucleotide (cAMP) [66] or $Ca^{2+}$ [67] are able to modulate the response of axons to netrin-1 distributions. The two other genes discovered in *C. elegans* with *unc-6* (coding for netrins homologue) that were responsible for proper guidance of pioneering axons in *C. elegans* are evolutionary conserved in vertebrates and code for DCC (*unc-40* gene) and UNC-5 (*unc-5* gene) [68], two receptors of netrins.

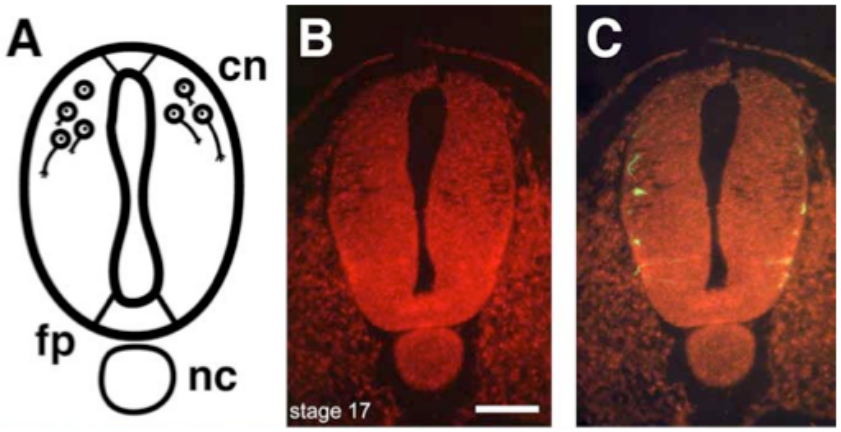


Figure 1.5: Netrin-1 (red) distribution secreted from the floor plate (fp) in a cross-section of spinal cord which contributes to the guidance of axons from commissural neurons (cn) towards the ventral midline (reproduced from [61]).

The DCC receptor controls attraction to netrins [68-70], while UNC-5 seems only to be involved in repulsion [65]. It was also found in *Xenopus* spinal neurons that DCC and

UNC-5 could form a complex via their cytosolic domain to regulate the repulsion to netrin-1 [71]. It was also reported that the adenosine 2b receptor was also able to bind netrin-1 [72], however this finding has been challenged by other researchers [73]. Netrins are not only involved in the guidance of commissural neurons; they also help the navigation of RGCs [70, 74] to their correct target and it has been found that at the optic disk, the presence of laminin turns netrin-1 from an attractive to repulsive cue [75] (Fig. 1.6). Similarly, the presence of laminin stops the attraction of vagal sensory axons by netrin-1 [76]. Recently, the influence of netrins on angiogenesis was demonstrated *in vitro* on human endothelial cells as well as *in vivo* on zebrafish [77].

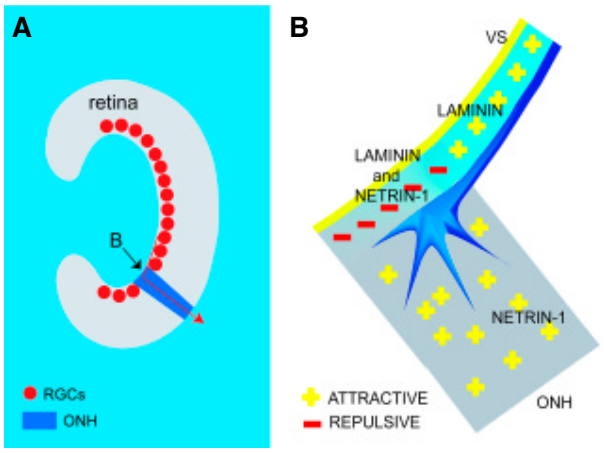


Figure 1.6: In the presence of laminin, netrin-1 becomes repulsive to growth cone from RGCs. (a) RGCs' axon need to do a right turn to enter the optic nerve head (ONH). (b) Laminin and netrin-1 both act as attractive cues when acting individually, but when combined at the entry of the optic nerve head, netrin-1 act as a repellant which ensure the growth cone turning in the ONH (reproduced from [6]).

### 1.2.4 Slits

Genetic screening on *Drosophila* first allowed the discovery of two new genes influencing commissural projections: *commissureless* and *roundabout* [78]. Subsequent work showed that Roundabout (Robo) is a new family of receptors evolutionary conserved [79] and Commissureless (Comm) is regulating surface levels of Robo at the growth cone [80]. The midline line repellant of Robo is Slit, a large extracellular matrix protein secreted by midline glial cells [81, 82]. It was also found that Slit repulsive function was evolutionary conserved in vertebrates in the presence of three Slits (1-3) and three Robos (1-3) [83, 84]. Slits presence is necessary to avoid commissural axons to cross the midline a second time, suggesting that the growth cone sensitivity to Slits can switch at the midline. In vertebrates, this switching is coordinated with other guidance cues in such a manner that before crossing axons are attracted by netrin-1 [57, 58] and insensitive to Slits and semaphorin-3s [47], but after crossing they lose their attraction to netrin-1 [85] and become repelled by Slits and semaphorin-3s (see Fig. 1.10). The precise molecular mechanism underlying this switching is not fully understood, but has begun to be elucidated [86]. For example, Rig-1 (Robo3) is acting as a negative regulator of Robo1 before midline crossing, making the growth cone insensitive to Slits [84, 87]. After crossing, Rig-1 is downregulated, which leads to the upregulation of Robo1 and prevents axon recrossing at the midline. In *Drosophila*, Comm, which is involved in intracellular sorting, when activated traffics Robo for degradation, therefore decreasing the concentration of Robo at

the growth cone surface [80, 88]. After crossing the ventral midline, Comm is probably inactivated and Robo concentration at the growth cone increases again preventing the axon to cross a second time (see Fig. 1.7).

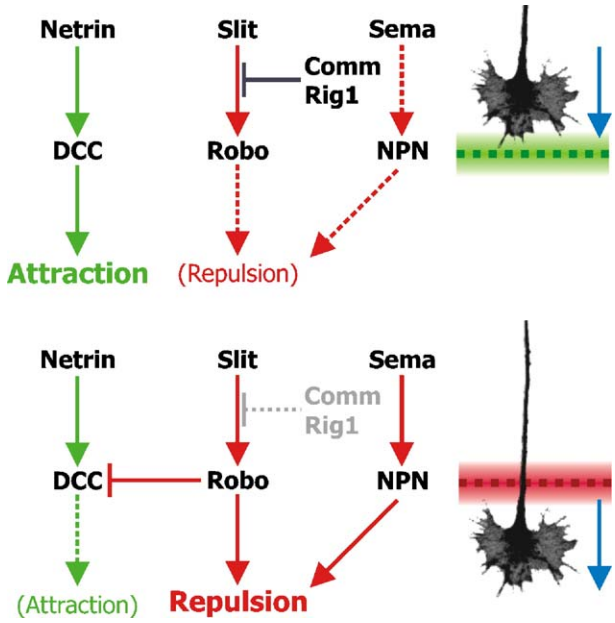


Figure 1.7: Switching response to Slits, netrin-1 and semaphorin-3s at the ventral midline of the spinal cord and the role of Comm and Rig-1. Before crossing the midline, commissural neurons are attracted by netrin via their DCC receptors, but are insensitive to Slits due to Comm or Rig1 acting as negative regulators of Robo. After crossing the midline, Comm and Rig1 are inactivated and neurons become repelled by Slit to avoid recrossing and lose their attraction to netrin. Semaphorin is also implicated to avoid recrossing of axons (reproduced from [5]).

Slits are also implicated in the guidance of several neuronal cell types; they act as a repellent for axons from the olfactory bulb [89] and restrict RGCs growth to a defined

regions at the optical chiasm [90-93] and along the optic tract [94] (see Fig. 1.8). Similarly to netrins and semaphorins, Slits can have various functions since they also influence branching and elongation of sensory neurons [95].

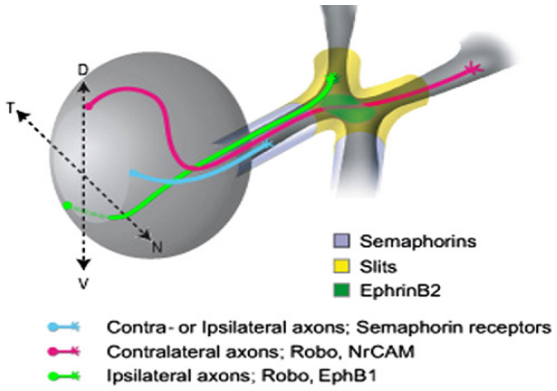


Figure 1.8: Schematic view of RGCs axon elongation and the presence of Slits around the chiasm which allow growth only in restricted regions. Semaphorins are also present and act as repellant to restrict growth before the chiasm. EphrinB2 is as well present at the chiasm to determine which axons are allowed for crossing, depending on their original location in the retina (reproduced from [74]).

## 1.2.5 Morphogens

Even if ephrins, netrins, semaphorins and Slits are still considered the main four families of guidance molecules, they can't explain the entire axonal path finding decisions. Recently, three families of morphogens have also showed their effect in the proper wiring of the nervous system: Hedgehog (Hh), Wingless/Wnt and Decapentaplegic/Bone Morphogenetic Protein/Transforming Growth Factor-β (Dpp/BMP/TGF-β) [96, 97]. We

have seen in previous sections how netrin-1, Slits and semaphorin-3s collaborate to appropriately guide axons from commissural neurons towards the floor plate, and subsequently turn and cross the midline [47, 57, 58, 84, 87]. As if this was not complicated enough, three morphogens also contribute to the guidance of commissural axons [96].

Morphogens are secreted proteins that control differentiation in the developing organisms, and they are often found in graded distributions [98, 99]. Along a morphogen gradient, cells are subjected to different absolute protein concentrations that will result in modulated gene expression. This will result in cell fate that will vary as a function of position in the gradient. A good example of their implication in neuroscience is the neuronal specification in the developing spinal cord [100]. More specifically, a gradient of the morphogen Sonic hedgehog (Shh) secreted from the notochord and the floor plate is in part responsible for the fate of neuronal progenitors in the ventral spinal cord [101, 102]. Other mophogens are also implicated in the fate of neuronal progenitors in the spinal cord; Wnt (contraction of wingless and integration) and BMP (bone morphogenetic protein) [97] (Fig. 1.9a).

Two BMPs secreted from cells in the roof plate, BMP7 and GDF7, have shown to repel commissural axons away from the floor plate [103] by forming heterodimers [104] (Fig. 1.9b). A gradient of Shh, similar to the Netrin-1 gradient also attracts the axons towards the floor pate [105] (Fig. 1.9b). Then once the axons have crossed the midline, they

turn along the antero-posterior axis and are now repelled by Shh [106] and attracted towards a gradient of Wnt4 [107] (Fig. 1.9c).

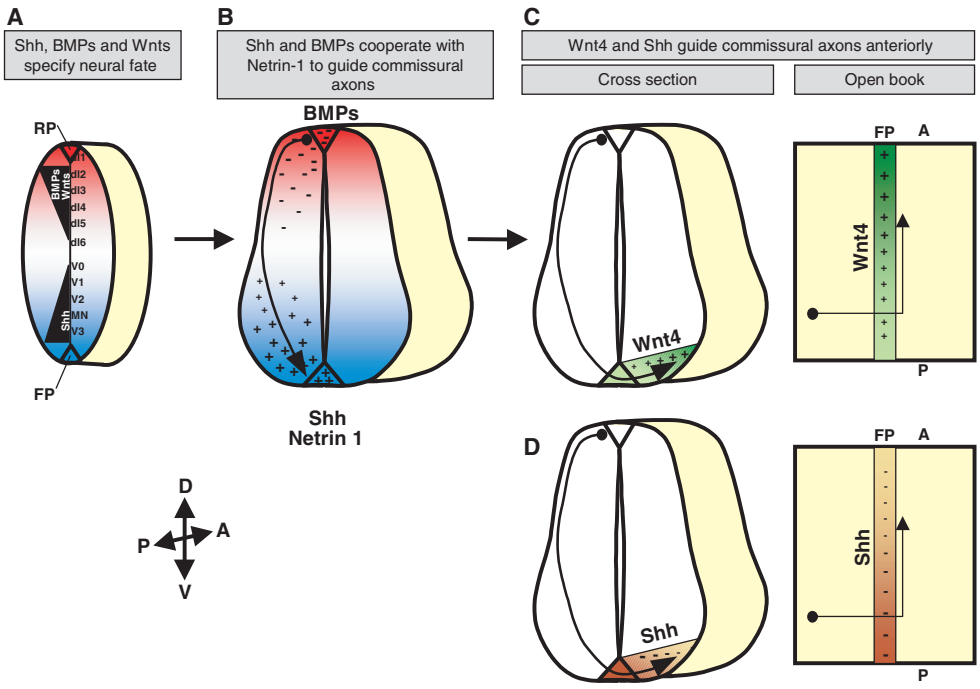


Figure 1.9: Gradients of the mophogens BMPs, Shh and Wnts first contribute to specify cell fate and later in the appropriate guidance of axons from commissural neurons. (a) Morphogens are first responsible to specifying cell fate as a function of the cell position along the gradients, here we see Shh, BMPs and Wnts. (b) Axons from commissural neurons are repelled by BMPs and attracted by Shh and netrin-1. (c) After crossing the midline at the floor plate, Wnt4 attracts while Shh repels axons to guide them in the anterior direction (reproduced from [96]).

### 1.2.6 Extracellular matrix, growth factors and neurotransmitters

Moreover, to the four main families of guidance cues and morphogens, other proteins or molecules play a significant role in axon guidance. These include extracellular matrix proteins, secreted growth factors and neurotransmitters.

The extracellular matrix protein laminin plays a particularly important role in the proper navigation of growth cones. Early work on neurons from the sympathetic ganglia of chick embryos didn't show any evidence of influence from a substrate-bound laminin gradient upon the orientation of axons [108]. However, subsequent experiments showed that DRGs from chick embryos where turning on substrate-bound gradients from a laminin peptide, IKVAK [109]. It was shown that laminin gradients were influencing the direction of the presumptive axon (longest neurite) of rat hippocampal neurons [110] or neurites from PC12 cells [111], as well as to induce turning in axons from chick retinal explant [112] or *Xenopus* spinal neurons [113]. *In vivo* experiments with laminin zebrafish mutants showed axons from various neural types made specific pathfinding errors [114], therefore suggesting that laminin is implicated in guidance.

Growth factors such as nerve growth factor (NGF) [48, 115-117], brain-derived neurotrophic factor (BDNF) [113, 118-120] and neurotrophin-3 [120] are also implicated in axon guidance. The neurotransmitter, acetylcholine, also showed its ability to induce axon turning in *Xenopus* spinal neurons [121].

### 1.2.7 Cytoskeleton remodeling

It is also important to understand how growth cone turning is actually happening. Once the growth cone is asymmetrically exposed to guidance molecules, a signal transduction cascade triggers several structural changes that ultimately induce growth cone turning [122]. Several second messengers are implicated in the signal transduction; we have seen that cyclic nucleotides (and their related protein kinases) and calcium levels [53, 66, 67, 120, 123-127] are part of these pathways; however, we only have partial knowledge of the signaling cascades occurring for each guidance cue, and these cascades could get overly complicated when multiple cues are simultaneously involved. Recent discoveries allow us to better understand how the effective end of these pathways influence membrane trafficking [128] and cytoskeletal dynamics [129] in order to induce growth cone turning. Here we will briefly look at the cytoskeleton modifications occurring during guidance; the following review covers this topic in detail [129].

The growth cone cytoskeleton is composed of microtubules and filamentous actin (F-actin), which can be found in bundles or meshworks. The fine finger-like projections at the end of the growth cone are called filopodia and are filled by F-actin bundles, in between filopodia, we found lamellipodia which is filled with an F-actin meshwork. Figure 1.10d shows in green mostly F-actin meshwork in lamellipodia and the white arrows show F-actin bundle at the base of a filopodia extending further up and the black arrows show an adjacent microtubule depicted in red. Several proteins are involved with F-actin and

microtubules to regulate polymerization, bundling or meshing, as well as linking between both. These proteins are often at the effective end of the pathways induced by guidance cues.

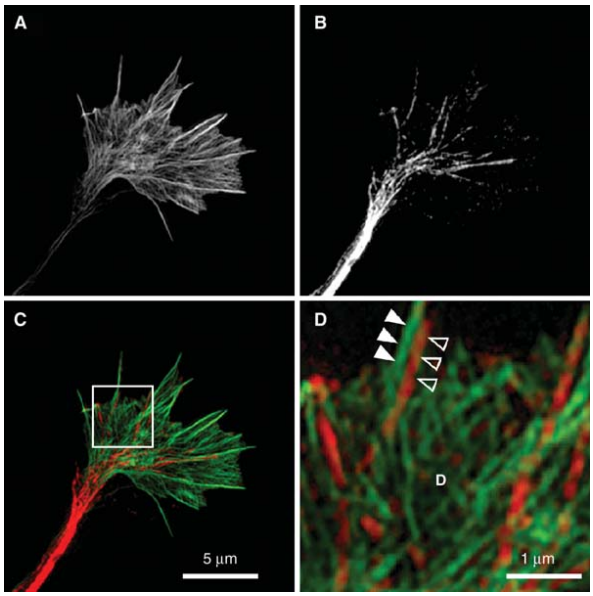


Figure 1.10: Growth cone fluorescent image showing F-actin (a) and microtubules (b) and an overlay of both (c and d), actin in green and microtubule in red (reproduced from [129]).

The dynamics of F-actin are first regulated by a proper balance of its retrograde flow from the front edge to the center of the growth cone as well as polymerization and depolymerization. An actin motor protein, Myosin is involved in regulating the rate of retrograde flow [130]. Capping proteins and barbed-end binding protein modulate the polymerization close to the leading edge of the growth cone. Barbed-end proteins such as ENA/Vasp [131, 132] and DAMM1 (a formin family member) [133] facilitate

polymerization, while capping proteins, including ESP8 [134] and CapzB2 [135], stops polymerization at the leading edge. Other proteins help cross-linking F-actin together such as Fascin [136] to form bundles of Arp2/3 complex [137] to nucleate new F-actin on the side of existing ones in order to form a meshwork. F-actin severing proteins such as cofilin [138] or depolymerization proteins such as Mical [139] are implicated in its disassembly. All these protein related to F-actin are also implicated in growth cone turning.

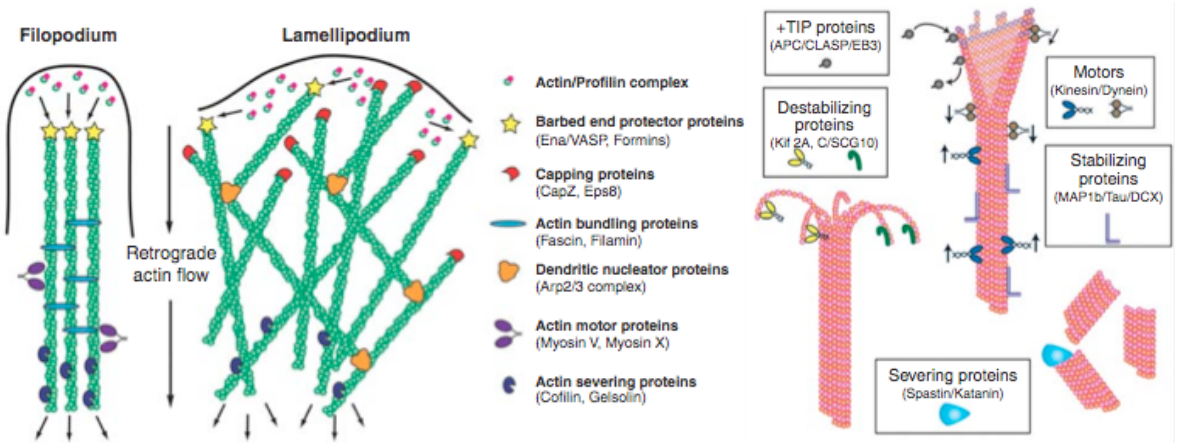


Figure 1.11: Proteins directly implicated in cytoskeletal modifications of F-actin (green) and microtubule (pink) during axonal guidance (adapted from [129]).

The polymerization of microtubules during axon guidance is regulated by plus-end-tracking proteins (+TIPs) such as CLASP [140, 141]. Microtubule stabilizing proteins (MAPs) also play a crucial role, MAP1B is a particular example that is also a downstream effector of Netrin-1 mediated-guidance [142]. Moreover, MAP1B serves as a cross-linking protein between F-actin and microtubules as it binds both [143]. Other proteins either destabilizing

microtubules such as SCG10 [144] or severing them like Spastin [145] are also regulated in axonal guidance.

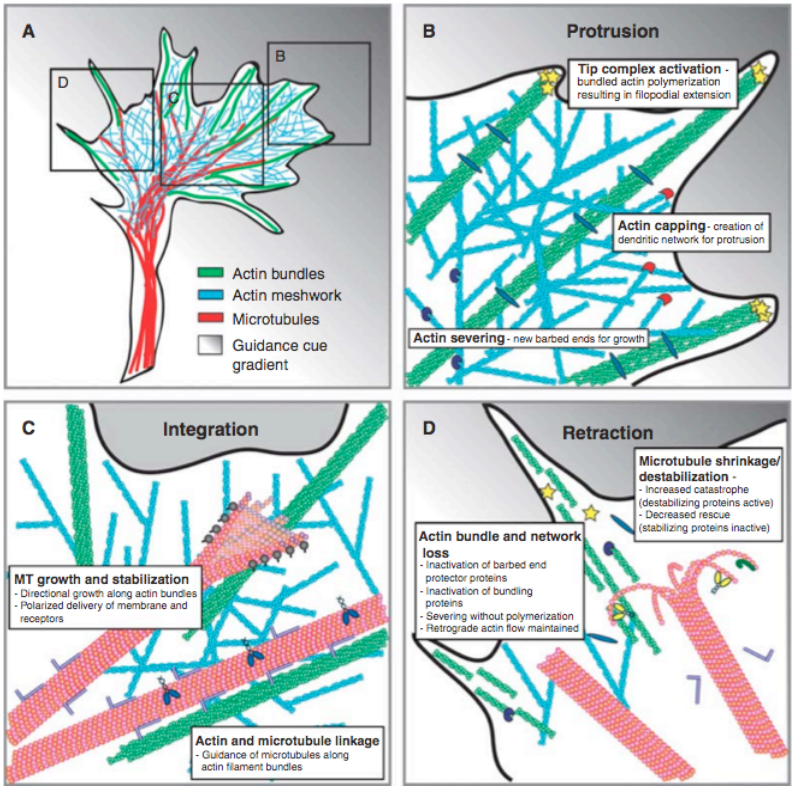


Figure 1.12: Model of cytoskeletal reorganization during growth cone turning due to an attractive guidance cue. (a) Subsections of the growth cone will react differently depending where they are located as a function of the guidance cue gradient. (b) Barbed-end and nucleating acting protein contribute to filopodial protrusion. (c) Microtubule growth and stabilization as well as linkage with F-acting support the protrusion in the integration zone. (d) Proteins responsible for severing F-actin or destabilizing microtubules are activated while barbed-end actin protectors and microtubules stabilizers are less effective in the retraction region (reproduced from [129]).

Cytoskeletal changes occurring in growth cone turning can be summarized by an oversimplified model describing, protrusion, retraction and integration of different regions of the cone due to the exposition of a graded concentration of a guidance cue [129] (Fig. 1.12). It is most probable that barbed-end and nucleating actin proteins activation contributes to the protrusion in the direction indicated by the concentration gradient (Fig. 1.12b). Closer to the center of the growth cone, in the integration zone, linkage between F-actin and microtubules is most likely occurring to stabilize the cytoskeleton directed protrusion (Fig. 1.12c). F-actin severing and microtubule destabilizing proteins are probably activated while barbed-end actin protectors and microtubule stabilizing proteins are less effective in the retraction region of the growth cone (Fig. 1.12d).

In this section, we have discussed the different molecular cues taking place in axon guidance as well as their effect on the cytoskeleton. These guidance cues are either secreted or bound to the membrane of cells, and as we have seen they often collaborate to properly guide axons. Working with genetically modified models such as *C. elegans* or *Drosophila* contributed in the identification of new guidance proteins and their receptors while experiments on rats and mice allowed visualizing their homologs distribution in mammals. However, to study neurons behavior in controlled conditions, it is necessary to work with isolated cultures, which requires reproducing *in vitro*, the molecular distributions that are found *in vivo*. In fact, several papers previously cited in this introduction featured experiments with artificially produced protein distributions, as they are necessary to

understand the molecular mechanism underlying axonal guidance. During the last 40 years, several methods were developed to better mimic protein distributions; the next section will present several of these methods, either soluble or substrate-bound depending on the nature of the distribution found *in vivo* of the particular protein.

## 1.3 Protein patterning

The effects of protein gradients on axonal guidance and morphogenesis have been discussed in the previous section, however it has to be noted that biomolecule distributions also have important roles in angiogenesis [146], wound healing [147] and immunology [148]. *In vivo* experiments can answer general questions about the implication of guidance cues at different time point or location, but more specific questions necessitate working with isolated cells. Therefore, the need for *in vitro* assays to reproduce protein patterns found *in vivo* is required for major advances not only for neuroscience, but also for chemotaxis in general. During the last forty years, several methods were developed and can be distinguished from each other by the type of distributions they produce, soluble or substrate-bound, their relative complexity, the stability and the shape of the pattern. This section will describe the assays that are available for protein patterning; two reviews already well describe most of these methods [149, 150].

### 1.3.1 Zigmond and Dunn chambers

The functioning principle of Zigmond and Dunn chambers seem simple, diffusion from a source to sink, and they have been very effective to produce gradients with slopes that are quite constant across the ridge [151]; they are stable in time once the nearly steady-state is reached and allow multiple cells to be studied at the same time due to the large size of the gradient.

The Zigmond chamber is quite simple, it consists of two rectangular reservoirs that are separated by a glass ridge, a cover glass with cells plated on it is clamped over the channels and the ridge. The two channels act as sink and source; the medium with the guidance molecule fills the source channel and only medium is used for the sink channel. An important design feature is that the two channels must hold a volume that is much larger than the volume present in the ridge section where the gradient takes place. For example in the original design by Zigmond, the sink and the source contained approximately 100 μL each, while the volume in the ridge was about 1 μL [152]. This allows having a nearly steady-state gradient in the bridging section for a relatively long period of time. Due to open ends on each side of the channels (see Fig. 1.13), the Zigmond chamber is very sensitive to evaporation, which limits the period of time with steady gradient to approximately 1 h [149]. Therefore, this method is limited to study cells that will respond quickly to a molecular gradient, such as neutrophils [152-159], macrophages [160], osteoclasts [161, 162] or spermatozoa [163-166].

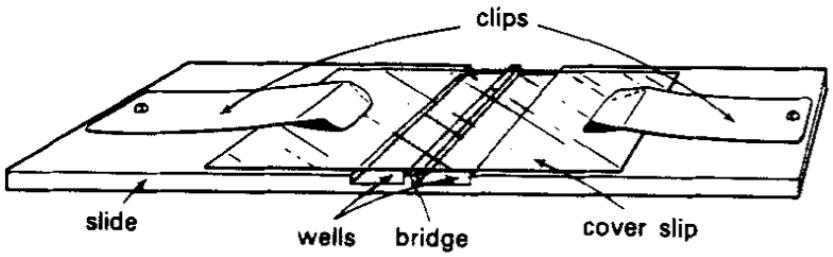


Figure 1.13: Zigmond chamber showing two wells acting as reservoirs that will produce a diffusion gradient from one well to the other in the section delimited by the bridge and the cover glass where the cells are plated (reproduced from [152]).

The Dunn chamber [167] was initially designed to study the chemotaxis of fibroblasts, which are slower than neutrophils and for which the Zigmond chamber was not suitable. Significant improvements compared to the Zigmond chamber were made by replacing the rectangular channels by a circular inner well that acts as a sink and a ring-shaped outer well as a source (see Fig. 1.14). Due to the geometry of the chamber, the gradient is formed radially with increasing concentration from the inner to the outer well. Moreover, while doing the imaging of cells, it is particularly important to know the angular position on the ridge where the imaging is done since it will define the direction of the gradient. Dunn chambers, being less prone to evaporation, can be used to obtain steady gradients (after 20-30 minutes) with uniform steepness for up to 20 hours [168], therefore allowing to study axon guidance by Sonic Hedgehog or retinoic acid [169, 170].

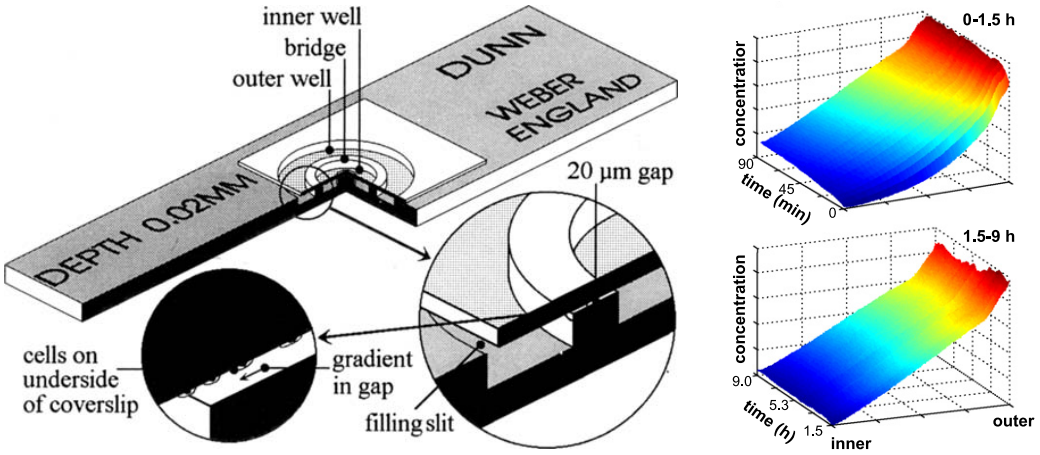


Figure 1.14: Left part of the figure shows the Dunn chamber with an inner well filled with regular medium and an other well filled with the guidance cue to produce a gradient by diffusion (reproduced from [171]). Right part of the figure shows that gradients obtained by Dunn chamber are linear and can be stable over several hours (reproduced from [169])

## 1.3.2 Micropipette

Soluble gradients generated by a micropipette were first used to study the guidance of axons from chick dorsal root ganglion cells by NGF gradients [115, 116]. The basic idea to create a gradient with a micropipette is to position the tip at a certain distance of the growth cone of interest and to inject a small amount of a guidance protein to create a diffusion gradient within the culture medium. The initial version of Gundersen and Barrett [115, 116] (Fig. 1.15) was using a steady outflow to create the diffusion gradient, this was later improved by using a microinjector to puff-in small amounts of biomolecules with pulses at a fixed frequency [121, 172]. Micropipette puffs have been extensively used and

clearly helped elucidating detail of axonal guidance: such as the role of cyclic nucleotides (cAMP and cGMP) as second messenger [53, 66, 120, 128, 172, 173], to confirm receptor-ligand interactions [70] and to improve our comprehension of the role of $Ca^{2+}$ [67, 174-176]. The shape of the micropipette tip, the frequency of the puffs, their volume and length, and the distance (radially and in height) from the micropipette tip to the growth cone, as well as the charge and the diffusion coefficient of the biomolecule in the media will determine the shape of the gradient [177]. Recent theoretical modeling and experimental work showed how critical the distance from the micropipette can be on the gradient steepness compared to the Zigmond chamber [151]. Despite the fact that 100μm is usually used as a standard distance between the pipette tip and the neuron [172, 178, 179], the moving growth cone will be subject to a change of slope during its growth as its position relative to the tip changes. Also, it has to be noted that most of the guidance experiments done with micropipette generated gradients have been performed on axons from *Xenopus* [66, 70, 121, 172, 179-181] due to their quick response to guidance cues. Despite this fact, work has also been carried out on neurons from rat [178, 182] and Syrian hamster [183]. Most neurons from mammals when they are in isolated culture will grow at irregular intervals, remaining most of the time stationary. Since the micropipette assay is only able to study one neuron at the time, the probability of performing the assay on a stationary neuron is relatively high; therefore, an assay where multiple neurons can be followed in parallel is more optimal for mammalian neurons [169]. Guidance of neutrophils also showed good

results with the micropipette assay due to their quick reaction to biomolecules distribution [184-186].

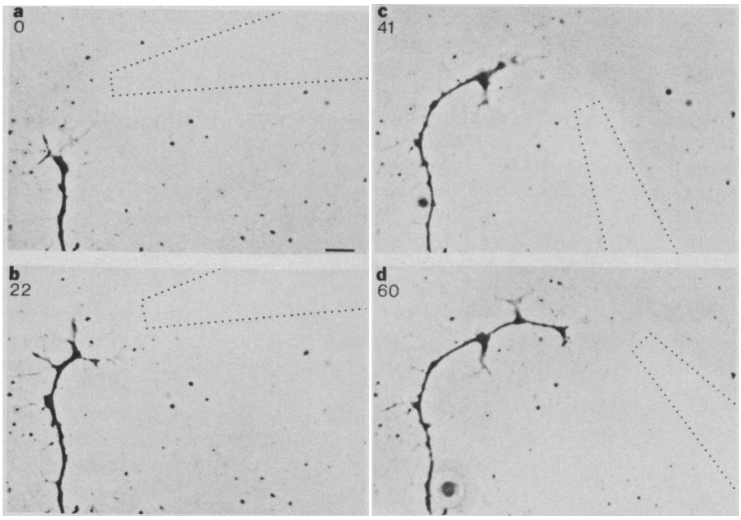


Figure 1.15: Guidance from micropipette generated gradient from chick dorsal root axon. Dotted lines show the location of the micropipette at different time points (reproduced from [115]).

### 1.3.3 Soft lithography

Advances in microfabrication techniques over the last few decades allowed researchers to produce cell culture environments that better mimic those found *in vivo* compared to traditional culture methods [187-190]. Soft lithography helped develop both microfluidics [191, 192] and microstamping [193], moreover both techniques can be used to produce protein patterns. The key steps to fabricate microfluidic devices or a microstamp are: a master is first made by photolithography using the appropriate mask, ultraviolet (UV) light and photoresist and silicon wafer; then elastomeric material, most of the time

polydimethylsiloxane (PDMS), is poured on the master and cured to create the microfluidic system or the microstamp. PDMS can later be chemically bound to glass using oxygen plasma for the case of microfluidic devices [194]. The next two sections will describe the use of microfluidics and microstamps to produce protein patterns.

## 1.3.4 Microfluidics

The development of microfluidic devices to study the behavior of cells exposed to molecular gradients has grown significantly over the last decade. These devices can be grossly divided in four categories depending on the way gradients are produced: flow and diffusion, flow only, diffusion only or depletion. One particularly interesting feature of microfluidic devices is that most of them allow temporal modulation of the molecular distribution [195]. Further reading specifically on microfluidic devices to produce biomolecular gradients can be found in this review [196].

### 1.3.4.1 Flow and diffusion devices

The serpentine premixer is a popular example of a microfluidic device that relies both on flow and diffusion to produce sophisticated concentration gradients. It consists of two or more inlets with solutions that will repeatedly mix and divide in a series of parallel serpentine channels growing in number for several mixing steps [197]. The serpentine channels are designed in a way that two solutions with different concentrations reach equilibrium by diffusion before they divide again. After a few mixing steps, these channels

are then merged in the cell culture area to produce a transverse soluble gradient in a laminar flow (Fig. 1.16).

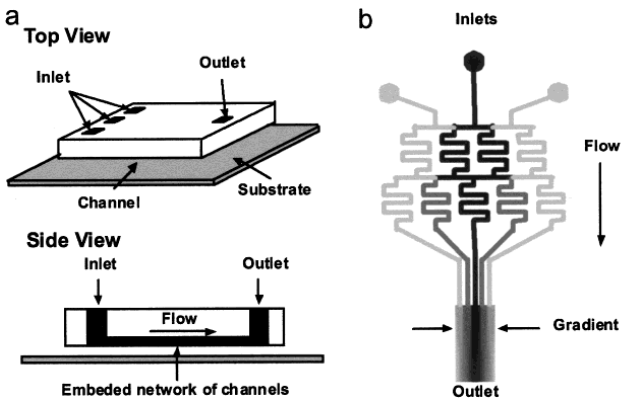


Figure 1.16: Schematic representation of the serpentine premier to produce substrate-bound or soluble gradients. (a) Several inlets allow introducing various solutions that will mix and exit via the outlet. (b) In this example, the central inlet is filled with the molecular cue and the two side-inlets with regular medium. The channels corresponding to each inlet will repeatedly mix and divide in a series of parallel serpentine channels growing in number for several mixing steps (in this illustration, only 2). After mixing, the channels are all merged in a chamber to expose cells to a transverse soluble gradient or to transfer proteins to a surface in a graded manner (reproduced from [197]).

One particularly interesting feature of the premixer is its ability to produce both soluble and substrate bound gradients. For example, it has been used to produce soluble gradients of interleukin-8 (IL-8) to guide neutrophils [198, 199], substrate bound gradient of laminin via adsorption for 6 hours to study axonal guidance of hippocampal neurons from neonatal rats [110] and both soluble and substrate-bound gradients of BDNF and laminin respectively [113]. The profile of the gradient depends on the concentration of guidance molecules

injected in the selected inlet as well as the flow speed [197]. Improvements in design also allowed to produce patterns with complex shapes or multicomponent gradients with opposing slopes [200]. The premixer has also been used to show the effect of epidermal growth factor (EGF) gradient slopes on the chemotaxis with breast cancer cells [201], proliferation of neural stem cells (NSC) in a gradient of growth factor (GF) mixture [202] and bacterial chemotaxis [203].

It is also possible to produce flow and diffusion gradients without premixing. One notable device is the T-sensor where two solutions are directly combined together it a T-shaped device [204, 205]. Modified versions of the T-sensor have been used to study bacterial chemotaxis from chemorepellant and chemoattractant [206, 207]. This device is particularly useful in the assessment of attraction or repulsion since the cells' position can be easily quantified in one of the 22 outlets. Other devices inspired from the T-sensor design to produce protein gradients were used in chemotactic experiments. For example, endothelial cells have been guided by producing hill-shaped gradients of vascular endothelial growth factor A (VEGFA) in a three inlet direct mixing microfluidic devices [208] (Fig. 1.17). However, gradients produced with direct mixing have profiles that can change significantly depending on the position inside the growth chamber. Another method to produce gradients by flow and diffusion is the universal microfluidic generator. It has also been demonstrated that it was possible to produce various profiles by placing parallel dividers at various positions in a flow where the mixing of two solutions occurs [209].

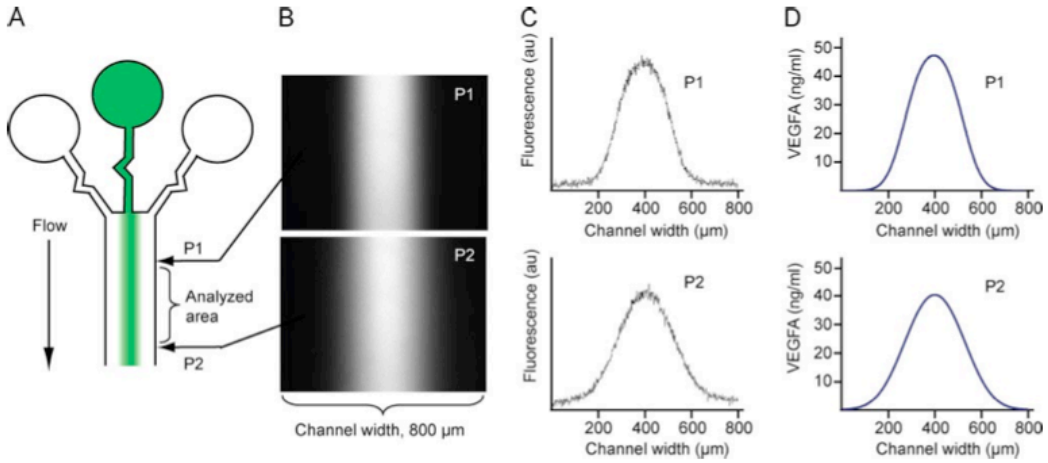


Figure 1.17: Hill-shape gradient profiles at various positions in the growth chamber. (a) Schematic representation of direct-mixing device with three inlets to produce hill-shaped gradient. (b) Images of the gradient profiles at position P1 and P2 in the chamber. (c,d) Intensity and simulated profiles show the variability in the slopes depending on the position along the chamber (reproduced from [208]).

The mixing is then restricted between two dividers or one divider and one of the limits of the channel. The number of dividers increases by one for each dividing step along the direction of the flow; the number of steps defines the precision of the concentration profiles while the position of the divider determines the profile itself (see Fig. 1.18). The universal microfluidic generator also inspired modifications to the serpentine premixer in order to produce various concentration profiles [210]. The main drawback of devices relying on flow and diffusion is they expose the cells to flows that induce shear stress. Diffusion-only devices offer the possibility to produce molecular gradients without flow.

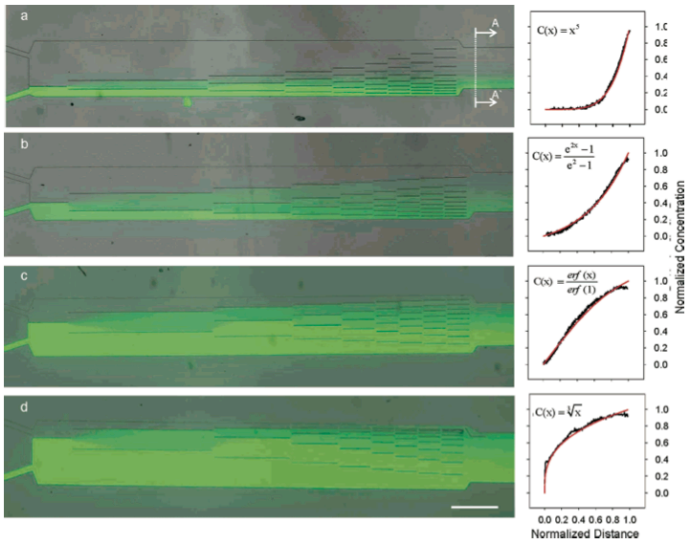


Figure 1.18: Universal microfluidic gradient generator. Various dividers configuration allow to obtain profiles corresponding to (a) fifth power, (b) exponential, (c) error, and (d) cubic root functions (reproduced from [209]).

### 1.3.4.2 Diffusion-only devices

The membrane-based gradient generator is a good example of a microfluidic device relying solely on diffusion to produce molecular distributions [211] (Fig. 1.19). It has a large source (100µL) that is separated from the gradient region by a membrane with high fluidic resistance in order to avoid flow but to allow diffusion of molecules. A steady state gradient is produced within 6 hours and few changes in the profile can be observed within 24 hours. The functionality of the device was demonstrated by guiding neutrophils toward a gradient of a short bacterial peptide. Another design by Michel Maharbiz's group allows the cells to be cultured on top of the porous membrane for greater flexibility [212].

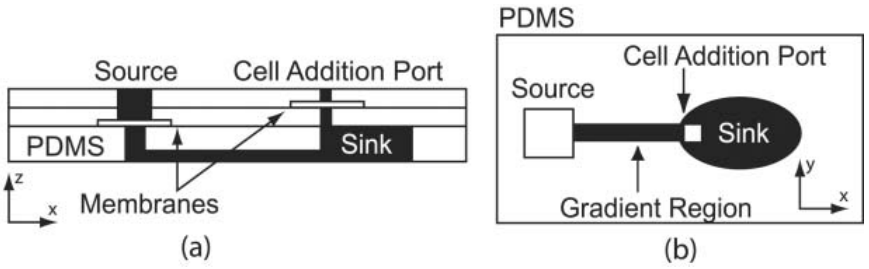


Figure 1.19: Membrane-based gradient generator that produce a graded molecular distribution by diffusion while the membranes high fluidic resistance avoid flow (reproduced from [211]).

Another option to produce gradients where cells are not subjected to flow is the use of a cross channel gradient generator. The initial configuration comprised two large parallel flow-through channels interconnected by perpendicular cross channels that act as chambers to study cell chemotaxis [213]. As proof of functionality, one of the flow-through channels was filled with a solution of pheromone, while the other with regular medium, the pheromone was then diffusing in the cross channels to produce a linear gradient to guide yeast in a high-throughput manner. The method was later improved by changing the cross channels length [214] or shape [215] to produce gradients with various profiles. It is also possible to produce gradients in cross channels filled with collagen to produce 3D patterns [216]. It is also possible to produce 3D patterns by replacing the cross channels with a central channel parallel to the flow-through channels where cells will be introduced within a hydrogel. To allow diffusion from the source to the sink flow-through channels to create a gradient in the central channel, the device must however be in part built from agarose [217, 218] or nitrocellulose [219]. It has to be noted that these 3D gradients have concentration

that mainly changes in one direction. Diffusion through agarose was also used to produce complex patterns [220]. Small fluidic channels with specific user-define shapes were placed in contact with agarose containing a diffusion gradient; the position inside the microchannel relative to the diffusion gradient inside agarose determines the molecular concentration (Fig. 1.20).

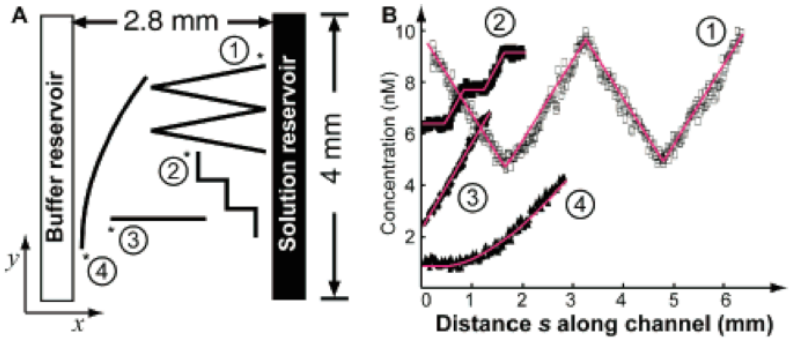


Figure 1.20: Complex-shaped concentration profiles inside microchannels in close contact with a diffusion gradient inside agarose. Within the agarose, a simple linear gradient is formed, but along the adjacent channels, profiles can be modulated depending on their shape (reproduced from [220]).

A particularly interesting method to produce soluble gradients is the microjets device (Fig. 1.21) whose main advantage over other flow-resistive gradient generators is its open cell culture chamber which allows to control pH or perform electrophysiology experiments [221]. Moreover, the change in pressure of the source and the sink allows changing the position of the gradient across the culture chamber without interfering with the slope. The microjet device was used to study desensitization of human neutrophils to IL-8 gradients [222].

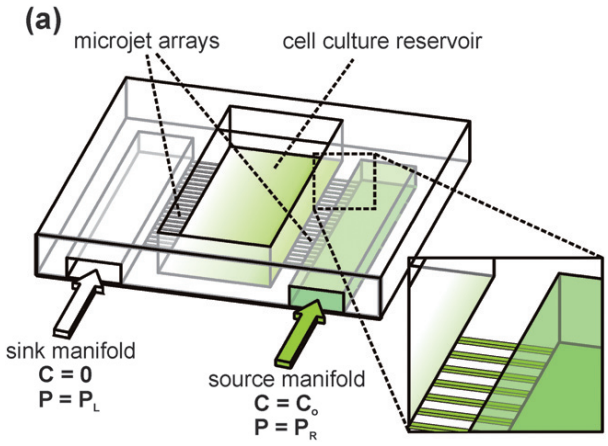


Figure 1.21: Microjets device produces a gradient in an open chamber configuration and its position can be controlled by changing the pressure of the sink and the source (reproduced from [222]).

Another method, the microvalve chemotaxis device (μVCD) allows the production of diffusion gradients by pneumatically controlling a microvalve connecting a source and a sink, which is also the cell chamber [223]. Four other pneumatic valves control the filling of the source with the molecular cue and the sink with cells in regular medium. Once filled, the four valves are closed and the one connecting both chambers together is open to create a diffusion gradient. The functionality of μVCD was demonstrated by guiding neutrophils toward a gradient of the chemotactic factor IL-8.

### 1.3.4.3 Flow-only device

A device that relies mostly on flow and is used like a pen close to a glass surface showed its ability to produce substrate-bound protein gradients; this device was named multipurpose microfluidic probe [224]. The device can move freely relative to a glass substrate and

consist of injection and aspiration apertures that are responsible to adsorb proteins on the surface in a spatially controlled manner (Fig. 1.22). The device is operated to approximately 10 µm of the glass surface and is scanned to produce protein gradients; the scanning velocity can be varied to modulate the amount of adsorb proteins. The probe can also be used to selectively remove proteins adsorbed to a surface or cells in culture one at a time.

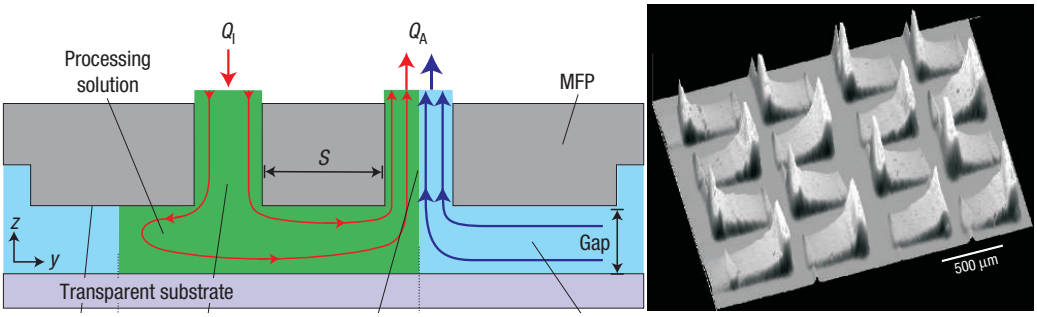


Figure 1.22: On the left, a cross-section sketch of the multipurpose microfluidic probe showing the injection aperture ($Q_I$) and the aspiration aperture ($Q_A$) that allow to adsorb controlled amount of proteins on a adjacent substrate. On the right, protein gradients obtained by scanning close to a surface (adapted from [224]).

### 1.3.4.4 Depletion device

When depletion was first observed in microfluidic devices destined to the surface adsorption of antibodies, it was first considered as a problem to circumvent [192, 225]. However, the effect has proven useful to produce gradients where protein are adsorbed to the walls of microchannels and a glass surface with decreasing concentration from the

reservoir to the other end [226]. Surface-to-volume ratios of the channels allow modulating the slope of the gradients.

### 1.3.5 Microcontact printing (μCP)

Microcontact printing is technique allows transferring proteins or chemicals to various substrates [193, 227-229]. It is possible to replicate the negative of the silicon master either by lift-off or casting methods [230]. Despite good results obtained to study morphogenesis [231], locomotion of fish keratocytes [232] or to produce neuronal networks [229, 233], the concentration of transferred proteins by μCP remains binary; where the stamp makes contact with the substrate a constant concentration of protein is found, while elsewhere no protein is transferred. A clever stamp design (see fig. 1.23) allowed the fabrication of concentration gradients perceived on large scale by printing lines or spots with increasing sizes [230]. The technique was then used to show that RGCs from the temporal region stop at a position in an ephrinA5 gradient that is dependent on the steepness and absolute concentration [234]. Lately, the possibility to produce continuous gradients using an agarose stamp was demonstrated [118]. Netrin-1 and BDNF were introduced in a microchannel, allowed to diffuse inside agarose and transferred to a pretreated glass substrate. Dissociated rat hippocampal neurons showed for the first time axonal guidance on substrate-bound netrin-1 gradients [118].

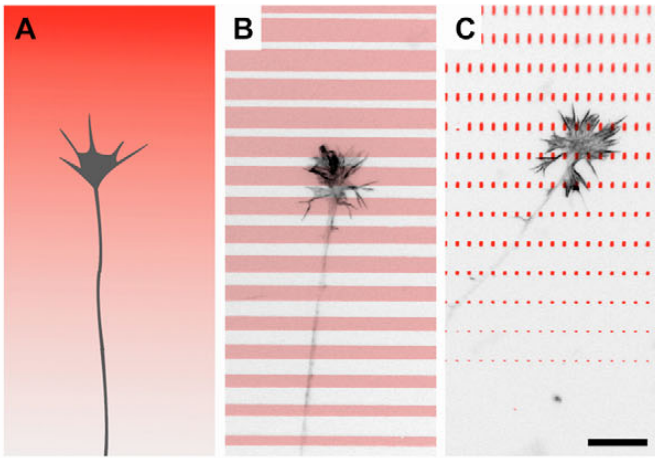


Figure 1.23: Gradients of ephrinA5 produced by μCP (a) A schematic representation of a growth cone on a gradient. (b,c) Growth cone on a gradient produced by (b) lines of increasing thickness or (c) dots of increasing size. Scale bar is 15 μm (reproduced from [234]).

### 1.3.6 Biological hydrogels

We have seen in the two preceding sections that it is possible to use biological hydrogels such as agarose or collagen to slow down diffusion and avoid flow in microfluidics [217-220] or to produce a stamp with a continuous distribution [118]. However, their usage in microfluidics or stamping is relatively new; their initial use solely depended on bulk diffusion. They were used in co-culture to have guidance molecules diffusing away from one of the cultures in order to guide cells from the other [34]. For example, it was used to study the growth of commissural axons toward a diffusion gradient created by an explant of the floor-plate of the developing spinal cord or transfected COS cells expressing netrin-1 [56, 57] (Fig. 1.24).

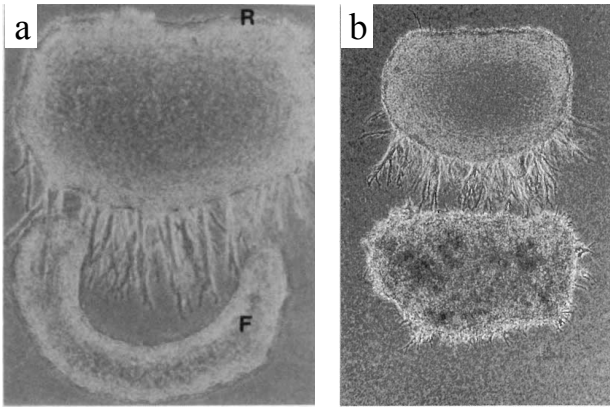


Figure 1.24: Commissural neurons attracted by (a) the floor-plate of the spinal cord or (b) an aggregate of COS cells expressing netrin-1 (adapted from [56, 57]).

Alternatively, the secreting explant can be replaced by directly adding a solution of the purified chemoattractant (or chemorepellant) [235-238]. Mixing liquid form of an hydrogel with the guidance molecule at various concentration and solidifying thin layers at different concentrations one over the other can produce gradients in 3D [111]. More recently gradients of NGF in a thin collagen gel were produced by using a pump allowing to release nanoliter droplets in a controllable manner and by using a 2D axis stage to move the sample [238]. The method was also used to show the extreme sensitivity of rat dorsal root ganglion (DRG) cells to low slope gradients of NGF gradients [237].

Cross-linking molecules in hydrogels using UV light or two-photon absorption is another option to obtain bound protein distributions that don't change in time [239]; for example, DRG cells were guided on IKVAV peptide helices patterned inside hyaluronan [240] (Fig. 1.25).

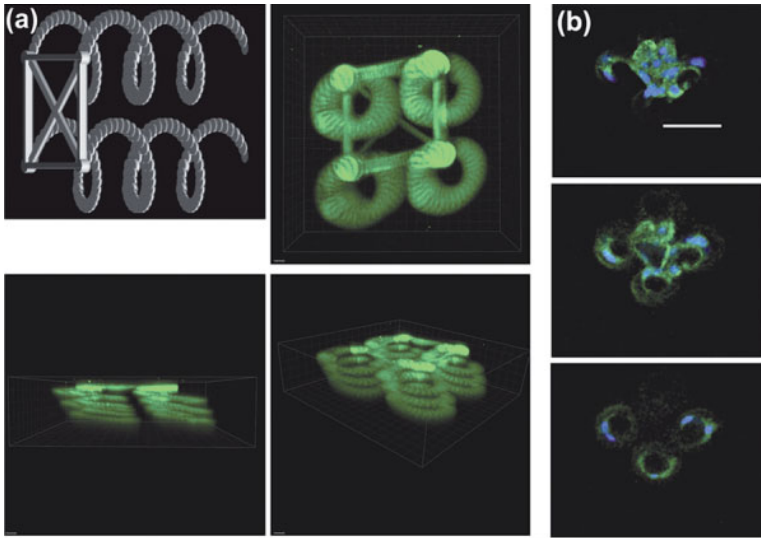


Figure 1.25: 3D guidance of DRG cells on helical patterns of IKVAV peptide. (a) Schematic representation (gray) and 3D reconstruction from confocal microscopy images of IKVAV helical patterns (green). (b) DRG cells stained by DAPI (blue) on IKVAV patterns in green (reproduced from [240]).

## 1.3.7 Photopatterning

The use of light to create patterns in a hydrogel was briefly discussed at the end of the previous section, however photopatterning can also be used to produce substrate bound patterns [150]. Three strategies are readily available to produce patterns with UV light: the use of photoresists, photosensitizers and thin layers. Recently, methods using visible light were also developed.

### 1.3.7.1 Photoresists

The advances in microfabrication techniques not only helped the development of soft lithography, but also allowed to produce in a few steps substrate-bound protein patterns based on the one created by the photoresist. Here are key steps to produce a typical pattern: first a photoresist is spin coated on the substrate, then exposed with UV-light via a photomask; the photoresist is then developed, and a first chemical or protein is added (promoting or inhibiting cell growth); the photoresist is striped and another chemical or protein can be added. Pioneering work was done using silanes (Fig. 1.26); amino-trihydroxysilane was first used to promote the growth of dissociated neurons, while alkyl-trichlorosilane was used as an inhibitor [241]. Similarly, EDS (3-[(2-aminoethyl)amino]propyltrimethoxysilane) and DMS (dimethyldichlorosilane) were used respectively as promoters and inhibitors to study the kinetics and organization of bone cells [242, 243]. Laminin, collagen, fibronectin and bovine serum albumin were patterned either directly on glass or via EDS binding, and cellular adherence on the patterns was clearly demonstrated [244]. The technique was also used to produce patterns of horseradish peroxidase (HRP) where the catalytic activity of the enzyme was retained as well as patterns of synthetic peptides [245]. More recently, the development of a new method using pH-sensitive photoresist now allows patterning of two different proteins without exposing them to irradiation or solvents [246]. This method was then used to produce patterns of anti-CD3 and intercellular adhesion molecule-1 (ICAM-1) to mimic immunological

synapse of T cells with antigen presenting cells [247]. The patterns mimicking the antigen presenting cells were able to fully activate T cells, which increased their production of Interleukin-2 (IL-2) and Interferon-gamma (IFN-γ). The recent development of a protein friendly photoresist allowed even the production of patterns from three different proteins [248]. It has to be noted that photoresist patterns can be altered by the cell culture.

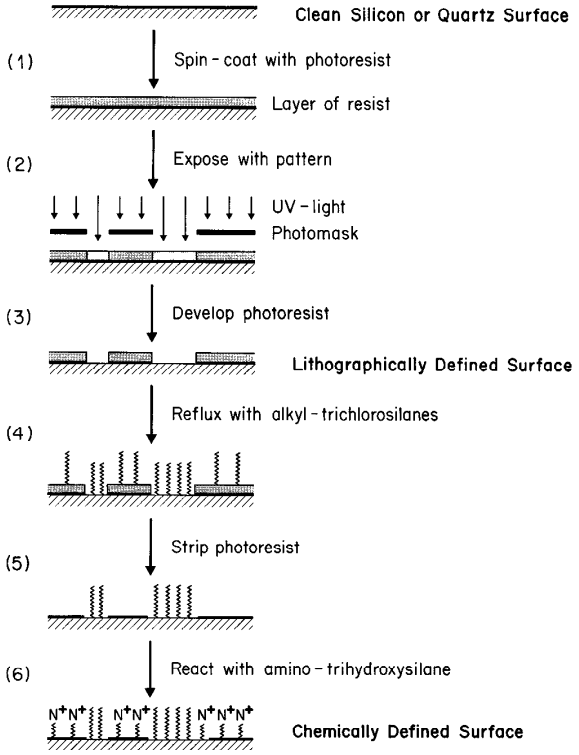


Figure 1.26: Key steps in photolithographical patterning of alkyl-trichlorosilane (inhibitor) and amino-trihydroxysilane (promotor). (1) Surface is spin-coated with a photoresist and (2) exposed to UV light through a photomask. (3) After being developed (4) alkyl-trichlorosiliane can be bound in open areas and (5) non-desired bounding can be remove by striping the photoresist. (6) Amino-trihydroxysilane is then bound to the areas previously protected by the photoresist (reproduced from [241]).

### 1.3.7.2 Photosensitizers with near UV light

The use of chemicals that can be easily altered by near UV light in order to activate them to bind target molecules on various substrates allows the production of protein patterns [249-251]. Several molecules that react to UV light have been used to selectively bind molecules of interest: benzophenone [109, 252], arylazide [250, 253], nitrobenzyl [254-256] and aryldiazirine [252, 257, 258]. Benzophenone, arylazide and aryldiazirine can be covalently attached to the molecule of interest or to a molecule that will facilitate the binding of the protein of interest such as antibodies. Benzophenone and aryldiazirine have been used conjugated to peptides in solution to produce patterns onto glass substrate by scanning a 325 nm Cd/He laser [109] or by near UV exposure via a photomask [252]. The laser scanning allowed obtaining continuous substrate-bound gradients (see Fig. 1.27) and could, in theory, be applied for all photosensisers in the near UV region to produce gradients. An arylazide biotin-conjugate (photobiotin) coated to a surface via streptavidin linking was used to pattern several antibodies on a silicon wafer [251, 253] using a photomask UV exposure. Since it is the photobiotin linked to the surface that becomes reactive, generic proteins can be patterned following this strategy without chemically modifying the protein itself. Nitrobenzyl is used as a caging agent to prevent the normal function of an active molecule. For example, caged biotin linked to the substrate can be selectively uncaged by a photomask of UV light, after the region with uncaged biotin can bind to streptavidin that will later bind a biotinylated protein to produce the final pattern

[254, 256]. Nitrobenzyl can also be used to cage a reactive amino group to produce spatially defined peptide synthesis [255]. Several other chemicals can be used as well [250], for example hydroquinone protected by nitroveratryloxycarbonyl (NVOC) can be irradiated with 365nm light to later bind a ligand conjugated with cyclopentadiene [259].

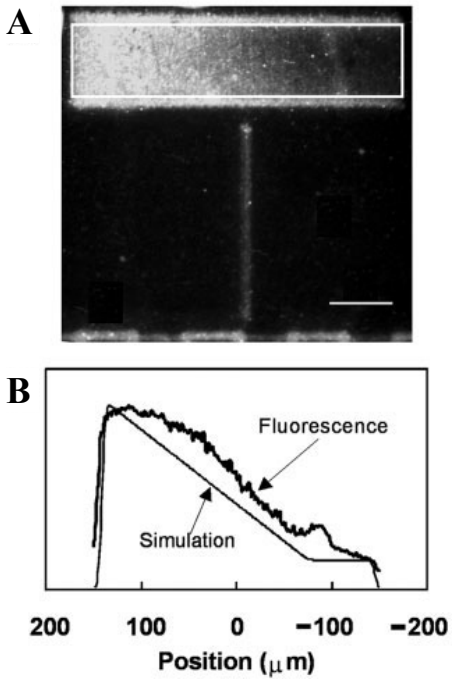


Figure 1.27: (a) Continuous IKVAV gradient produce by UV laser scanning revealed by immunofluorescence labeling and (b) profile of the fluorescence image compared to simulation (reproduced from [109]).

### 1.3.7.3 Thin layer modifications with far UV light

Another option for photopatterning is the modification of a thin layer by far UV light which allows to break chemical bonds without the use of specific photosensitizers. However, at these wavelengths, air absorbs light significantly, which forces the work to be done in

vacuum conditions and the use of a photomask material transparent to these wavelengths. Self assembled monolayer (SAM) [260-262], polymers [263-268] and even neutravidin [269] were used in combination with far UV to create molecular patterns. SAM of EDA, an organosilane that act as a promoter, can be formed on a glass surface and irradiated by far UV light; the irradiated regions can then be exposed to another silane (13F) that will then act as an inhibitor for the growth of human neuroblastoma cells [260]. The same procedure can also be used to later bind a full protein to EDA patterns by a simple overnight incubation; for example, fibronectin patterns where used to study the proliferation and differentiation of endothelial cells [261]. Polymers such as polycarbonate (PC) and polymethylmethacrylate (PMMA) can also be irradiated with far UV light resulting in changes in surface chemistry that later allows to selectively adsorb other proteins such as human serum albumin [266]. The same technique was used to make patterns of laminin and culture PC-12, a cell line that differentiate when treated with NGF, to show neurite guidance [265]. It is also possible to produce protein patterns by adsorbing neutravidin on a glass surface, followed by exposition to 185nm light patterns to locally break peptide bonds, therefore denaturing the protein [269]. More recently, a simple technique to produce protein patterns from a thin layer of poly-L-lysine-grafted-polyethylene glycol (PLL-g-PEG) coated on glass was developed [263, 264]. Far UV irradiation allowed breaking several bonds in PEG while having less impact on the PLL; moreover, carboxyl groups were formed on the exposed surface, contributing to the later adsorption of proteins such as fibronectin.

### 1.3.7.4 Photopatterning with visible light

We have seen that photopatterning with UV light is a particularly good technique to produce substrate-bound protein patterns and that it was even possible to fabricate continuous gradients [109]. However, it would be particularly convenient to develop photopatterning techniques using visible light, since it is already used in microscopy; simple software changes on a confocal microscope or minimal modifications on a fluorescence microscope could allow typical life science lab to possess the hardware necessary for protein patterning. It was recently demonstrated that a 633nm HeNe laser is able to unbind fluorescently tagged antibodies linked to a thin layer of proteins coated on a glass surface, therefore allowing to produce patterns of the newly exposed proteins [270].

Recent work, without which this thesis would simply not exist, showed it was possible to bind biotin-4-fluorescein (B4F) and a Alexa 594 labeled antibody via photobleaching of the fluorophores [271] (Fig. 1.28).

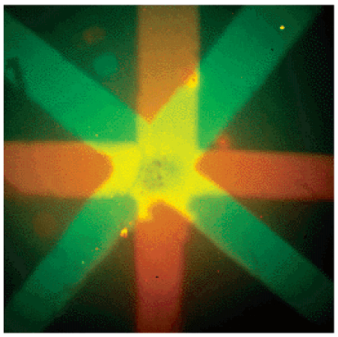

Figure 1.28: Alexa 488 labeled streptavidin (green) and Alexa 594 antibody (red) shows the ability to produce dual component protein patterns via photobleaching of florescent dyes with visible light (reproduced from [271]).

Chapter 2 of this thesis will show how we improved this method by using laser scanning to produce protein patterns with absolute spatial control on concentration as well as providing a detailed characterization of the technique. As a proof of functionality, axons from DRG cells were guided on gradients of the laminin peptide IKVAV.

Chapter 3 will demonstrate how we can create patterns of several components using antibodies conjugated with different dyes and corresponding laser lines. It also demonstrates how a fluorescent microscope can be modified with a common spatial light modulator, such as those found in video projectors, to produce protein patterns as well as a characterization of this new technique.

Chapter 4 will show how we can use thousands of laminin patterns and automated image analysis to study axonal guidance in a high-content manner to identify very subtle changes in neuronal morphology.

# 2 First article

This chapter presents the first article, which was published in *Lab on a Chip* showing the basics of LAPAP. It shows how it can create complex 2D patterns, a full characterization and proof of functionality by guiding DRG cells on IKVAV peptide gradient.

I built the optical setup and programmed the Matlab and Labview software necessary to fabricate the patterns. I also established the incubation procedures in order to fabricate patterns with little non-specific binding and I did the characterization of the technique. For the proof of functionality, I fabricated all the IKVAV patterns and James Correia cultured commissural neurons on them. Once the neurons fixed and stained, I did the imaging and Santiago Costantino did the guidance analysis in a blind manner. I prepared all the figures of the article and wrote a first version of the manuscript, which was greatly improved by Santiago Costantino and reviewed by all the co-authors.

## 2.1 Patterning protein concentration using laser-assisted adsorption by photobleaching, LAPAP

*Lab on a Chip*, 2008, doi:10.1039/b813897d

Jonathan M. Bélisle[1,2], James P. Correia[3], Paul W. Wiseman[4], Timothy E. Kennedy[3], Santiago Costantino[1,2,5]

1. Maisonneuve-Rosemont Hospital, University of Montreal, QC, Canada

2. Institute of Biomedical Engineering, University of Montreal, QC, Canada

3. Montreal Neurological Institute, Department of Neurology and Neurosurgery, McGill University, QC, Canada

4. Departments of Physics and Chemistry, McGill University, QC, Canada

5. Department of Ophthalmology, University of Montreal, QC, Canada

### 2.1.1 Introduction

The study of cellular responses to changes in the spatial distribution of molecules in development, immunology and cancer, requires reliable methods to reproduce *in vitro* the precise distributions of proteins found *in vivo.* Here we present a straightforward method

for generating substrate-bound protein patterns which has the simplicity required to be implemented in typical life science laboratories. The method exploits photobleaching of fluorescently tagged molecules to generate patterns and concentration gradients of protein with sub-micron spatial resolution. We provide an extensive characterization of the technique and demonstrate, as proof of principle, axon guidance by gradients of substrate-bound laminin peptide generated *in vitro* using LAPAP.

### 2.1.2 Article

Microfabrication techniques are increasingly being applied to refine cell culture methods in order to precisely reproduce in vitro, the spatial distributions of proteins found *in vivo* during key events in development [149]. Nevertheless, the technical challenges of fabricating effective biomimetic protein patterns using existing methods have restricted the use of these new technologies. Here we report a relatively simple technique to tailor arbitrary protein patterns at subcellular resolution that can be implemented using readily available reagents and equipment typically used in life science research labs.

Precise distributions of extracellular proteins are crucial for cellular responses in a myriad of processes that include migration, differentiation and ultimately tissue organization [61, 98, 272, 273]. During neural development, axonal growth cones extend and retract filopodia and lamellipodia to determine the path and speed of process extension in order to appropriately wire the nervous system. Several families of guidance cues

including netrins, semaphorins, slits and ephrins have now been identified. These bind to specific receptors presented by axonal growth cones which trigger signal transduction pathways that direct cytoskeletal remodeling [4, 5]. Neuronal responses to these guidance cues are being investigated biochemically; however, many of the precise details of the pathfinding mechanisms remain elusive, in part due to the lack of adequate *in vitro* assays to mimic the responses made by growth cones *in vivo.*

Several methods have been used to investigate protein gradient function *in vitro.* Passive procedures include Boyden, Zigmond and Dunn chambers, however limitations of all these methods are their inability to maintain a stable gradient over periods of several hours to days and major limitations in their capacity to tailor gradients with specific spatial profiles. The simplicity of generating gradients puffed from a micropipette has made them a convenient tool to study axon guidance [115, 121], but the concentration and shape of gradients produced with this assay have shown important instabilities [177]. Other methods to mimic gradients of membrane or extracellular matrix proteins to study axon guidance were limited in their capacity to reproduce the small scale and steepness of gradients present *in vivo* [108, 274]. In addition, the deposition of nanodrops of protein solution [237] and several microfluidic devices [110, 275] have also been successfully used to produce gradients, however the requirement for specialized equipment has restricted the use of these methods in subsequent biological studies. Recently, gradients of ephrinA5 were fabricated by soft lithography, changing protein spot densities to influence axon extension of retinal neurons [234]. While this method provides precise and reproducible graded patterns at a

macroscopic scale across a few tens of micrometers, it is limited by the fact that the concentration of protein present in each spot remains constant across the entire gradient, and the distribution is only graded in terms of spot size and density. Finally, gradients can also be obtained by varying nanoparticle spacing on a substrate via self-assembly of micelles [276] or just using a miniature squeegee [277].

Photonic techniques offer an alternative [109, 278], but generally require the use of UV-lasers and specific chemical cross-linkers that are not commercially available. By contrast, in the approach we describe here, fluorescently tagged molecules are bound to glass substrates by photobleaching the dye molecules. Previous reports of this phenomenon used Hg lamps and large scale photomasks to covalently bind biotin-4-fluorescein (B4F) to BSA adsorbed on a glass surface and thereby generate patterns of substrate-bound protein [271]. Biotin binds to BSA via the generation of free radicals after fluorescein photobleaching and this mechanism was tested varying the oxygen concentration of the buffer solution [271]. However, like the soft-lithography approach [234], the concentration of substrate-bound protein remained constant within the patterned surfaces.

For the approach we have developed here, laser assisted protein adsorption by photobleaching (LAPAP), B4F is adsorbed to a BSA coated glass substrate using a visible Argon or diode laser and is used as a scaffold to bind protein, and potentially multiple different proteins. In this first step of the protocol, custom patterns of substrate bound biotin are produced by moving the focal spot of the laser with respect to the surface. Moreover, since the intensity of the laser illumination regulates the amount of proteins

bound to the substrate, the concentration of protein deposited on cell culture substrates can be controlled. The spatial resolution of the technique is determined by the diffraction limit size of the laser focus and the precision of the motorized translation stage. The macroscopic size of the overall pattern is only limited by the size of the surface to be patterned and the range of the motorized microscope stage. The final density of protein linked to the substrate is determined by the total amount of energy applied during photobleaching. Therefore, the scanning velocity, the solution concentration and the intensity of the laser regulate the dynamic range of the number of proteins that can be linked on the substrates.

Typically, after the laser-adsorption of B4F, the second step is to incubate streptavidin on the sample, which binds to the patterned biotin. For the final step, multiple options are available: either biotinylated peptides or a set of biotinylated antibodies or proteins can be added to the substrate to produce spatially definite patterns of substrate bound, biologically active protein. The full procedure is depicted in Fig.1.

The LAPAP setup consisted of a 473 nm diode laser (Laserglow, ON, Canada), a motorized xyz translation stage (Thorlabs, NJ) and a 60x 1.2 NA water immersion objective (Olympus, Japan). The movement of the motorized stage and laser intensity were controlled by a custom-made Labview (National Instrument, TX) program. A solution of 3% bovine serum albumin (BSA) was added for 20 min to minimize non-specific protein adsorption in 10 mm microwell culture dishes (MatTek Corporation, MA). A 40 μL drop of 50 μg/mL of B4F (Anaspec, CA) in 3% BSA was placed on the surface of glass-bottom culture dishes before performing the photobleaching process. The total number of gradients

on a culture dish was user-defined and depending on the complexity of shape and slope of the gradient, approximately 30 s to 3 min were required to generate each gradient.

The B4F solution was then rinsed with PBS and then incubated with 5 μg/mL streptavidin-CY5 (Invitrogen, CA) in 3% BSA solution for 30 min. To produce functional peptide gradients, 5 μg/mL of a biotinylated peptide (CSRARKQAASIKVAVSADR, commonly named IKVAV peptide) in 3% BSA was then incubated on the microwell plate for 25 min. Fig. 1a and Fig. 1b present schematics of gradients obtained using biotinylated peptides and of the patterning setup.

Various examples of protein gradients and patterns fabricated using LAPAP are shown in Fig. 1. Panel 1**c** illustrates a gradient of streptavidin-Cy5 composed of 100 lines 50 μm in length, spaced by 1 μm. The first 60 lines were made at a constant laser scan velocity of 50 μm/s and increasing laser intensity incrementally from line to line from 0.5 to 160 μW. A constant intensity of 160 μW and a sequentially decreasing line scan velocity (from 49 to 5 μm/s) were used for the final 40 lines.

Additionally, using biotinylated antibodies, patterns of specific antigens can be fabricated. To create full protein gradients (in this case using antibodies against the extracellular matrix protein laminin-1), the peptide incubation step is replaced by three 30 minutes steps of biotinylated anti-rabbit IgG (5 μg/mL), followed by rabbit anti-laminin (5 μg/mL) and then Alexa 594 goat anti-rabbit (20 μg/mL). The first biotinylated antibody is used to link the target protein (rabbit anti-laminin) to the substrate. The fluorescently tagged IgG is then used to visualize the distribution. Fig. 1e illustrates several gradients of

rabbit anti-laminin revealed with the Alexa 594 goat anti-rabbit IgG, all created using the same parameters as for the gradient shown in Fig. 1c. Finally, the flexibility and precision of this method to fabricate substrates with a wide dynamic range of adsorbed protein concentration is demonstrated by reproducing a 200x293-pixels image of Vermeer's "Girl With a Pearl Earring" (Fig. 1d). Each pixel from the image scales to $1\mu m^2$ on the pattern.

To characterize the dynamic range of LAPAP as a function of laser power, an analysis of photobleaching dwell time compared to B4F concentration was performed. Lines were first scanned at different beam focus velocities from 200 to 2 μm/s and we compared the fluorescence intensity present in different regions of the pattern generated while assuming a linear relationship between fluorescence signal and protein concentration. We applied a simple model where the adsorption rate of B4F is proportional to the available B4F-free surface within the area delimited by the focal spot of the laser. Therefore, the adsorbed protein concentration ($\theta$) as a function of the laser dwell time (t) behaves exponentially: $\theta=\theta_{max}(1-e^{-t/\tau})$, where $\theta_{max}$ is the maximum protein concentration that can be adsorbed and $\tau$ is a characteristic time constant. As shown in Fig. 2a, protein concentration was relatively well modeled by this function yielding a time constant of 0.14 s. However, this model is overly simplified and could be improved since experimental conditions allow B4F binding to previously substrate-bound B4F and possibly grow in an arborized manner. Better models could explain discrepancies between the data and the fitted curve.

The amount of substrate bound protein was found to increase with laser power from 1.9 to 160 μW when using a 1.2 NA objective. For laser intensities beyond this threshold a plateau can be observed in protein concentration up to an intensity of 3.1 mW, likely due to photobleaching saturation (Fig 2b). The protein concentration as a function of B4F solution concentration follows a Langmuir isotherm (Fig 2c).

To test the biochemical activity of the peptide gradients generated, dorsal root ganglion (DRG) cells isolated from E15 Sprague Dawley rat embryos were plated on gradients of a laminin fragment that has been previously demonstrated to be sufficient to evoke axonal growth cone turning by these cells[109] (Fig 2d). Dissociated DRG cultures were cultured in neurobasal supplemented with 2% B-27, 2 mM GlutaMAX-1, 100 unit/mL penicillin, and 100 μg/mL streptomycin, 50 ng/mL NGF. Before LAPAP, the substrates were coated with poly-D-Lysine (2 μg/mL) for 10 min to promote attachment of the neurons to the coverglass. DRG cells were grown on IKVAV gradients and also on control samples where the laminin peptide was replaced by B4F (5 μg/mL). After 24 to 36 hours, the cultures were fixed in 4% paraformaldehyde and neurons were immunostained using 0.8 unit/mL Alexa 546 coupled phalloidin and 500 ng/mL Hoechst 33258.

In order to quantify the behavior of growth cones on the peptide patterns, the samples were imaged using fluorescence microscopy and analyzed. Axons were counted as "guided" if they entered the patterned area and traveled up the gradient, and as "non guided" if they traveled down the gradient before exiting the pattern. The images were randomly numbered and analyzed by an observer blind to the experimental conditions, i.e.

unaware if the sample substrate consisted of IKVAV peptide or were controls (Fig. 2e). The number of axons extending in the positive direction on the IKVAV gradient was three times greater than the number turning in the opposite direction. On control substrate, axons showed no preferential direction. Fig. 2d illustrates an example of an axon that was scored as turning and extending up a gradient of the IKVAV peptide. Fig. 2e shows the cumulative results of a total of 400 gradients (200 controls and 200 IKVAV peptides), on which 30 axons were identified and scored as having encountered a gradient, independent of interactions with other cells. Both continuous gradients as in Fig. 1c (400 in total) and gradients composed of separated lines (694) to reduce fabrication time were patterned. Line gradients consist of 11 lines of a 100 μm length spaced by 10 μm with a measured thickness of 1.26±0.07 μm. A six-fold reduction in the fabrication time of the discrete gradients allowed doubling of the covered area as compared to continuous gradients. The guiding capacity of each type of gradient, continuous and spaced, was quantified independently and no guidance observed on the striped pattern for 131 growth cones. In addition, the total number found on the peptide patterns doubled the number of those on control samples (considering the 1094 patterns).

As compared to conventional assays, LAPAP can create protein patterns that have a resolution close to one micron (1.26±0.07 μm for the 1.2 NA objective used), their spatial distribution is arbitrary and their full size is only limited by the range of travel of the stage used. The simplicity of LAPAP allows for straightforward implementation on a motorized confocal microscope, with only software customizations. Moreover, the fact that laser light

does not interact with the final protein patterned, eliminates the chances of protein photodamage as compared to other photonic techniques[109]. Fabricated gradients remain stable over extended periods of time as we have found that they can still be visualized after more than three months of storage at 4 $^{o}$C. Finally, by varying beam dwell time and solution concentration, it is possible to change the amount of protein bound by an order of magnitude for each parameter (Fig. 2a and c). Manipulation of the laser power provides additional control, readily providing the ability to vary the fluorescence from the bound protein by over two orders of magnitude (Fig. 2b). By combining adjustments of the laser power and dwell time we show that the range of bound protein can be extended by three orders of magnitude (**Supplementary Fig. 1**). Furthermore, minimizing non-specific binding of proteins to the substrate could further increase this range.

The studies presented demonstrate the versatility and potential of this simple approach. Nevertheless, chemotaxis in a living organism implies complex distributions of a plethora of guidance cues and to understand and manipulate this requires a means to generate more complex protein distributions and combinations. Our current studies aim to extend LAPAP to link more than one guidance cue by increasing the number of fluorescent tags and laser lines, and additionally to carrying out functional chemotaxis assays using full-length proteins.

In conclusion, we report a novel assay for precise and flexible generation of protein distributions on cell culture substrates. LAPAP provides a relatively straight forward

method that allows the generation of graded distributions of substrate bound protein at subcellular levels of resolution.

### 2.1.3 Acknowledgements

Support is acknowledged for SC from the NSERC and FQRNT, for PWW from NSERC and CIHR, for TEK from FRSQ and CIHR, and for JMB from NSERC (CGS D). We acknowledge Simon W. Moore for helpful discussion during the beginning of this project. PWW and TEK acknowledge the support of the CIHR funded program in neuroengineering for this work.

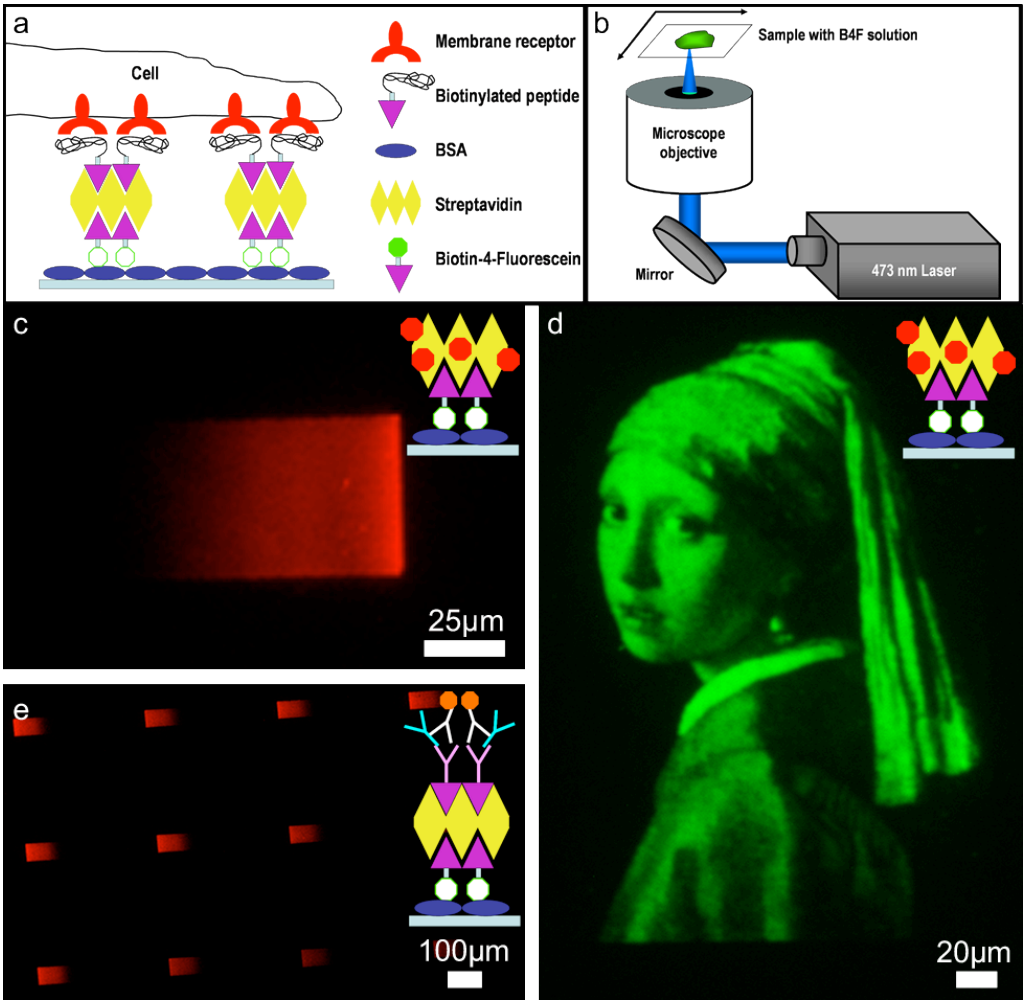


Figure 2.1: Examples of protein gradients and patterns obtained by Laser-Assisted Protein Adsorption by Photobleaching (LAPAP) and Setup. **(a)** Schematic of the B4F, streptavidin and biotinylated peptide combination required to produce functional protein patterns. B4F is first adsorbed by LAPAP to a BSA-coated substrate, next streptavidin is incubated on the sample and finally a biotinylated peptide is added to produce functional gradients. **(b)** The simple patterning apparatus includes a blue diode laser, a microscope objective and motorized translation stages to move the sample with respect to the focal spot. **(c)** Continuous gradient of streptavidin-Cy5 produced by changing both the laser intensity and the velocity of the focal spot displacement. **(d)** Streptavidin-Cy5 miniature reproduction of Vermeer's Girl With a Pearl Earring that

demonstrates the flexibility and dynamic range of the technique **(e)** Gradients of rabbit anti-laminin with the same shape as that shown in (c), immunostained using Alexa 594 goat anti-rabbit IgG. To produce and visualize these gradients, B4F was first adsorbed by LAPAP, followed by 4 subsequent incubation steps: streptavidin, biotinylated anti-rabbit IgG, rabbit anti-laminin and Alexa 594 goat anti-rabbit IgG.

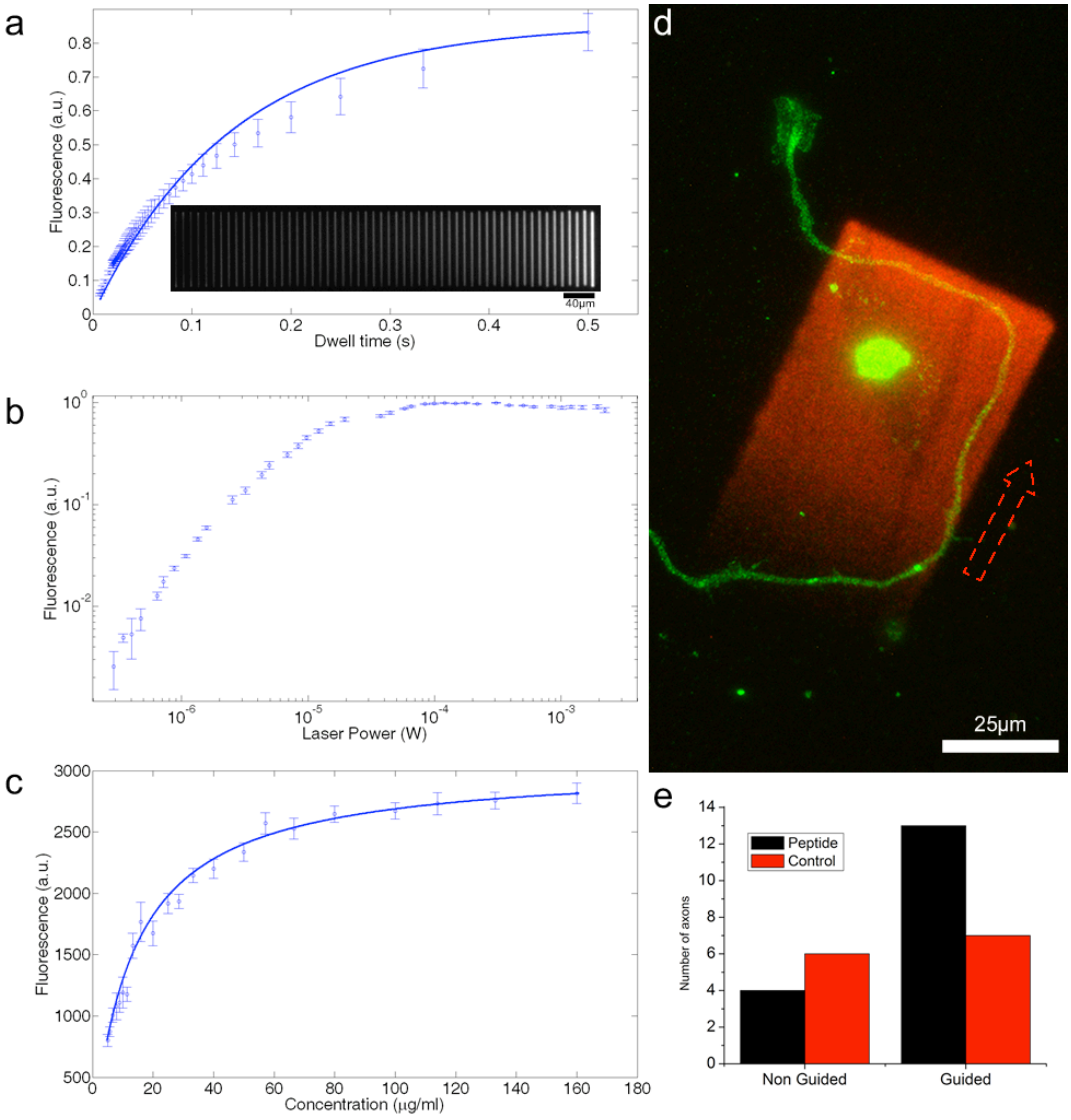


Figure 2.2: Characterization of the patterning method and growth cone guidance assay. **(a)** Adsorbed protein concentration as measured by fluorescence as a function of beam dwell time nearly shows an exponential behavior. It has to be noted that this model is overly simplified and therefore only fits partially the data. The inset shows one of the 10 patterns created to produce this graph. **(b)** Adjusting the laser power allows the user to modulate the protein concentration range over more than two orders of magnitude. Maximum protein concentration is reached at approximately 160 µW. **(c)** By varying the concentration of B4F, we show that

bound protein concentration follows a Langmuir isotherm. **(d)** An example of axonal guidance by a gradient of IKVAV peptide. DRG neuron stained with Alexa 546 in green and laminin peptide gradient visualized by streptavidin-Cy5 in red. The red arrow points to the direction of increasing concentration. The green circular spot in the middle of the gradient is due to debris resulting from tissue dissection. This neuron was scored as guided. **(e)** Histograms showing axonal response on laminin peptide gradients and on control samples. Axons were considered "guided" if they traveled along the gradient's positive slope, and "non guided" when they traveled in the opposite direction.

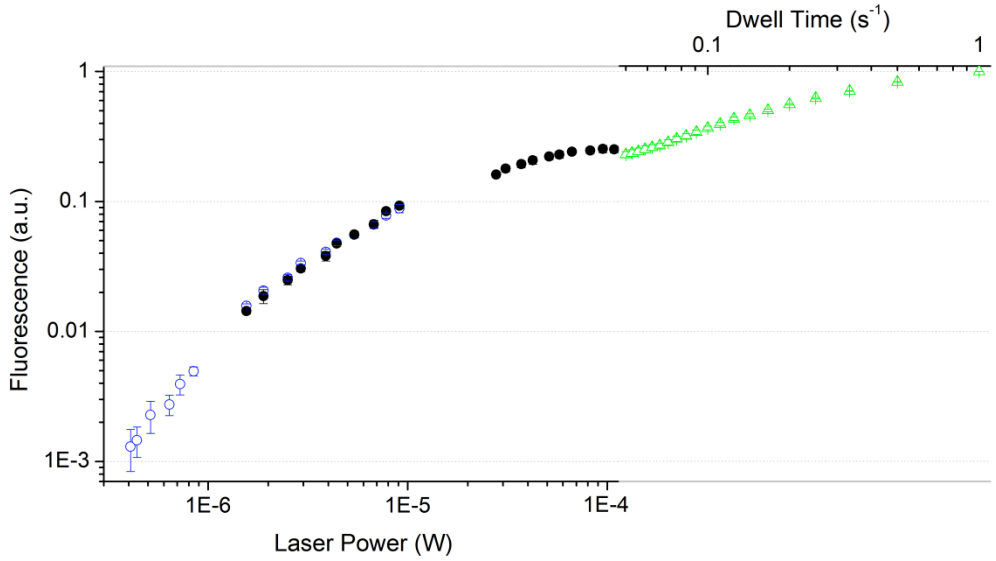


Figure. 2.3: Concentration of substrate-bound protein (Streptavidin-Cy5) as a function of both laser power and dwell time. Data represented by green triangles were obtained at constant laser power by only varying the velocity of the laser scan (top right x-axis). Blue circles and filled black circles were obtained at constant dwell time, while laser power was varied (bottom left x-axis). The images obtained to create this plot were acquired at two different ccd exposure times in order to avoid artifacts due to a nonlinear response of the camera over a very large dynamic range. Blue circles were acquired using an integration time ten times longer than the filled black circles and the green triangles. To combine all measurements on one graph, the ten overlapping points located between laser powers of $10^{-6}$ to $10^{-5}$ W were used as a reference.

# 3 Second article

This chapter presents a follow up paper from the article presented in chapter 2 and was accordingly published in *Lab on a Chip*. It presents three major advances to the original LAPAP technique. The first one is the ability to link several different molecules to the substrate by using several laser lines and still achieve full control on the individual concentrations. This is particularly important since *in vivo* several guidance proteins are responsible for accurately guiding axons, not just one. The second improvement is the simplification of the method and the reduction in time for the patterning step, which was accomplished by introducing widefield illumination. Finally, we also establish patterning protocols using standard antibodies that most cellular biology laboratories usually have in stock.

I built the new widefield LAPAP setup and fully characterized patterning performed with this setup. Dario Kunik contributed to the time exposure characterization. I developed the new protocol for using antibodies instead of B4F as a first binding molecule and also improved the LAPAP setup by adding a new laser line for multicomponent patterning. I prepared all the figures and wrote the first version of the manuscript that was later improved by Santiago Costantino and Dario Kunik.

## 3.1 Rapid multicomponent optical protein patterning

*Lab on a Chip*, 2008, doi: 10.1039/b911967a

Jonathan M. Bélisle[1,2], Dario Kunik[1,2] and Santiago Costantino[1,2,3]

1. Maisonneuve-Rosemont Hospital, University of Montreal, QC, Canada

2. Institute of Biomedical Engineering, University of Montreal, QC, Canada

3. Department of Ophthalmology, University of Montreal, QC, Canada

### 3.1.1 Abstract

Cells sense spatial distributions of molecules which trigger signal transduction pathways that induce the cell to migrate or extend by remodelling the cytoskeleton. However, the influence of local and small variations of extracellular protein concentration on chemotaxis is not fully understood, due in part to the lack of simple and precise methods to pattern proteins *in vitro*. We recently developed a new technology to fabricate such patterns which relies on photobleaching fluorophores to adsorb proteins on a cell culture substrate: *laser-assisted protein adsorption by photobleaching* (LAPAP). Here we report several key improvements to LAPAP: we created arbitrary patterns made of several different proteins simultaneously, we reduced the fabrication time more than one order of magnitude and we used secondary antibodies to significantly enlarge the spectrum of proteins that can be

employed. As a result, multicomponent protein gradients can be produced using reagents that are typically available in life science research laboratories on a standard inverted microscope equipped with a camera port.

### 3.1.2 Introduction

Spatial distributions of proteins are essential to the normal development and life of organisms; central nervous system wiring [5, 74], muscle formation [279], and defence against pathogens [148] are examples where protein distributions play a fundamental role. Indeed, understanding the function of these spatial distributions in cellular mechanisms is critical to achieve major advances in regenerative medicine. For example, a profound comprehension of how molecular cues are read by axonal growth cones is a prerequisite for repairing nerve damage after injury, which is one of the ultimate challenges of neuroscience [280, 281]. Growth cones integrate information from different molecules in the environment to extend in the correct direction and to connect with their appropriate targets [9] during development. The arrangement of chemoattractants and chemorepellants encountered by growth cones dictate the reorganization of microtubules and actin filaments to steer the axons [4, 272]. Therefore, the need for a precise and reproducible *in vitro* assay to create protein patterns is vital for a deeper understanding of axonal guidance. Moreover,

a low-cost and user-friendly technology is required to allow an increasing number of research groups to carry out studies leading to major advances in the field.

Laser-Assisted Protein Adsorption by Photobleaching (LAPAP) was recently introduced in an attempt to overcome most of the limitations that constrained the applications of protein patterning [282]. Simplicity and robustness make LAPAP an attractive alternative to existing techniques [149] in obtaining protein gradients and even arbitrary spatial distributions of molecules. LAPAP-made protein gradients are more stable in time and reproducible as compared to micropipette puffed generated gradients [115, 121] and unlike patterns generated by microcontact printing [230, 234], the protein concentration can be continuously varied over three orders of magnitude. LAPAP is relatively straightforward as compared to microfluidic implementations [110, 113, 275] as it has a very simple setup, high spatial resolution and even the ability to be implemented on commercial confocal microscopes. Finally, the use of low power visible lasers and all commercially available reagents is simpler than UV illumination [109, 278].

Briefly, in LAPAP, biotin-4-fluorescein (B4F) molecules are photobleached by a blue laser in order to adsorb them to a glass surface [282]. The photobleaching of fluorescein creates free radicals [271] that react and bind these molecules that are in close proximity to the surface. To produce on-demand arbitrary patterns, the laser is focused at the glass surface and scanned across the substrate, while varying the illumination intensity and the scanning velocity [282]. In the second step, streptavidin is incubated which binds B4F and finally, biotinylated proteins or antibodies can interact with streptavidin.

Three fundamental improvements are presented in this work. First, we describe how to bind several different molecules with full control of their individual concentrations and spatial distributions. The level of complexity of the protein patterns that can now be achieved is highly improved. Secondly, in order to further simplify the method and reduce the time required to produce patterns, we introduce widefield illumination LAPAP. This novel setup can be implemented using any standard inverted microscope equipped with a camera port. Finally, we illustrate how to carry out the patterning protocol using chemical reagents that are usually in stock in most cellular biology research laboratories. Primary and fluorescently tagged secondary antibodies can be used to link most proteins of interest.

Overall, we extended LAPAP to achieve protein patterns of high complexity while simultaneously simplifying and accelerating the fabrication time.

## 3.1.3 Results

### 3.1.3.1 Widefield illumination LAPAP

The widefield illumination setup that we implemented (Fig. 1a) is an add-on device that can be coupled to the camera port of any standard inverted microscope. Such a device makes use of a light spatial filter located at the image plane of the microscope that is here used as an illumination port instead of an imaging port. Illuminating this spatial filter produces its image on the focal plane of the objective. Thus, instead of scanning a laser to tailor a desired pattern, the same pattern can be achieved by widefield illumination. Such

illumination modality speeds up the process, does not require automation software and almost no optomechanical elements are needed.

To obtain a perfectly focused image of the spatial filter on the sample, the spatial filter must be precisely placed at the position where the CCD chip would normally be located if that port was equipped with a camera instead of the patterning setup. An extended light source is ideal for this application with light-emitting diodes and lamps probably being the best options. Several objects can be used as spatial filters, but photography slides and liquid crystal displays (LCD) are the most convenient for this application. The advantage of LCDs is that they can be controlled using a standard VGA or SVGA computer output that allows a very simple setup and no need for specialized software. An example of how flexible protein patterns can be is shown in Fig. 1b, where streptavidin-Cy5 was used to reveal the pattern.

Using widefield illumination LAPAP, two options are readily available to vary the protein concentration: using a greyscale image as a spatial filter or using binary black and white image series. In order to characterize the dynamic range of both possibilities, a pattern of 12 squares was fabricated by generating a greyscale image as a filter where each square had a linearly increasing intensity from 21 to 255. We show that the amount of protein can be modulated by 1 order of magnitude only by changing the pixel value within the image on the spatial filter (Fig. 2a), where 0 is black and 255 is white.

Similarly, a white square filter was used to subsequently fabricate 12 square patterns using a 60x 1.35NA objective with various exposure times for each square ranging

from 5s to 85min at a constant power after the objective of 15.5µW. This gives the possibility of changing the protein concentration by 50-fold (Fig. 2b).

To evaluate the amount of protein bound as a function of the exposure time, the bound B4F was revealed using streptavidin-Cy5 and the fluorescence intensities were plotted in Fig. 2a and Fig. 2b respectively. The experimental details including protein concentrations and incubation times can be found elsewhere [282].

Finally, to assess the typical resolution that can be obtained by widefield illumination LAPAP, a protein pattern of a modified USAF resolution target was produced using a 60x objective yielding 1µm as a result (Fig. 2c and d).

### 3.1.3.2 Fluorescently tagged secondary antibody patterns

In order to decrease the number of incubation steps required to produce full protein patterns, we developed a protocol to directly bind fluorescently conjugated antibodies to the glass surface by either standard or widefield illumination LAPAP. In this case, fluorescently tagged secondary antibodies replace B4F as the molecule that first binds to the substrate by photobleaching the fluorophores. Subsequently, primary antibodies and full proteins are bound to create patterns.

We produced patterns of various concentrations to characterize the technique using rabbit anti-laminin antibodies following the binding of FITC goat anti-rabbit IgG to the glass substrate. The antibody pairs were revealed using Cy5 conjugated antibodies Different concentrations were obtained by either changing the laser intensity or the

scanning velocity of the laser focus. For both methods, we show that the dynamic range obtained is approximately one order of magnitude (Fig. 3).

#### 3.1.3.3 Single step multicomponent antibody patterns

Multicomponent protein patterns can be obtained by combining multiple laser wavelengths and different fluorophores. We demonstrate that it is possible to tailor superposed gradients of two different antibodies. Provided that the absorption maxima of the two fluorophores are distinct (so that each laser line photobleaches only one specific molecule), the binding of each species can be controlled by the intensity of the corresponding wavelength, thereby controlling their individual concentrations.

In Fig. 4c one two-component sample consisting in four different gradients is shown. The top-right region appears yellow as FITC goat anti-rabbit IgG (green) and Cy5 goat anti-mouse IgG (red) gradients are precisely superposed. The bottom-left pattern shows gradients of opposing slopes therefore appearing half-green and half-red with fading intensity toward the middle. The remaining two patterns are both made of one type of antibody and appear red and green respectively. It is important to state that some level of cross talk from one component to the other was observed. In the location where only the blue laser is on (top left corner of Fig. 4c), a small amount of Cy5 goat anti-mouse IgG is adsorbed and where only the red laser is on (bottom right corner of Fig. 4c), FITC goat anti-rabbit antibodies are also adsorbed. This non-specific binding is approximately 10%

for FITC and 30% for Cy5. Control experiments were performed to assess the origin of such cross-talk and showed that most probably several fluorophores could be photobleached on a single antibody, allowing to both covalently bind the substrate and another antibody in close proximity.

### 3.1.3.4 Multicomponent patterns using subsequent illumination

Subsequent widefield illumination LAPAP steps with different FITC conjugated antibodies have lead to the production of multicomponent patterns avoiding cross-talk from one component to the others. We were able to combine three different molecules on the same pattern by photobleaching them sequentially and changing the solutions between each exposition: two different primary antibodies (mouse anti-myc and rabbit anti-thy1) as well as streptavidin were patterned. A glass-bottom culture dish was placed on the microscope positioned at the focal plane of the objective and three circles were patterned by widefield illumination. The dish was clamped to the microscope to avoid possible displacement during the iterative illumination and rinsing steps. The result obtained is shown on Fig. 5 where the streptavidin is reavealed by B4F (blue), mouse anti-myc (9E10) by TRITC-goat anti-mouse IgG (green) and rabbit anti-thy1 by Cy5-goat anti-rabbit IgG (red). Seven regions are clearly distinguishable in the image where the different proteins are combined.

## 3.1.4 Experimental

### 3.1.4.1 Widefield illumination LAPAP

An extended light source is ideal for this application and we used a 470nm 380mW blue collimated light-emitting diode (LED) (Thorlabs, NJ). We used an 800x600 translucent liquid crystal microdisplays (LCD) (Holoeye, Berlin, Germany) combined with two linear polarizing filters placed on each side with a polarization efficiency of 95% (Edmund Optics, NJ).

The LCD was positioned at the right side port of an Olympus IX71 microscope and since it followed the C-mount standard, the LCD was placed 17.5mm from the flange of the camera port. Patterns of 12 squares were fabricated by generating an 8-bit greyscale image as a filter where each square had a linearly increasing intensity from 21 to 255. This image file sent to the LCD as a spatial filter was generated by a custom program in Matlab (MathWorks, MA). A B4F (50μg/ml) solution was exposed for 30min using a 20x 0.75NA objective and the pattern was later revealed by streptavidin-Cy5 (5μg/ml). Both solutions were prepared using 3% bovine serum albumin (BSA) in phosphate buffered saline (PBS).

An 800x600 pixels image of the USAF resolution target was produced on the LCD spatial light modulator (Fig 2c). We also modified the resolution target by adding 12 white lines of a single pixel thickness, 6 of them separated by 1 black pixel and the remaining 6 by 2 black pixels.

### 3.1.4.2 Patterns using fluorescently tagged antibodies

In order to minimize non-specific protein adsorption, a blocking solution (1% goat serum and 1% BSA in PBS) was incubated for 30min on a 14mm microwell culture dish (MatTek Corporation, MA). A 20µL drop of 2mg/mL of FITC goat anti-rabbit IgG (Jackson ImmunoResearch Laboratories, PA) in 2% BSA and 80% goat serum was placed onto the coverglass of the dish. Patterning was then performed by moving the focus of a 473nm laser diode across the sample. Rabbit anti-laminin (5µg/mL), biotinylated goat anti-rabbit IgG (5µg/mL) and streptavidin-Cy5 (5µg/mL) all in 3% BSA were subsequently incubated for 30min each to reveal the pattern obtained by FITC goat anti-rabbit IgG

The dynamic range obtained with the antibody was characterized in terms of laser dwell time and power using the standard LAPAP setup [282]. For dwell time characterisation, lines at beam focus velocities from 30µm/s to 1µm/s were scanned at a constant 160µW laser power and after all the incubation steps, streptavidin-Cy5 fluorescence was measured and assumed to be proportional to the bound FITC goat anti-rabbit IgG concentration. The laser power characterisation was performed by scanning lines at a constant 1µm/s velocity and by increasing laser power from 1.8µW to 277.2µW and by measuring the streptavidin-Cy5 fluorescence after the last incubation step.

### 3.1.4.3 Single step multicomponent antibody patterns

The blocking solution was incubated for 30min on a glass-bottom culture dish. Then, a drop of FITC goat anti-rabbit IgG and Cy5 goat anti-mouse IgG (each 2mg/mL in BSA 4% and goat serum 60%) was placed on the coverglass and was scanned simultaneously by the moving focal spot of two diode lasers (473nm and 671nm, Fig. 4a). A total of four patterns were produced by scanning 50 lines 25µm long and by increasing the laser intensity every next line between 0.2µW to 90µW for the 473nm laser and by increasing the intensity between 0.2µW to 430µW for the 671nm laser. One pattern was made by increasing both laser lines in the same direction, giving two superposed gradients. Another one was drawn with the lasers increasing their intensity in opposite directions giving two gradients of opposing slopes. The remaining two patterns were obtained by scanning only one laser line for each of them to assess the presence of non-specific binding. After laser illumination, two incubation steps of 30min were required to reveal the patterns: rabbit anti-laminin (5µg/mL) and mouse anti-myc (9E10) (5µg/mL) in 3% BSA in PBS followed by FITC goat anti-rabbit IgG (5µg/mL) and Cy5 goat anti-mouse IgG (5µg/mL) in 3% BSA in PBS (Fig. 4b).

### 3.1.4.4 Multicomponent patterns using subsequent illumination

A solution of BSA 3% was incubated on a microwell culture dish for 30min and was later rinsed with PBS. The culture dish was then placed on the microscope stage with

the top surface of the coverglass positioned at the focal plane of the objective. The dish was tightly fixed with clamps to avoid displacement during the subsequent illumination and rinsing steps. A drop of B4F (50µg/mL) in BSA 3% was then placed on the coverglass and exposed by a top-center circle using widefield illumination LAPAP for 15min. The sample was then rinsed several times with PBS while maintained at a fixed position and next a drop of FITC goat anti-rabbit IgG (2mg/mL in BSA 2% and goat serum 80%) was placed on the coverglass. The sample was again exposed with the blue LED, but this time with an image of a bottom-right circle for 30min. The sample was again rinsed while kept in a fixed position for the final exposure step where the blue light image of a bottom-left circle adsorbs FITC goat anti-mouse IgG (2mg/mL in BSA 2% and goat serum 80%) onto the coverglass for 30min. A mix of streptavidin (5µg/mL), mouse anti-myc (9E10) (5µg/mL) and rabbit anti-thy1 (5µg/mL) was then incubated on the pattern for 30min. In order to reveal the pattern, B4F (5µg/mL), TRITC-goat anti-mouse IgG (5µg/mL) and Cy5-goat anti-rabbit IgG (5µg/mL) were finally incubated on the sample.

### 3.1.5 Discussion

The improvement made to LAPAP[282] by implementing the technology using a standard microscope equipped with a camera port highly simplifies the method with the aim of making the technique amenable to be used in a standard life science lab. The time needed to

produce a pattern was significantly reduced as the Einstein miniature (Fig. 1b) only took 5 minutes of exposure compared to 80 minutes needed for similar patterns produced with original LAPAP [282]. Furthermore, there is no sophisticated control and automation software required for producing these patterns.

Compared with standard LAPAP [282], the results we obtained (Fig. 2a) using widefield illumination shows a reduced dynamic range. This is not a limitation of the new illumination method itself, but is mainly due to the poor polarization efficiency of the low-cost polarizers we used, which reduced the contrast ratio of our spatial filter. Nevertheless, the dynamic range we obtained is enough for a large fraction of possible biological applications.

Regarding the resolution obtained (Fig. 2c and 2d), 1μm is considerably above the diffraction limit for a 1.35NA objective using 470nm light. One should consider that the smallest feature that can be patterned via this setup is basically limited by the pixel size of the spatial filter. The size we measured approximately matches what was expected given the characteristics of the LCD we used and the magnification of the microscope objective.

The use of antibodies yields the ability to produce patterns of several specific proteins, therefore allowing improved *in vitro* studies of cellular response. Furthermore, this change also reduces the number of intermediate molecules required to pattern the desired protein.

It is important to note that the molecular mass of tagged antibodies being roughly 200 times the mass of B4F, an IgG concentration of 10mg/ml should be used to obtain a

similar amount of fluorescent molecules per volume unit. However, significant non-specific binding was obtained at this concentration during preliminary experiments and the final concentration was decreased by 5-fold to obtain optimum results. Even if the final concentration we used is much larger (1000 times) than what is currently utilized for immunostainning, commercially available lyophilized antibodies can be used to prepare the solution while maintaining a remarkably low cost per sample. The results obtained showed that it is possible to vary the amount of adsorbed antibodies by one order of magnitude (Fig.3).

Regarding multicomponent protein patterns, this is, to our best knowledge, the first technique that is capable of providing such patterns with micron resolution and a total control of the local spatial concentration. The limitation to the number of molecules that can be mixed is determined by the width of the absorption spectra. It is challenging to find more than two molecules whose absorption spectra do not overlap significantly. Indeed, despite the direct visual results obtained by this technique (Fig. 4c), the quantitative analysis of the profile of each fluorescence channel showed relatively small cross talk. Control experiments were then performed to understand the binding of Cy5 goat anti-mouse IgG with the 473nm laser and of FITC goat anti-rabbit IgG with the 671nm laser. We found that the 671nm laser was not able to bind FITC goat anti-rabbit IgG when it was not mixed in solution with Cy5 goat anti-mouse IgG. The most probable explanation for the cross-talk binding of FITC-goat anti-rabbit IgG illuminated by 671nm laser is the non specificity of the chemical reaction that allows single Cy5 goat anti-mouse IgG to

covalently bind to the surface and while also linking FITC-goat anti-rabbit IgGs. For the binding of Cy5-goat anti-mouse IgG with the 473nm laser, we found that approximately one third of the cross talk is due to direct photobleaching of Cy5 by the 473nm laser. This cross-talk became significant when a third fluorescently tagged antibody was mixed and a 532nm laser was added to the setup. The undesirable mixing of molecular species when adding TRITC conjugated antibodies yielded serious cross talk with the two other tagged IgGs.

To circumvent this cross talk problem and be able to add a third protein, we designed an assay with subsequent illumination steps. Simply using FITC conjugated antibodies against different antigens opened the possibility to obtain three component patterns (Fig. 5). In this case, the limitation in the number of different molecules that can be attached is their availability on the market. Since most secondary antibodies bind mouse and rabbit immunoglobins, the possibility of further expanding the number of proteins requires the use of chemical reagents that are not of general use.

### 3.1.6 Conclusion

The novel technology we presented made possible to pattern different proteins on the same substrate. We can now fabricate multi-protein patterns at high levels of resolution. Two and three different molecules were bound to glass substrates using very simple technology and commercially available reagents. Furthermore, simple improvements to the

illumination setup allowed the fabrication of micron resolution protein patterns using a standard microscope. We designed a device that mounted on the camera port of an inverted microscope would render substrate bound protein patterning simple, inexpensive and user-friendly.

### 3.1.7 Acknowledgements

Support is acknowledged for SC from the NSERC, FQRNT, CNIB and FRSQ. For JMB from NSERC (CGS D). We thank Stephane Lefrançois for a critical reading of the manuscript.

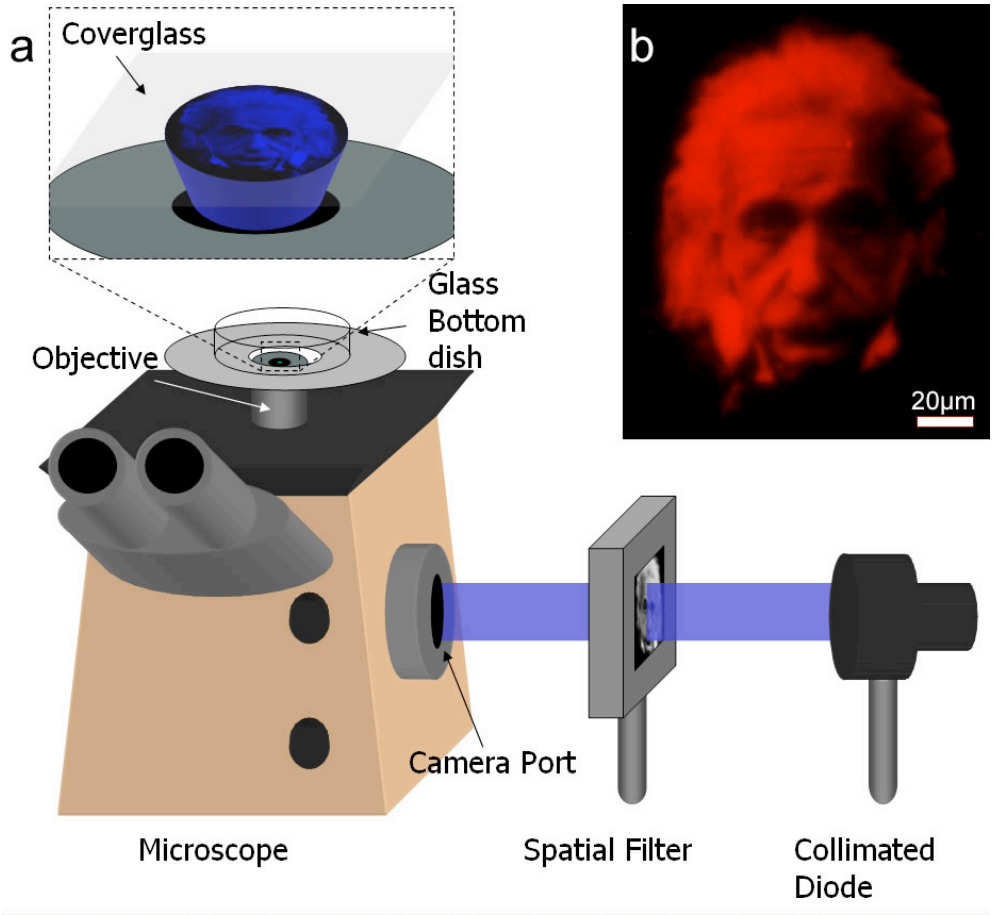


Figure 3.1: Widefield illumination LAPAP. **(a)** A collimated blue diode (470nm) illuminates a spatial filter which is positioned at the image plane of the camera port. This scheme produces an image of the spatial filter at the focal plane of the objective which is focused at the top surface of a glass-bottom dish. Biotin-4-Fluorescein or FITC conjugated antibodies are then photobleached following the pattern represented in the image sent to the spatial filter. In this case, a grayscale image of Einstein is recreated using blue light on the top surface of the coverglass. **(b)** The Einstein protein pattern made using a 60x objective and B4F was later revealed with streptavidin-Cy5 and imaged by fluorescence microscopy.

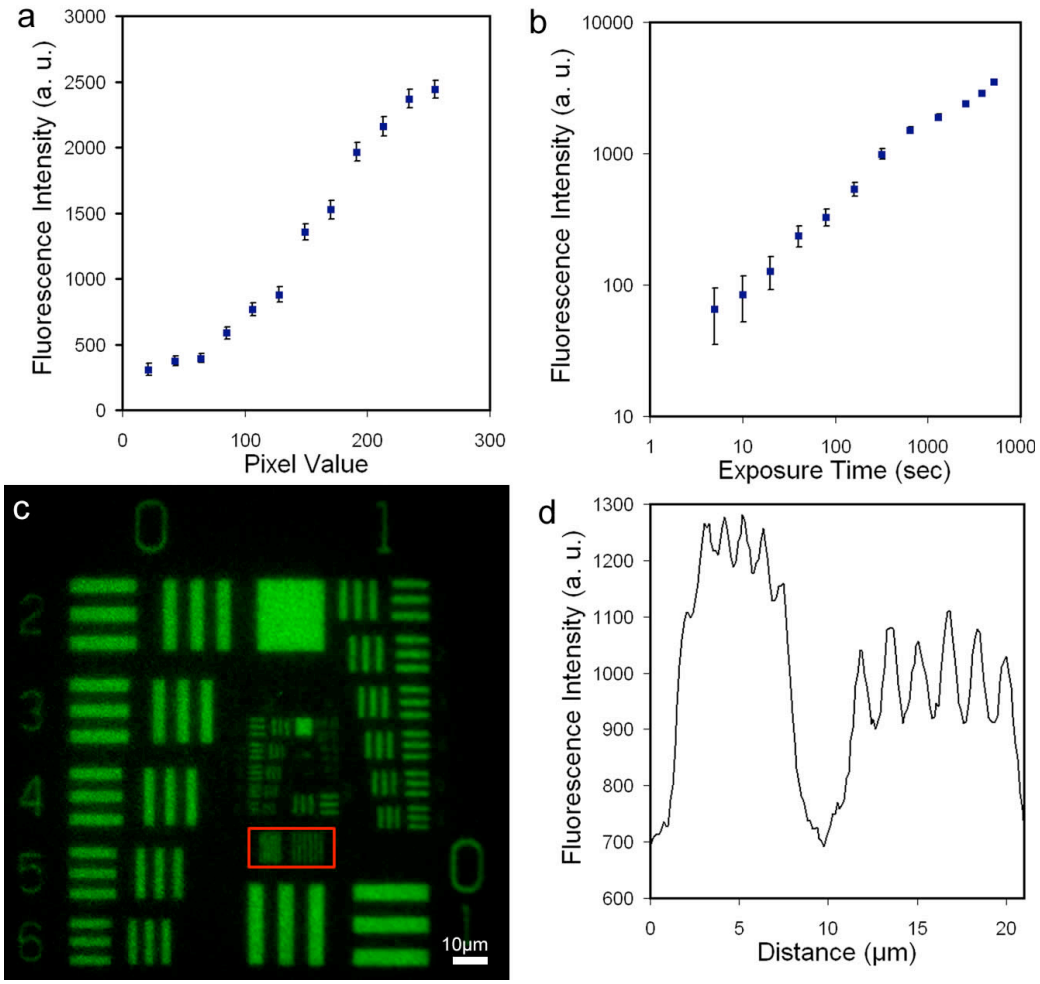


Figure 3.2: Characterisation of widefield illumination LAPAP. (a) Fluorescence intensity as a function of the spatial filter's pixel value. Our results show that the amount of bound protein can be changed by one order of magnitude. (b) Protein quantity as a function of exposure time was modulated by 50-fold using exposure times ranging from 5s to 85min. (c) Image of a resolution target produced by widefield illumination LAPAP with a 60x objective (1.35 NA). The red rectangle shows a region where 6 lines (on the left) were separated by 1μm and the other 6 lines (on the right) by 1.5μm. (d) Average linear profiles of this region show that it is possible to resolve individual lines separated by 1μm (left) and 1.5μm (right).

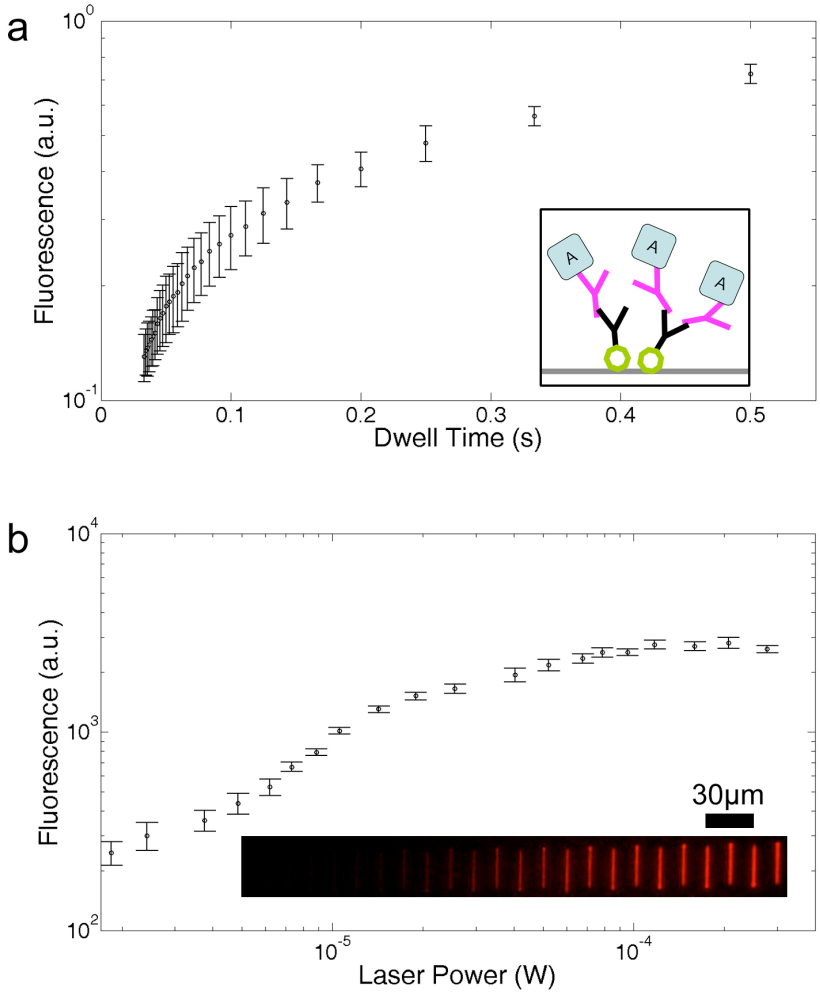


Figure 3.3: Patterns of antibodies produced by LAPAP. FITC conjugated goat anti-rabbit IgGs were directly bound to a glass substrate by a focused 473nm laser. Rabbit anti-laminin, biotin conjugated goat anti-rabbit and streptavidin-Cy5 were subsequently incubated on the pattern for visualization. (a) Semi-log plot of antibody concentration as a function of dwell time shows a dynamic range close to one order of magnitude. The inset shows how a specific protein pattern is made using a fluorescently conjugated secondary antibody (in black), a primary antibody (in pink) and the protein of interest (rounded square). (b) Log-log plot of bound antibody concentrations as a function of laser power shows a one order of magnitude dynamic range. The inset shows one of the 10 patterns used to obtain this graph.

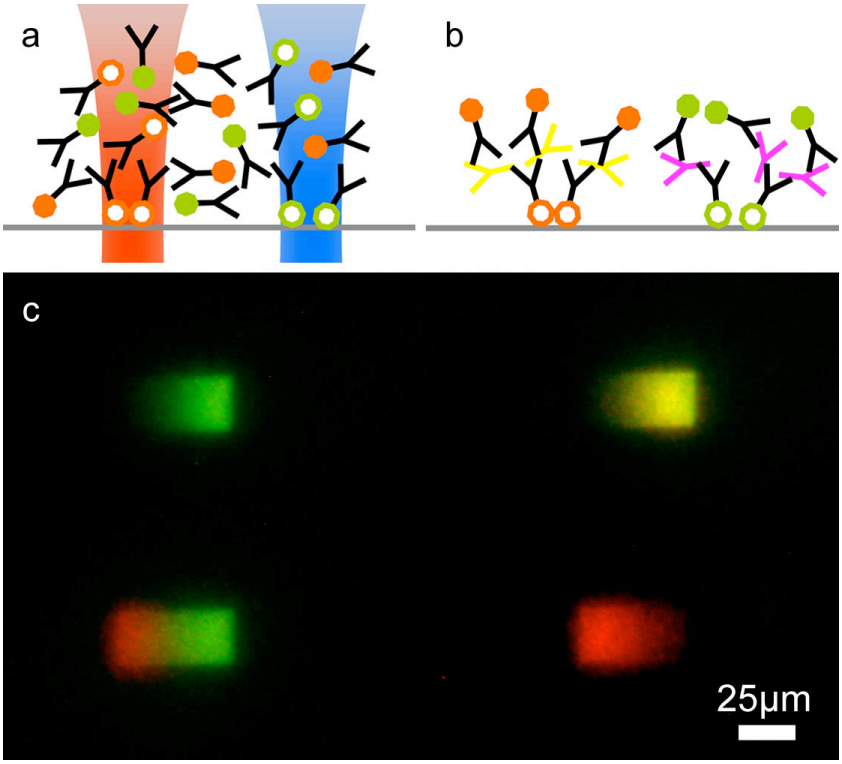


Figure 3.4: Two-component patterns by photobleaching FITC and Cy5 conjugated antibodies simultaneously illuminated by 473nm and 671nm lasers. (a and b) Schematic representations of antibody patterns fabricated using two lasers. The blue (473nm) and red (671nm) lasers in the scheme are not superposed for better clarity. The red laser photobleaches Cy5 goat anti-mouse IgG to adsorb them onto the surface, which later binds to mouse anti-myc (9E10) shown in yellow and finally Cy5 goat anti-mouse IgG is again used to reveal the pattern. The blue laser photobleaches FITC goat anti-rabbit IgG, which binds to rabbit anti-laminin (in pink) and FITC goat anti-rabbit IgG finally reveals the pattern. (c) For this image, FITC is shown in green and Cy5 is shown in red. Bottom-left pattern was obtained by scanning 50 lines by increasing the laser intensity from left to right for the blue laser and by decreasing the intensity for the red laser. The top-right pattern was produced by increasing the both lasers in the same direction given precisely superposed red and green gradients, therefore appearing yellow. The top-left gradient was obtained using only the blue laser and the bottom-right one with the red laser alone.

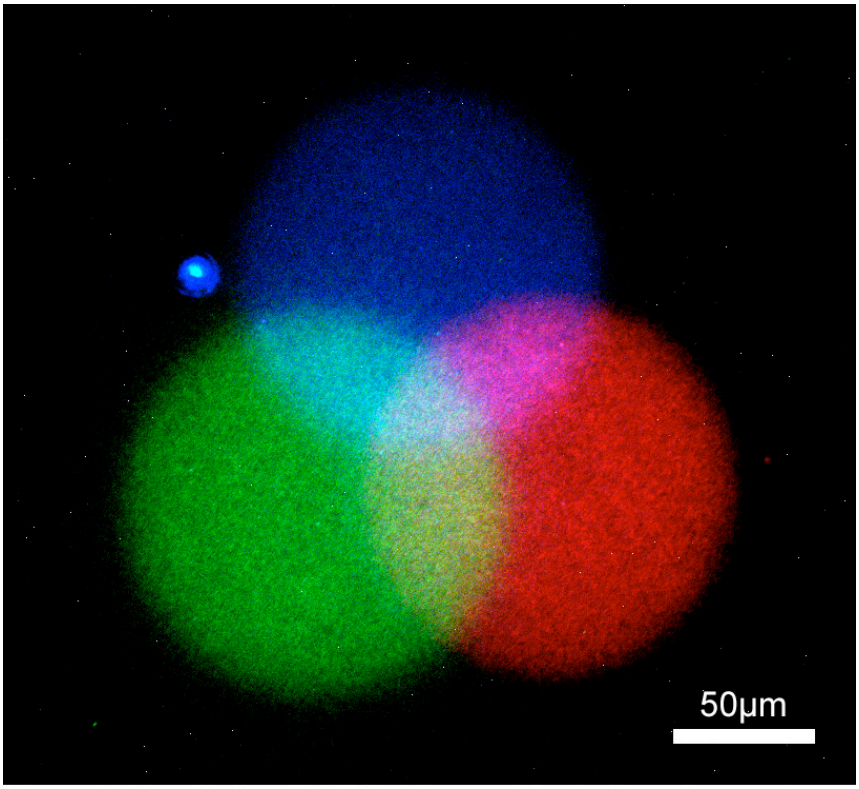


Figure 3.5: Three-component protein pattern. Using widefield illumination LAPAP, an image of a circle was positioned at top-center of the spatial filter while illuminating the sample containing a drop of B4F to adsorb it to the glass surface. The sample was then rinsed and a drop of FITC goat anti-rabbit IgG was placed on the sample to be illuminated by a bottom-right positioned circle. The sample was again rinsed and a drop of FITC goat anti-mouse IgG was illuminated by a circle positioned at the bottom left of the image. The sample was rinsed and then incubated with a solution containing streptavidin, mouse anti-myc (9E10) and rabbit anti-thy1. To reveal the pattern, the sample was incubated with B4F (blue cicle), TRITC goat anti-mouse IgG (green circle) and Cy5 goat anti-rabbit IgG (red circle).

# 4 Third article

This chapter presents a manuscript the will be submitted to *Plos One* and demonstrate how laminin patterns by LAPAP can be used for high-content analysis of neurite guidance. We first show how to produce large-scale gradients taking less then a minute per pattern to fabricate, which allows to culture RGC-5s on thousands of laminin gradients. The cells were then imaged on the gradients during differentiation by staurosporine to visualize the changes induced by the laminin. Since several thousands images were taken, an algorithm that does automatic detection and morphological analysis of cells from bright field images was developed to allow to assess axonal guidance in a quantitative manner.

I performed all the experiments presented in this article as well as developing the automated analysis algorithm. I prepared all the figures and wrote a first version of the manuscript that was then revised by Santiago Costantino and Leonard Levin.

# 4.1 High-content neurite guidance assay using optically patterned substrates

Jonathan M. Bélisle[1,2], Leonard A. Levin[1,3] and Santiago Costantino[1,2,3]

1. Maisonneuve-Rosemont Hospital, University of Montreal, QC, Canada

2. Institute of Biomedical Engineering, University of Montreal, QC, Canada

3. Department of Ophthalmology, University of Montreal, QC, Canada

## 4.1.1 Abstract

The study of axonal guidance *in vitro* relies on the ability to reproduce the distribution of attractive and repulsive guidance molecules normally expressed *in vivo.* The identification of subtle variations in the axonal response to different conditions can be achieved by monitoring the behavior of cells on protein gradients. To do this, automated high-content screening assays are used to quantify the morphological changes resulting from growth on gradients of guidance molecules. Here, we present the use of laser-assisted protein adsorption by photobleaching (LAPAP) to allow the fabrication of large-scale substrate-bound laminin-1 gradients to study neurite extension. We produced thousands of gradients

of different slopes and analyzed the variations in neurite guidance of neuron-like cells (RGC-5). An image analysis algorithm processed bright field microscopy images, detecting each cell and quantifying the soma centroid and the initiation, terminal and turning angles of the maximal neurite.

### 4.1.2 Introduction

During embryogenesis, neurons extend their axons over long distances in order to form the complex circuitry of the central nervous system. At the tip of the axon, a specialized dynamic structure called the growth cone senses the distribution of specific proteins and in response, modifies its shape to guide such extension [4, 74, 272]. This reshaping process is based on the response to several molecules that act as guidance cues. These trigger specific signaling pathways to locally reorganize microtubules and actin filaments that appropriately steer the growth cone. Several *in vitro* methods have been developed to mimic the spatial distributions of proteins that are found in vivo [149, 150, 231] for studying the growth cone. Micropipette puffed generated gradients [115, 121] have been extensively used and help to better understand the molecular mechanisms of axonal guidance. However, this technique allows study of only one axon at a time, and usually 10-50 cells per condition in total are analyzed [66, 120, 121, 178, 180]. Even with methods that allow study of multiple cells in parallel, such as microfluidic generated gradients [110, 283], the number of neurons analyzed per condition is often relatively low, making it difficult to identify subtle

variations in axonal guidance. Studying a few neurons per condition is helpful when axons turn *en masse* in response to a molecular gradient, but when only a fraction of the cell population responds, thousands of neurons may be necessary to understand the biological basis [284].

To overcome the limitation on the number of cells analyzed, high-content screening assays have recently been developed to obtain information about large populations of neurons. High-content analysis combines automated or semi-automated microscopy that obtain a large number of images with detailed image analysis to collect quantitative and standardized information about cell responses, e.g. morphology and protein expression [285]. High-content analysis has already been applied successfully in drug discovery [286, 287], RNAi screening [288, 289], and most recently to the study of neurite outgrowth [290-292]. Automated analysis of images using morphology filters allows extraction of particular features for multiple neurons. These include information about their somas, axons, and dendrites, as well as outgrowth and branching information for thousands of cells, permitting quantitative comparison of morphologies in different conditions.

The ability to fabricate several identical protein patterns is a prerequisite for performing high-content analysis of axonal guidance. To achieve this, we recently developed a technique for fabricating substrate-bound protein patterns, which allows the production of hundreds of patterns in parallel. Laser-assisted protein adsorption by photobleaching (LAPAP) [282, 293] uses a laser to photobleach fluorophores conjugated to various molecules as the basis for producing protein patterns, where the intensity of the

laser modulates the final concentration of protein bound. Typically, biotin-4-fluorescein is used as the first binding molecule, followed sequentially by binding of streptavidin, biotinylated antibodies, and the protein of interest. Originally, LAPAP was able to produce protein distributions with micrometer accuracy using a high numerical aperture objective lens, at the cost of relatively slow fabrication. For fabricating gradients more rapidly, a simple lens can be used to produce low-resolution protein patterns at approximately a minute per pattern.

The effects of laminin in neurite extension and guidance are actively being studied. Recently it has been shown that laminin triggers a new signaling pathway for neuritogenesis [294]. Furthermore, the attraction of Xenopus retinal ganglion cells to the guidance molecule netrin is turned into repulsion by the presence of laminin-1 [75], and guidance assays with substrate-bound laminin gradients also showed attraction of rat hippocampal neurons [110] and Xenopus spinal neurons [113]. However, neurite outgrowth of retinal ganglion cells on gradients of laminin has not previously been studied. Here we present the use of large-scale low-resolution LAPAP to produce 1350 gradients for high-content screening of a neuronal cell line (RGC-5). RGC-5 cells were derived from developing rodent retina; they differentiate and exhibit neuronal morphology when treated with low concentrations of staurosporine [295]. RGC-5 cells were sequentially imaged over a 4h period before and after differentiation with staurosporine. A total of 6852 bright-field images of neurons on laminin-1 gradients and control patterns were taken in a semi-automated manner and analyzed using a fully automated image processing algorithm.

Quantitative measures of cell morphology were obtained, e.g. position of the soma centroid, most distal neurite point, longest neurite length, and neurite initiation, terminal, and turning angles.

## 4.1.3 Materials and methods

### 4.1.3.1 Laser protein patterning

The laser protein patterning method has previously been described in detail [282]. Briefly, the LAPAP setup (Fig. 1a) consists of a 473 nm diode-pumped solid-state laser (Laserglow, ON, Canada) focused by a 100 mm plano-convex lens. The sample is moved with respect to the laser focal spot by a 3-axis translation stage (Thorlabs, NJ), with the laser power and translation stage positions controlled by a custom-written Labview program (National Instrument, TX).

A glass bottom dish (MatTek Corp., MA) was incubated with 3% bovine serum albumin (BSA) in PBS for 30 minutes at room temperature, followed by biotin-4-fluorescein (50μg/ml in 3% BSA). The laser scanned the sample at a speed of 150 μm/s, resulting in binding of the biotin-4-fluorescein to the glass. Fifteen equally spaced lines 400 μm long by 40 μm were patterned as the laser power was increased from 0.02 mW to 4 mW. This pattern size corresponds to the field of view obtained on the CCD when imaging with a 20x objective, and is therefore optimal for later imaging of the

cells extending their neurites on the gradient. To produce gradients of laminin-1, we subsequently incubated streptavidin-Cy5 (Jackson ImmunoResearch, PA), biotinylated goat anti-rabbit Fc-specific IgG (Jackson ImmunoResearch, PA), rabbit anti-laminin IgG (Sigma, MO), and laminin-1 from murine sarcoma basement membrane (Sigma, MO), each at 5 μg/ml in 3% BSA for 30 minutes at room temperature. The use of Fc-specific goat anti-rabbit IgG is necessary to bind the rabbit anti-laminin by its Fc region in order for the next antibody to have an orientation that facilitates laminin-1 binding. Between each incubation step the patterns were rinsed 4-5 times with phosphate buffered saline (PBS). To confirm the presence of laminin-1, we fabricated patterns where streptavidin-Cy5 was replaced by streptavidin-DyLight549 and added two supplementary incubation steps, chicken anti-laminin (5 μg/ml in 3% BSA) and Cy5 goat anti-chicken (5 μg/ml in 3% BSA), after laminin-1 incubation. Fig. 1b shows the fluorescence from Cy5 goat anti-chicken of this particular pattern and the red rectangle shows the region that is considered for neurite guidance. Fig. 1c shows the mean profile of 25 gradients where the first quartile (left) was used as a high-slope gradient and the last three quartiles (right) as a low-slope gradient. On average the change in protein concentration in the high-slope gradients is three times steeper than in low-slope ones. Control gradients were also patterned where all steps were performed up to rabbit anti-laminin incubation, and are depicted as control 1. Fifty

gradients (25 low-slope and 25 high-slope) were patterned per culture dish, totaling 800 laminin-1 gradients and 550 anti-laminin gradients for control 1.

#### 4.1.3.2 Cell culture and differentiation

RGC-5 cells (kind gift of Neeraj Agarwal, PhD) were cultured in Dulbecco's modified Eagle medium (DMEM) supplemented with 10% fetal bovine serum, 100 U/mL penicillin, and 100 μg/mL streptomycin. Cells were plated on glass-bottom dishes containing laminin-1 patterns, anti-laminin patterns (control 1) or no patterns (control 2) at a density of 1000 cells/$cm^2$ and incubated overnight at 37°C in 5% $CO_2$. RGC-5 cells were then differentiated the next morning by replacing culture media with staurosporine (316 nM).

#### 4.1.3.3 Microscopy

Fluorescence images of gradients and bright field images of cells were acquired with an inverted microscope (IX71 Olympus, Japan) equipped with a Retiga 2000R CCD camera (QImaging, Canada). The gain, exposure time and the other parameters of the CCD were identical for all image acquisitions. For samples with gradients, the culture dishes were first positioned manually by observing the fluorescence of streptavidin-Cy5 to image the protein patterns. The sample was rotated so that we positioned the high-slope gradient increasing horizontally from left to right and the low-slope

gradient from right to left. Then, patterns were imaged in fluorescence mode and the RGC-5 cells in bright field mode using a 20x 0.75NA objective. Each image contained both the low-slope and high-slope gradients, and was split in two for analysis. Images corresponding to high-slope gradients with cells on them were horizontally flipped to always have gradients with increasing concentration from right to left. For control samples with no gradients, semi-automated (fine focus adjustment was controlled manually) bright field microscopy was performed using a motorized translation stage (Thorlabs, NJ) controlled by a custom program written in Labview (National Instrument, TX). During each imaging session, cells were at room temperature and exposed to room air for less than 10 minutes, and were then placed back in the incubator at 37°C in 5% $CO_2$.

#### 4.1.3.4 Automated image analysis

This section describes an algorithm that combines basic image processing operations that are explained in detail elsewhere [296]. Image analysis was performed using an algorithm written in MATLAB™ (Mathworks, MA) and made use of built-in functions of the Image Processing Toolbox™ similar to what has been presented previously [297, 298]. All parameters that were manually set by the user for the image analysis were kept constant for all samples. The MATLAB code is available upon request.

Bright field images were first normalized, and then a Sobel filter was performed to find the edges of the cells. From the resulting binary image, isolated pixels were removed. The image was then dilated by 3 pixels in order to avoid breaks in neurites, and holes were filled to obtain masks for all objects in the image. Only objects with masks sized 685-4107 $\mu m^2$ (5000-30000 pixels) were considered neurons, with smaller objects removed.

Using these masks of individual neurons, a morphological opening was performed using a disk of 11.1 μm (30 pixels) diameter as a structuring element in order to create a mask of the soma. Objects with soma masks smaller than 274 $\mu m^2$ (2000 pixels) or larger than 1369 $\mu m^2$ (10000 pixels) were discarded. Neuron masks where no soma or more than one was detected were also removed from the analysis. For those containing only one soma, the centroid of the soma was detected using the function *regionprops* (*'centroid'*).

To find the skeleton of a neuron, a thinning of the neuron mask was performed using the function *bwmorph* ('thin') until minimally connected lines were obtained. The locations of the skeleton end-points and intersection-points were then obtained using the algorithms *find_skel_ends* and *find_skel_intersection* available in MATLAB Central (http://www.mathworks.com/matlabcentral/).

The most distal skeleton end-point from the soma's centroid was determined and further analysis was performed on the skeleton branch associated with that end-point. To find the initiation angle, the position where that single branch intersected the soma mask was determined (Fig. 2e, arrow i) as the initiating location of the neurite. The position on

the skeleton branch 16.7 μm (45 pixels) away from the initiating point was then found (Fig. 2e, arrow ii) and a straight line between those two positions was traced to determine the initiation angle. A 0° angle corresponds to a neurite initiating extension in the direction of decreasing slope (left to right) of the gradient and a ±180° angle to a neurite extending in the direction of increasing slope (right to left). Positive values were assigned to neurites initiating upwards and a negative value to neurites initiating downwards (Fig. 2a). The angle of neurite termination was determined from the segment between the most distal end-point from the soma centroid (Fig. 2e, big green disk) and the point 16.7 μm (45 pixels) away on the same skeleton branch (Fig. 2e, arrow iii). Branches smaller than 45 pixels in length were not analyzed.

### 4.1.4 Results and discussion

The morphological parameters obtained by automated analysis allowed us to observe the impact of laminin-1 gradients on neurite outgrowth. Subtle influences of the gradient could be measured and the collection of several parameters allowed us to better assess a variety of effects on neurite outgrowth.

Fig. 3 shows histograms of the location of the most distal end-point of the longest neurite compared to the position of the centroid of the soma. Guided neurites (black, +) are those extending in the direction of the gradient as described by the inset in Fig. 2a. Non-guided neurites (white, -) extend in the opposite direction and neutral neurites (not shown)

are those extending perpendicular to the slope direction. Fig. 3 shows the data corresponding to a total of 4514 cells analyzed (7100 if we include neutral cells).

When cells extended neurites on high-slope gradients (Fig. 3b), we observed statistically significant guidance ($p=0.0006$, $\chi^2$ test) 1 hour after differentiation for the most distal end-point data with 93 cells marked as guided and 52 marked as non-guided. This result raised other questions: Does the laminin-1 gradient increase the length of neurite outgrowth in the positive slope direction? Are neurites more likely to be initiated with an angle corresponding to the direction of the gradient, or is the neurite turning along the gradient during its extension?

The average neurite length, calculated as the distance from initiation point (Fig. 2e, arrow i) to the maximum end-point, for guided, neutral, and non-guided neurites is shown in Fig. 4a for high-slope gradients 1 hour after differentiation. No statistically significant difference could be observed for this parameter. We then compared the initiation angle (Fig. 4b) of the longest neurite and saw an influence of the laminin-1 gradient that was statistically significant ($p=0.005$, $\chi^2$ test) with 55 cells considered guided and 29 non-guided. Fig. 4c shows the turning angle (towards the gradient), defined as the difference between the absolute value of the terminal angle and initiation angles. A positive turning angle means that a neurite turned toward the increasing slope of the gradient. The histogram in Fig. 4c considers a turning angle greater then 5° as being guided (black, +), one between -5° and 5° as neutral (not shown) and one smaller than -5° as being non-

guided (white, -). Again, no statistically significant turning could be observed, therefore establishing that only the initiation of the neurite is influenced by the substrate bound gradient. The complete data obtained for all time points is presented in Supplementary Figures 1-6.

As shown in Fig. 3a, low-slope laminin gradients influence neurite outgrowth and is statistically significant 3 hours after differentiation guidance with 187 guided cells and 150 non-guided ($p=0.044$, $\chi^2$ test). Initiation, terminal, and turning angles data were not significantly influenced (see Supp. Fig. 1a-3a) by low-slope laminin gradients. In addition, the distribution of cell somas along the gradient was not significantly affected by high or low concentrations of laminin (see Supp. Fig 4), nor was neurite branching (see Supp. Fig. 5a).

The angular range for determining guidance was arbitrarily set at 120° for each possibility (see Fig. 2a): a 120° angle in the direction of the increasing slope (left) of the gradient was defined as guided, a 120° angle in the opposite direction (right) was defined as non-guided and the two 60° angles perpendicular (up and down) to the gradient was defined as neutral. In Fig. 5, we analyzed a data set (high-slope gradients 3 hours after differentiation) that did not show significant guidance (see Fig. 3b). The ranges of the angle were varied from 60° to 180° to show how the angular range influenced the ratio of guided to non-guided neurites (Fig. 5). By restricting the angular range, we observed statistically significant guidance for restriction angles of

60° and 90° (Fig. 5a). This result emphasizes the importance of establishing standards for user-defined parameters for high-content analysis of axonal guidance.

### 4.1.5 Conclusion

We used protein patterns produced by LAPAP for high-content screens to study neurite guidance. The novel image analysis tools developed for this study made possible automated neurite tracing from bright field images on substrate bound gradients. Previous studies of automated quantification of neurite outgrowth used fluorescence microscopy images because they allowed simpler neurite detection, necessitating use of stained cells or live cells expressing genetically encoded fluorescent probes [291, 297]. The morphological parameters obtained from the automated analysis allowed a quantitative understanding of the preferential neurite outgrowth of RGC-5 on laminin-1 gradients.

We showed that preferential neurite guidance could be observed by considering the position of the most distal end-point of the longest neurite relative to the soma on low and high-slopes laminin-1 gradients. On average, the longest neurites of cells had similar lengths, independently of their orientation with respect to the protein gradient. For high-slope laminin gradients, we also demonstrated that the guidance observed was mainly due to the initiation angle of neurites, which was preferentially in the direction of the increasing concentration of the gradient, and not turning of the longest neurite as it extended on the gradient. These finding are consistent with fact that neuritogenesis can occur through a

different signaling pathway in the presence of laminin [294], therefore having neurites more likely to initiate where laminin is of higher concentration.

The work presented here is a proof of concept for the application of high-content analysis to study axonal guidance on substrate-bound protein patterns. The use of LAPAP to produce multiple protein distributions and automated image analysis of the observed cells allows observation of large numbers of cells to tease out weak guidance cues, and is a first step towards a totally automated platform combining LAPAP, cell culture and microscopy for the screening of substrate-bound guidance cues in different types of neurons.

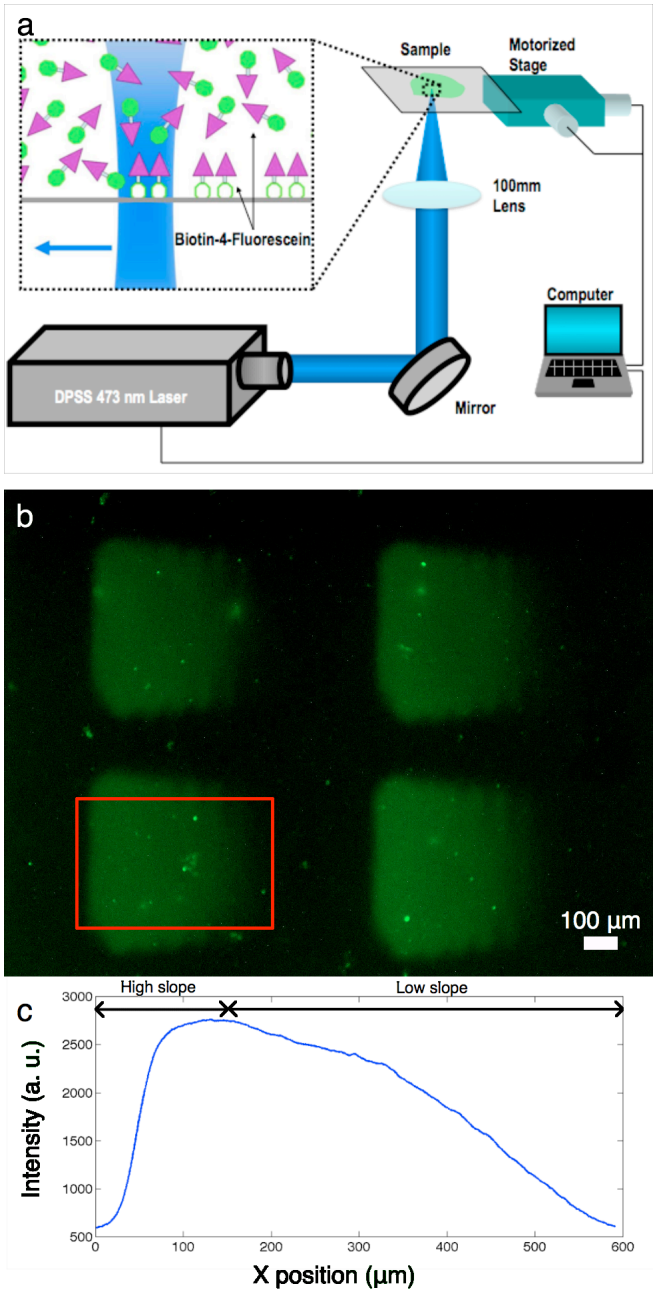


Figure 4.1: Patterns of laminin-1 were produced using LAPAP. (a) The platform consists of a 473 nm diode-pumped solid-state laser, a lens and a 3-axis motorized stage to produce the desired patterns of biotin-4-fluorescein. (b) Large gradients (400 µm x 600 µm) of laminin-1 were fabricated by sequentially incubating

streptavidin-DyLight549, biotinylated goat anti-rabbit IgG (Fc specific), rabbit anti-laminin-1 and laminin-1. This particular pattern was imaged using chicken anti-laminin-1 and Cy5 goat anti-chicken IgG to reveal the presence of laminin-1. The red rectangle delimits the section of the patterns considered for the RGC-5 guidance assay. It has to be noted that these gradients are made with a 100mm lens and have a lower resolution than those made with a 60x 1.2 NA objective lens in Chapter 2. (c) x-direction mean profile of 25 gradients. The first quartile (on the left) of the pattern was used as a high-slope gradient while the last three quartiles (on the right) were used as a low-slope gradient.

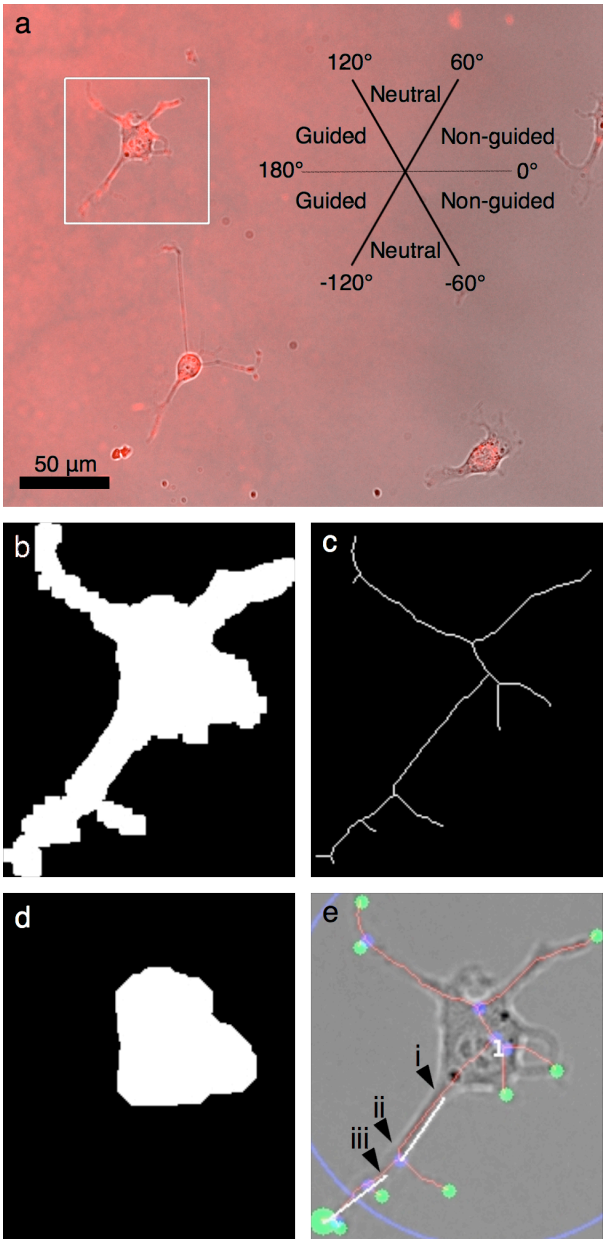


Figure 4.2: RGC-5 cells on a low-slope laminin-1 gradient where a streptavidin-Cy5 gradient was imaged by fluorescence microscopy with cells in bright field mode using a 20X 0.75 NA objective. (a) The properties of the longest neurite of each cell were classified as guided, neutral or non-guided. (b-e) In order to study

thousands of cells, classify them in an objective manner and collect information about each cell, an automated analysis algorithm was written in MATLAB™. Key steps of the algorithm are depicted here for the cell denoted by the white square in panel (a). (b) First, a Sobel filter, dilation, elimination of small objects and filling of remaining object was used to define a mask for each cell. (c) A skeleton was computed by performing a thinning of the mask corresponding to each cell until minimally connected lines were obtained. (d) A morphological opening of the mask was then performed to find the region corresponding to the soma and then its centroid (marked by the upper left position of the number in panel e). (e) The position of all end-points (green) and intersection-points (blue) of the skeleton were determined. The position of the most distal end-point (large green disk) relative to the soma's centroid and the length of the corresponding skeleton branch were computed, as well as the initiation angle and the terminal angle.

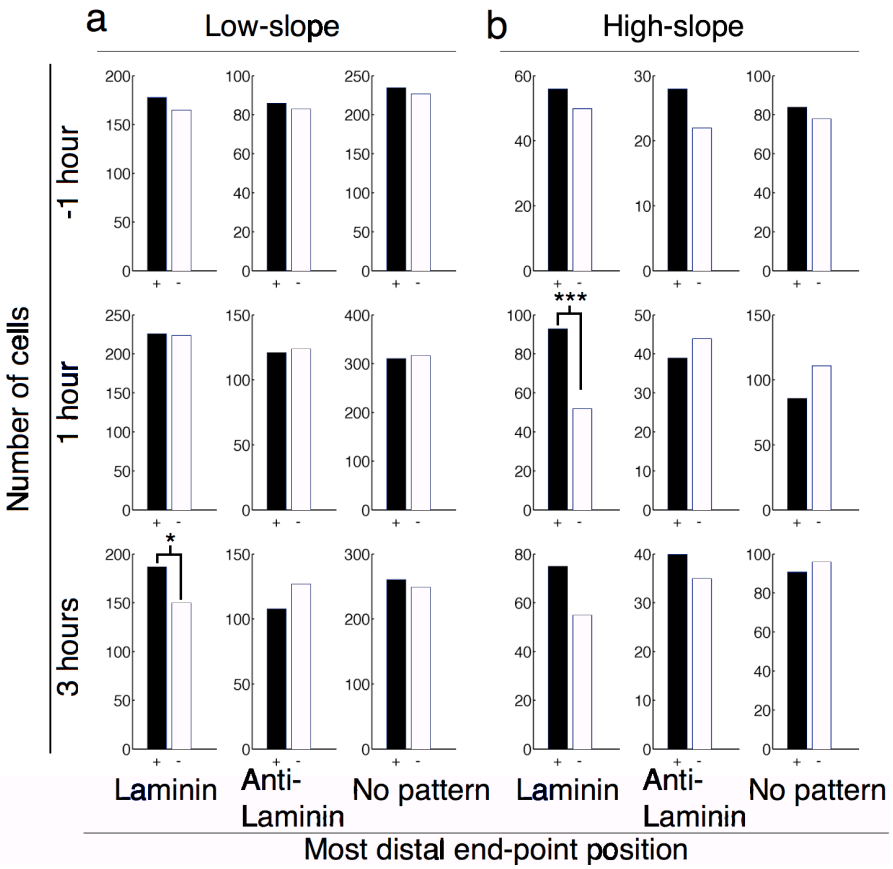


Figure 4.3: Histograms of most distal end-point relative to soma centroid position for all cell images in both low-slope and high-slope gradients at time points before and during differentiation with staurosporine. Guided (black, +) and non-guided (white, -) neurites were determined as described in Figure 2a. Low-slope gradients resulted in statistically significant guidance for laminin-1 three hours after differentiation ($p=0.044$ by $\chi^2$). High-slope gradients resulted in guidance that was statistically significant at 1 hour ($p=0.0006$ by $\chi^2$) after differentiation by staurosporine. $\chi^2$ tests were performed for every histogram and where nothing is mentioned about significance, p-values are above 0.05. Statistical significance is assessed for guided vs. non-guided pairs for each of the patterns type individually (Laminin, Anti-Laminin (control 1) or No pattern (control 2)), not between them.

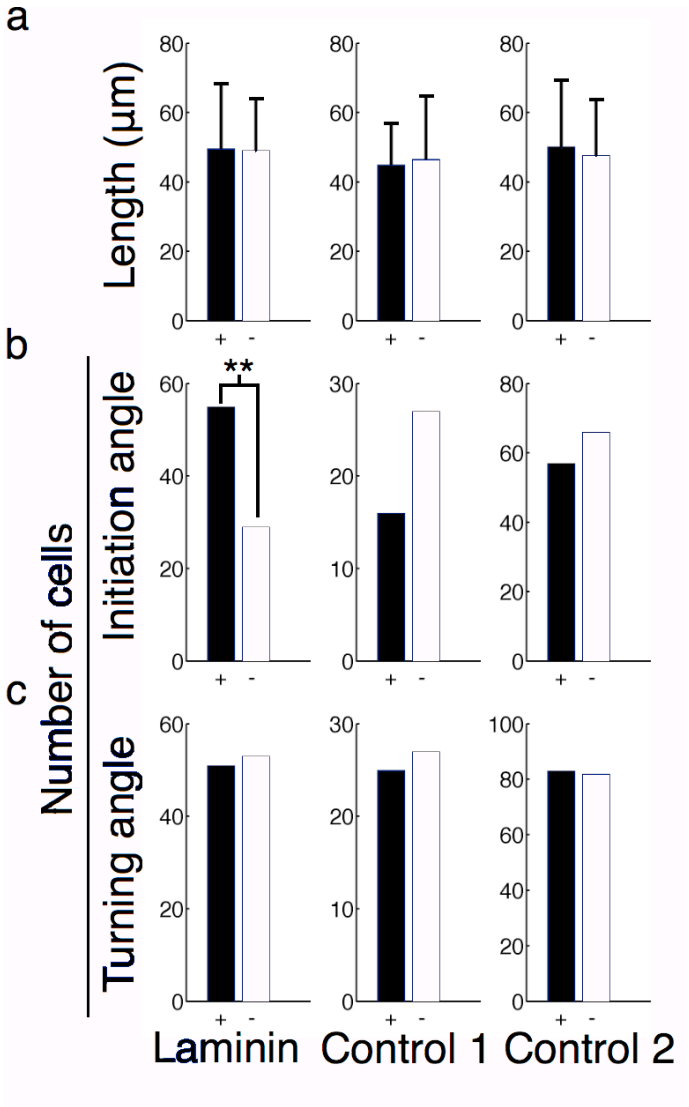


Figure 4.4: Various parameters of cells extending neurites on high-slope gradients 1 hour after differentiation. (a) The length of the neurite associated with the most distant end-point was similar for guided and non-guided cells (p=0.798 by t-test). (b) The histogram of the initiation angles of the neurites indicates that the angle at which they sprouted from the soma was responsible for the guidance (p=0.005 by $\chi^2$). (c) The histogram of the turning angle shows that turning while the neurite was extending was not responsible for guidance.

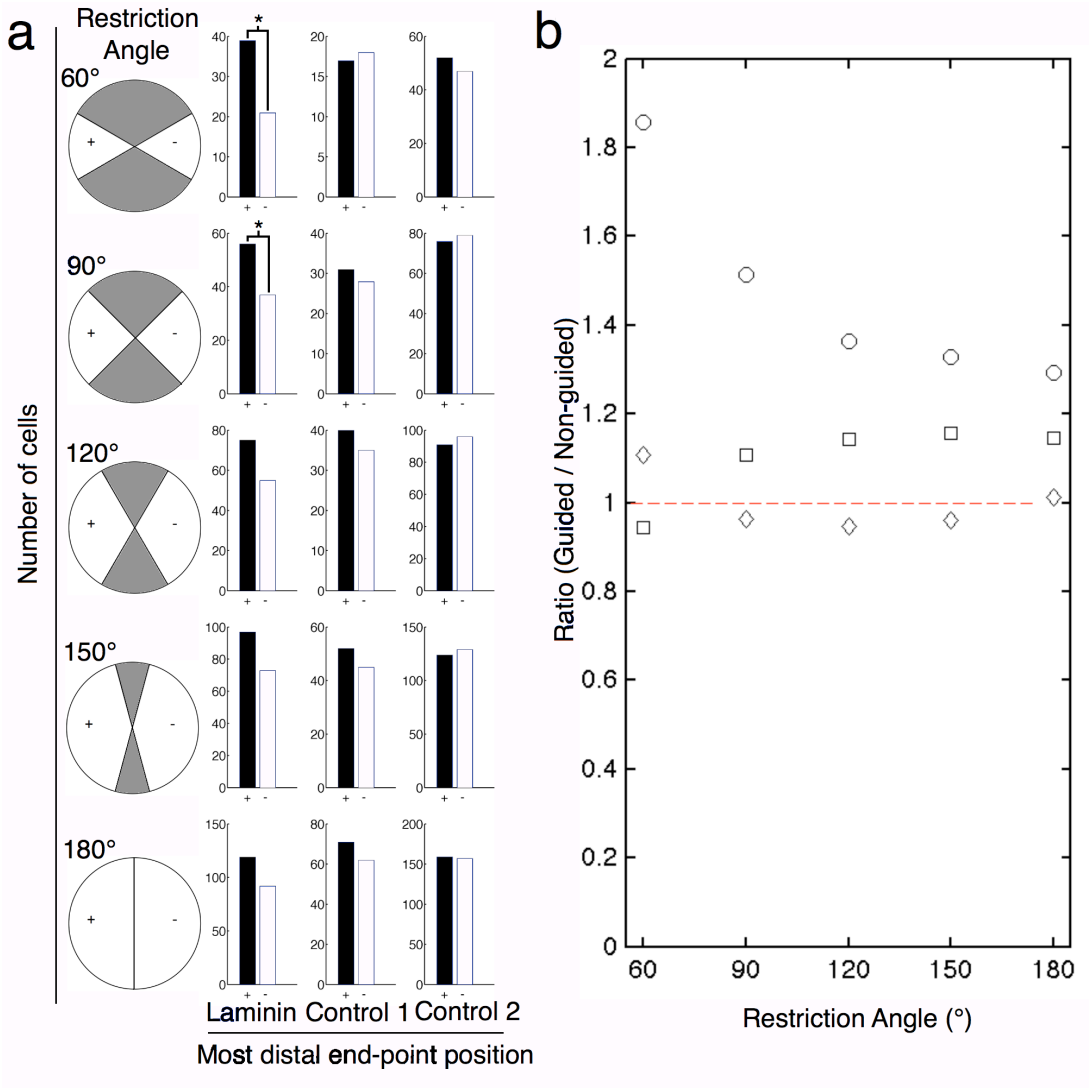


Figure 4.5: Effect of varying the restriction angle used to define whether an extending neurite was guided or unguided by the gradient, using data from high-slope gradients, three hours after differentiation. (a) Histograms of the most distal end-point position for different restriction angle. (b) Ratio of guided over non-guided neurites shows how this arbitrary parameter can greatly influence the outcome of the analysis. (Circles = Laminin, Squares = Control 1, Diamonds = Control 2). This analysis demonstrates that high-content screens of axonal guidance are strongly dependent on choice of critical user-defined parameters.

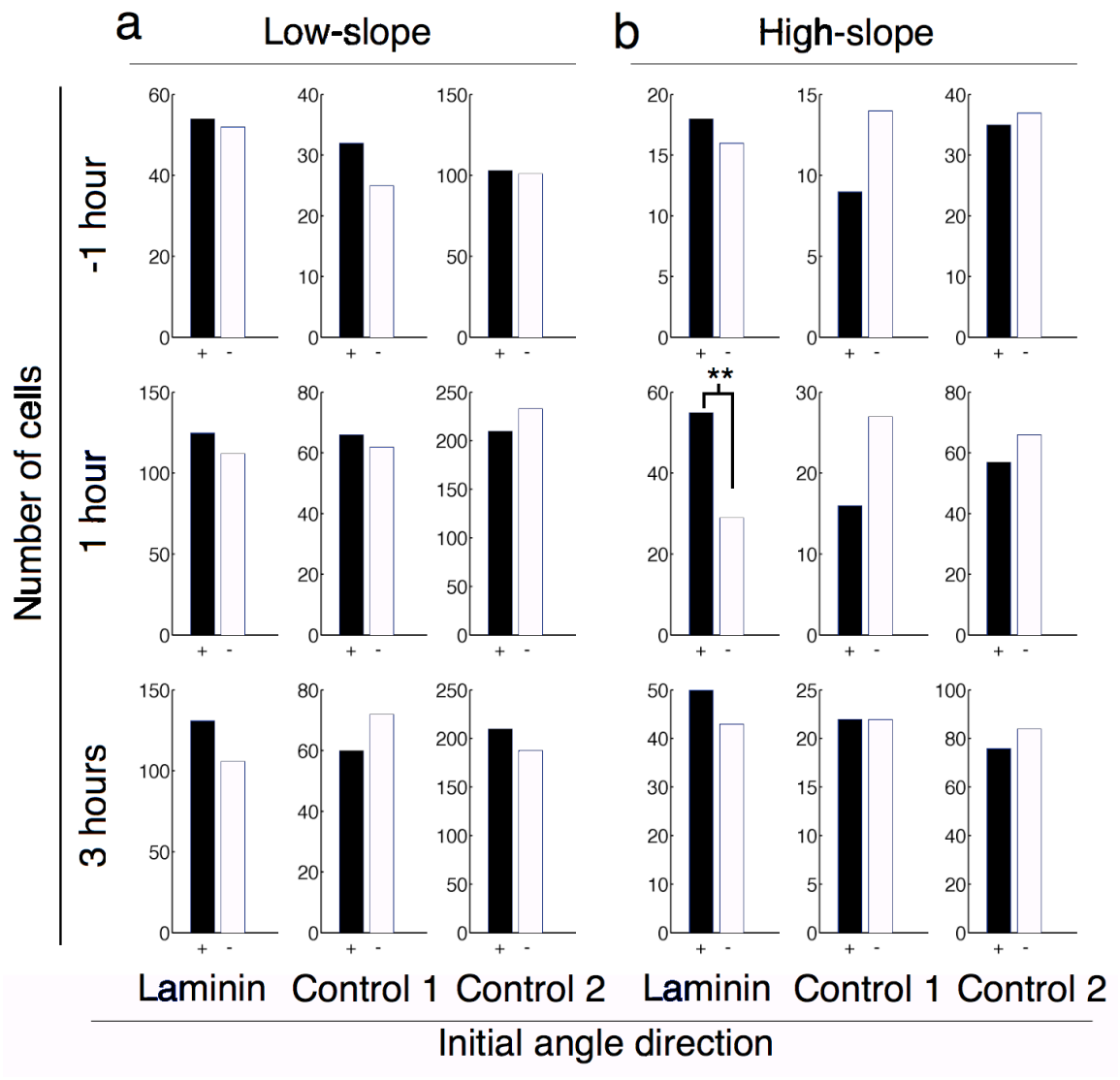


Figure 4.6: Histograms of the initiation angle of cells imaged on low-slope and high-slope gradients at different time points before and during differentiation by staurosporine. Guided (black, +) and non-guided (white, -) neurites were determined as described in Figure 2a.

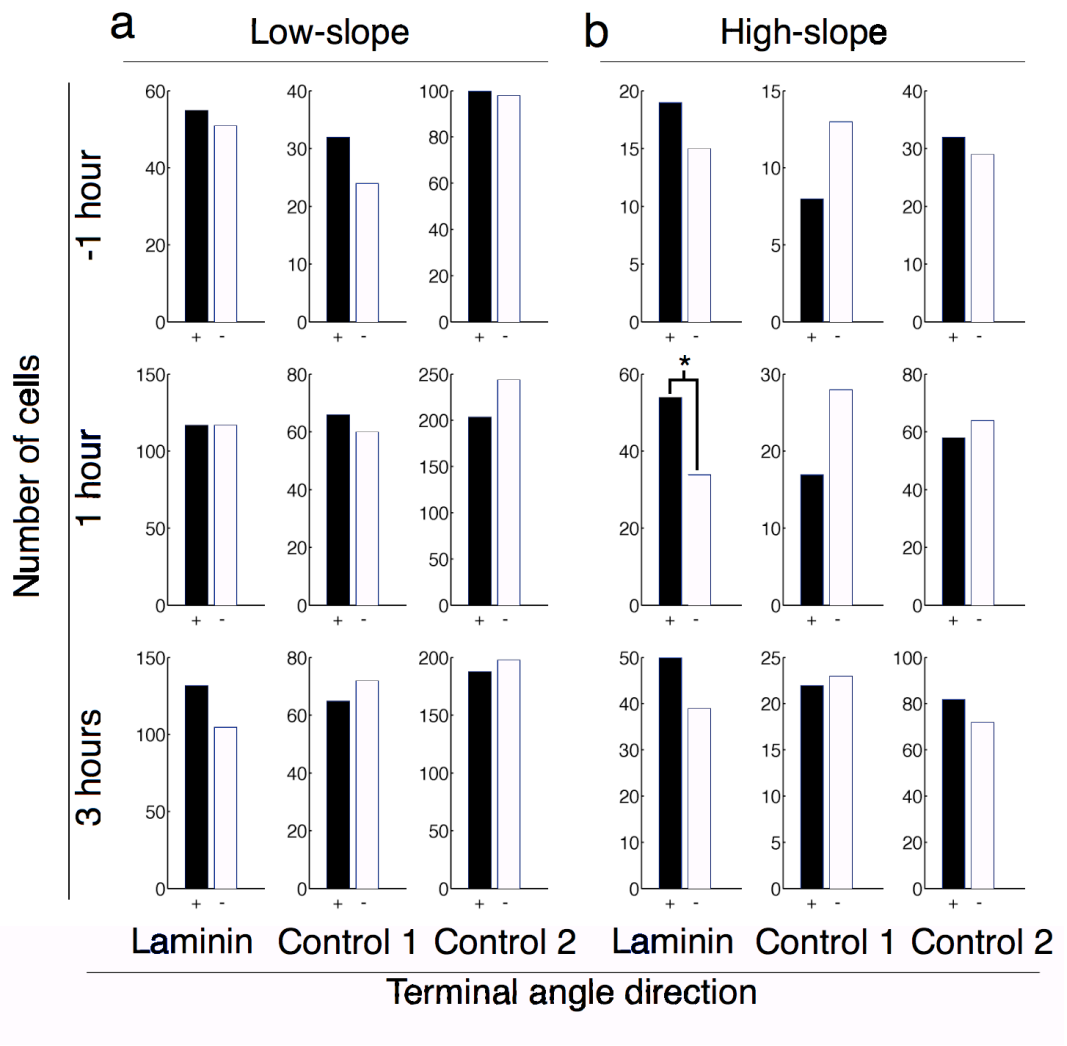


Figure 4.7: Histograms of the terminal angle of cells imaged on low-slope and high-slope gradients at different time points before and during differentiation by staurosporine. Guided (black, +) and non-guided (white, -) neurites were determined as described in Figure 2a.

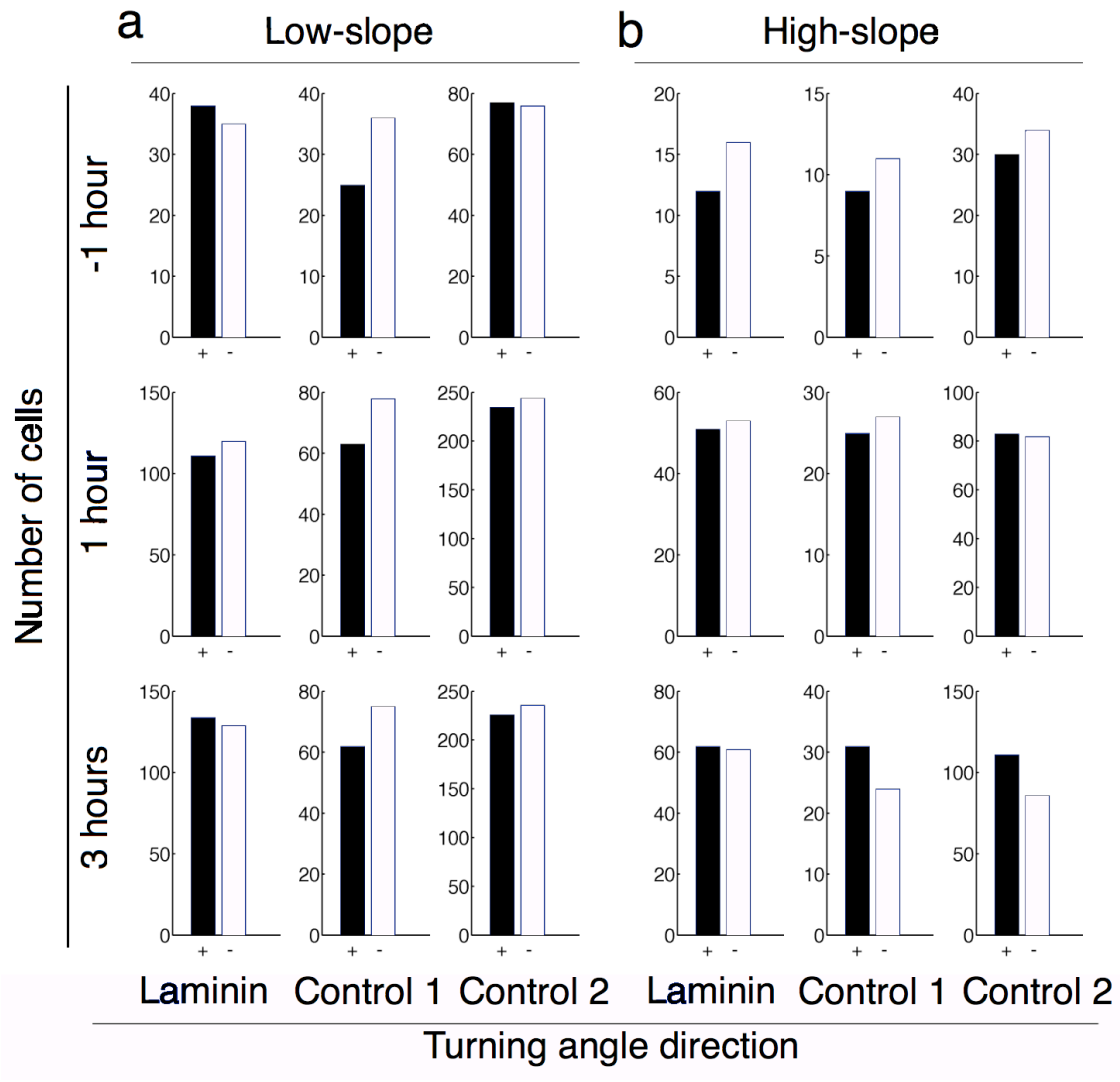


Figure 4.8: Histograms of the turning angle of cells imaged on low-slope and high-slope gradients at different time points before and during differentiation by staurosporine. Guided (black, +) and non-guided (white, -) neurites were determined as described in Figure 2a.

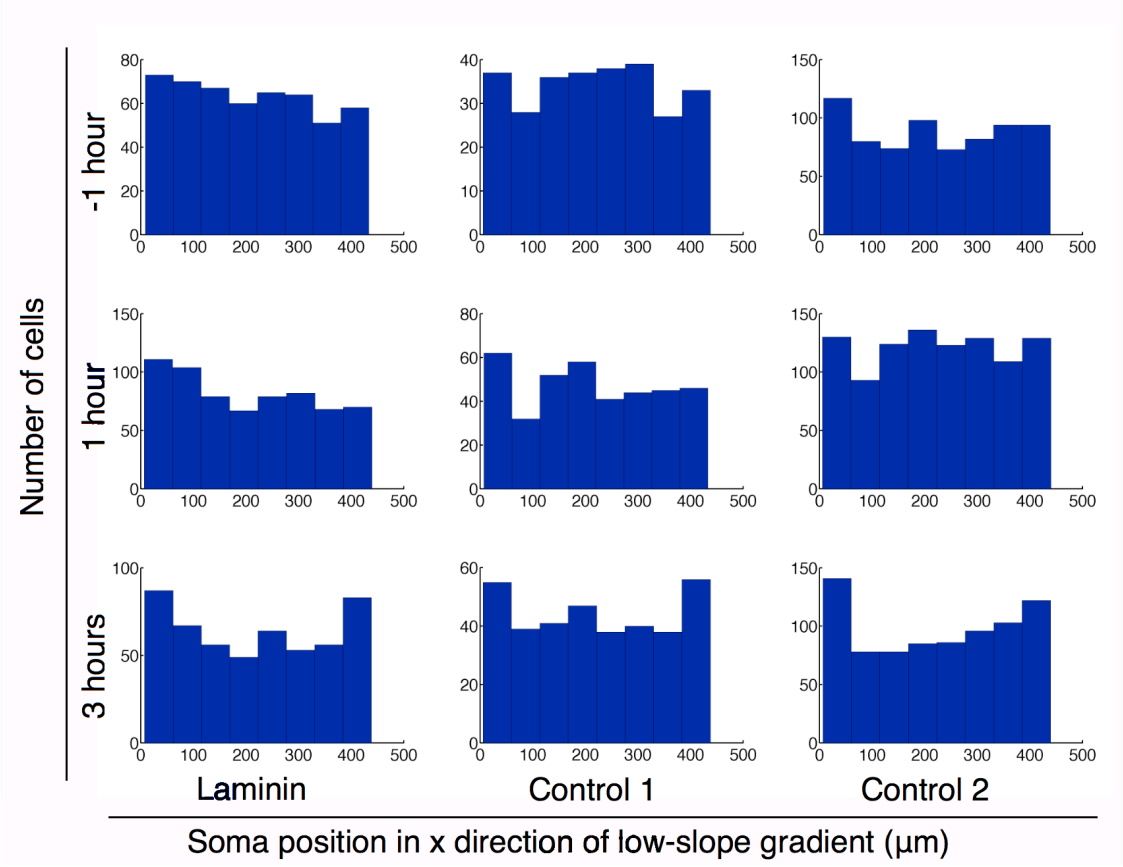


Figure 4.9: Histograms of the x-position of the centroid of the cell soma along the gradient (low-slope gradient). The laminin-1 or anti-laminin (control 1) concentration was highest at 0 µm and lowest at 444 µm.

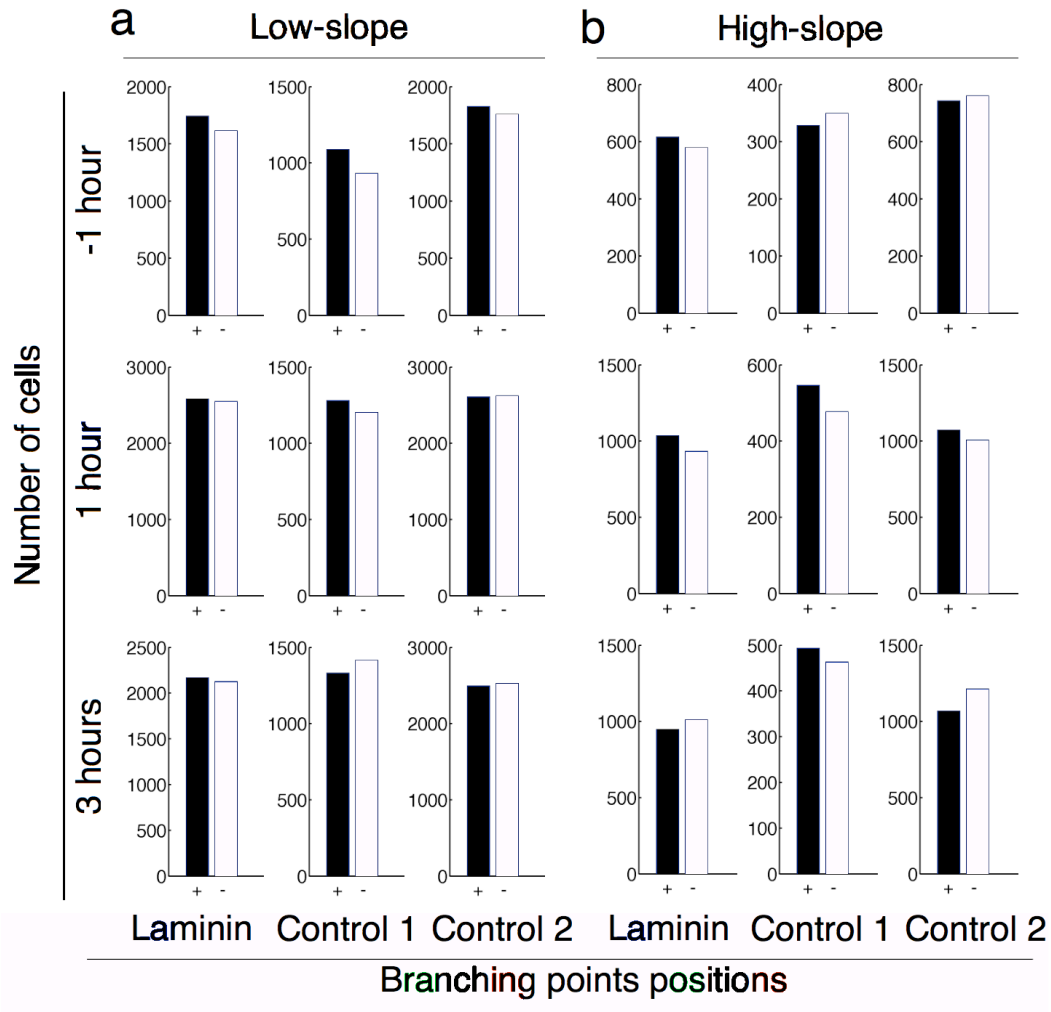


Figure 4.10: Histograms of the branching points of cells imaged on low-slope and high-slope gradients at different time points before and during differentiation by staurosporine. Guided (black, +) and non-guided (white, -) neurites were determined as described in Figure 2a.

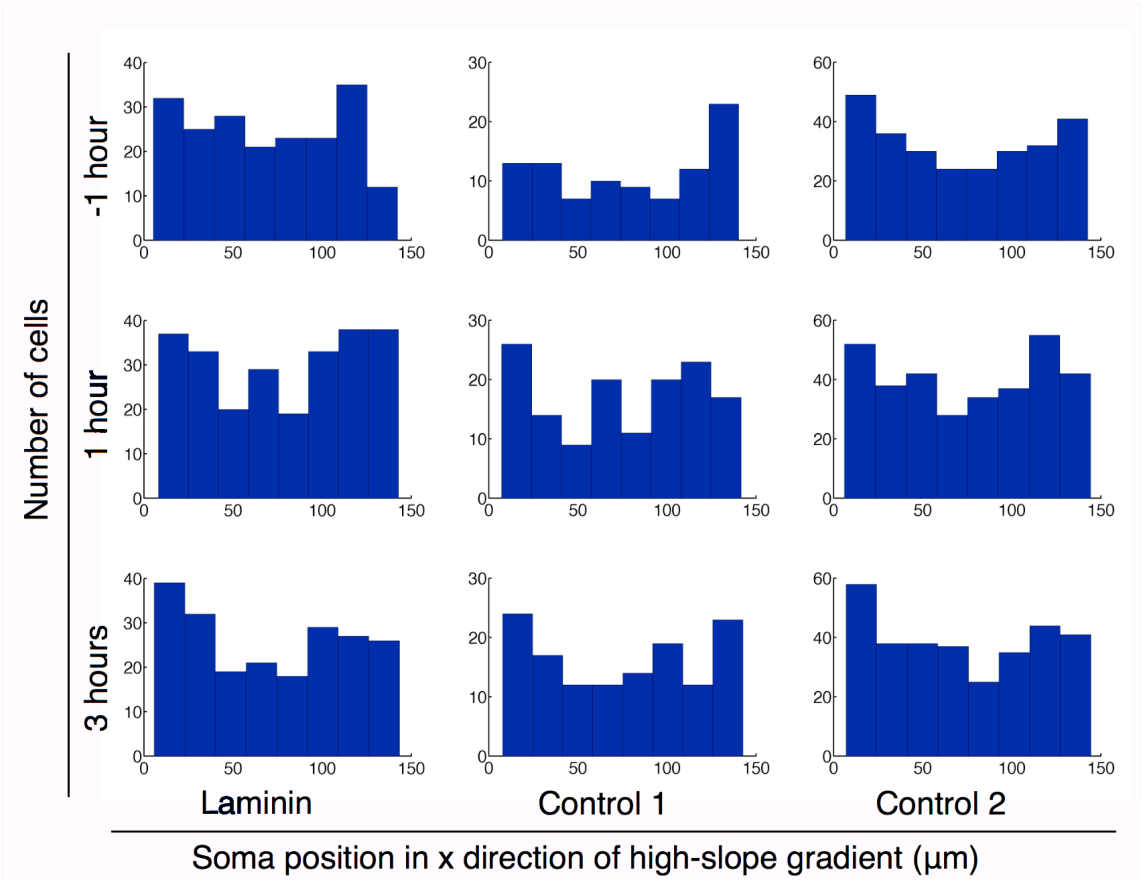


Figure 4.11: Histograms of the x-position of the centroid of the cell soma along the gradients (high-slope gradient). The laminin-1 or anti-laminin (control 1) concentration was highest at 0 µm and lowest at 148 µm.

# 5 Discussion

This thesis shows how protein patterning is important to answer questions about axonal guidance, as well as other chemotaxis phenomenon. It presented a new photonic technique to produce protein patterns with visible light and fluorophores, instead of UV light and specific cross linkers. The objectives of this thesis were to present the technique, characterize it and show its application for high-content analysis. Beyond these completed objectives, a lot of work lies ahead for LAPAP to become a standard technique for studying axonal guidance. We will first discuss the characteristics that make LAPAP a unique technique to produce substrate bound gradients. Then we will address several factors that could be improved to push the adoption of LAPAP on a broader scale.

## 5.1 LAPAP's advantages

One of the main advantages of LAPAP over other substrate-bound patterning methods is its ability to produce micrometer resolution patterns of highly controlled concentration. Microfluidics techniques to produce substrate-bound gradients via adsorption are only able to modulated protein concentration in one direction and only offer a poor resolution [110]. Microcontact printing is able to offer a micrometer resolution, but only two levels of concentration can be achieved [234]. Only UV-based photonic techniques are able to offer patterning possibilities similar as LAPAP. UV laser scanning allowed modulating the amount of bound peptides with micrometer resolution [109], but since the peptide concentration was modulated by the scanning speed, only gradients

changing in one direction were produced. Another group showed the possibility to produce substrate-bound micrometer resolution patterns in any direction with UV light illumination via a graded photomask which consisted of an image printed on a transparency, but a new photomask must be generated for each different pattern [278]. The use of solid state visible lasers makes it much easier to control laser intensity in a quick manner, the micrometer scale reproduction of Vermeer's Girl With a Pearl Earring is a convincing demonstration of flexibility of the method (Fig. 2.1d). As for widefield LAPAP, the use of spatial light modulators (SLM) makes it straightforward to modulate visible light in a patterned manner that can be modified on-demand. Another unique characteristic of LAPAP is its three-orders-of-magnitude dynamic range that allows fabricating gradients that smoothly increase over large range of concentration changes. This great dynamic range is allowed due to very little non-specific binding provided by a BSA coating of the substrate and the dilution of the reagents in high concentration BSA.

Moreover, since the photosensitizers that LAPAP uses are fluorophores, all the reagents can easily be found commercially. Biotins can be found conjugated to several fluorophores and offer a particularly interesting choice as a first binding molecule due to their size and high affinity to streptavidin. In this thesis, we only showed the use of BF4, biotin conjugated to fluorescein, but patterns were also made from two other biotin conjugated dyes (Atto 520-biotin and Atto 655-biotin) with two other laser lines 532nm and 671nm. The use of several molecules (biotin, streptavidin, antibodies) as a scaffold to bind the final protein is particularly interesting, since light cannot photodamage the functional

protein. Antibodies conjugated to various fluorophores can also replace biotin as a first binding molecule offering the possibility to produce patterns of several types of proteins. However, since antibodies are much larger in size compared to biotin (~150 kDa vs ~0.6 kDa), they can't be used at the same molar concentration, therefore limiting the dynamic range. Patterns of two different antibodies were obtained by photobleaching FITC and Cy5 conjugated antibodies with 473nm and 671mn lasers, respectively (Fig. 3.4). However, when adding a third laser line (532nm) and a TRITC conjugated antibody, significant cross-talk was observed with the two other antibodies. This could however be circumvented by the use of different FITC conjugated antibodies with sequential photobleaching steps.

When resolution is not a requirement, LAPAP is also able to produce several large-scale patterns promptly to allow studying guidance in high-content manner. By replacing the high NA objective by a 100 mm plano-convex lens, we were able to produce thousands of gradients with dimensions of about half a millimeter in approximately a minute each . The possibility to produce several gradients in parallel to observe guidance on thousands of cells is another advantage of LAPAP compared to techniques such as micropipette puffs where only one cell can be observed at the time [121]. However, imaging of thousands of cells on gradients creates a very large amount of raw data to analyze, which necessitates the use of automated image analysis. This type of analysis is particularly efficient and removes human bias.

## 5.2 Answering new questions about axon guidance

We have carried out several experiments with netrin-1 and Shh gradients produced by LAPAP (see Annex IV) with commissural neurons from rat embryos, but still we were not able to demonstrate significant axon guidance, preventing us to use the technique to address specific guidance questions. This is however not surprising since most of the work in guidance is being done on isolated neurons from *Xenopus* or chick embryos. To our knowledge, only one group was able to demonstrate *in vitro* guidance of mammalian commissural neurons, this was done by a soluble Shh gradients produced by the Dunn chamber [169]. It would be preferable to try other cell models, such as neurons from *Xenopus* or chick embryos, since they have clearly shown their ability to show guidance *in vitro*. After robust and reproducible guidance is obtained with a cell model by a specific protein gradient made by LAPAP, it could then be used to answer specific questions about the signaling pathways leading to growth cone turning or how gradients shape influence turning.

A specific example of unanswered question about axonal guidance that could be addressed is finding if $Ca^{2+}$/calmodulin protein kinase II (CaMKII) directly interacts with the cytoskeleton during growth cone turning. We know that CaMKII is implicated in the regulation pathway for $Ca^{2+}$ dependent response of growth cone to netrin-1 gradients [124]. On the other end, depending of the $Ca^{2+}$ cytosolic level, CaMKII is able to bind to F-actin [299] or microtubules, suggesting that CaMKII is directly implicated in cytoskeleton

remodeling. LAPAP could be used to systematically induce growth cone turning to verify the presence of interactions between CaMKII, F-actin and microtubules during this process.

LAPAP could also be used to answer quantitative questions no other method is able to do. One of the advantages of LAPAP is its micrometer resolution and total control on the 2D protein patterns produced. Other studies looked at the effect of slope of substrate-bound gradients [110, 234] either for attraction or repulsion, but none of them were able to add controlled noise or discontinuities in gradients to see how it can influence guidance. However, LAPAP is able to produce gradients with discontinuities of controllable size or to add stochastic noise with controllable mean amplitude within the gradient.

## 5.3 LAPAP by a confocal microscope

In chapter 2, it was suggested that the laser power used for photobleaching of fluorescein was so low that a confocal microscope could even be used to make patterns. Even if the possibility to make patterns by small software modifications to a confocal is obvious, this still needs to be shown and made easily available to life science laboratories. Very recently, another group used a Nikon Eclipse Ti to produce line patterns of (poly-D-lysine) PDL using LAPAP to study neurite dynamics on neurons while forcing them in having linear morphologies [300]. Even if this demonstration shows the capability of a confocal microscope to produce line patterns, no intricate patterns have been done. This task would need software modifications that would allow modulating laser power as a function of the scanning position. This could be easily done since acousto-optical tunable

filters (AOTF) or acousto-optical modulators (AOM) are usually used to modulate laser power in confocal microscopes. In order to have confocal microscopes able to produce complex patterns LAPAP, the technique demand would need to be relatively high for manufacturers such as Olympus, Zeiss or Nikon to include patterning in the software options. An open source software named ScanImage is also available to control nearly any type of laser scanning microscope [301], an interesting option would be to contribute to an expansion of the software that would allow for LAPAP protein patterning.

## 5.4 Improvements in widefield LAPAP

Chapter 3 discussed how protein patterns could be fabricated faster compared to standard LAPAP by using widefield-patterned illumination. However, several improvements could be made to improve widefield LAPAP, since most of the light in the present configuration is lost. First, the spatial filter used comprises a twisted-nematic device sandwiched in-between two orthogonal polarizers. In theory, even by using perfect polarizers, this configuration already losses 50% of the light. However, it is the use of a LED that mostly contributes to the greatest loss of light due to poor collimation compared to a laser. A more energy-efficient alternative for widefield illumination would be to modulate the phase of a laser beam at one of Fourier planes of the microscope; this is also called holographic illumination [302, 303]. The Fourier plane of the objective itself (back focal plane) is inaccessible in microscopes to position a phase modulator since it is very close (or even inside) to the objective structure, one must use another lens that will Fourier

transform the phase modulation on the image plane of the microscope, that will later be imaged at the focal plane of the objective (Fig. 5.1). There are two main advantages using this strategy for widefield LAPAP over the one presented in the third chapter. First, the laser being collimated, a very high amount of light will arrive at the focal plane of the objective compared to the use of standard light. Second, there is no light that is intentionally blocked for dark regions of the pattern, the strategy of Fourier transforming phase modulation leads instead to reattribution of light at the focal plane of the objective. However, one of the disadvantages is that it is non-trivial to find the proper phase modulation that will lead to the correct pattern compared to standard widefield LAPAP where the image sent at the amplitude light modulator is the pattern itself. For holographic illumination, one must use an iterative Fourier-transform algorithm to find the proper phase corresponding to the desired pattern [302, 304]. Another disadvantage is that patterns created via holographic illumination tend to contain speckles that could be problematic for some applications [302, 305].

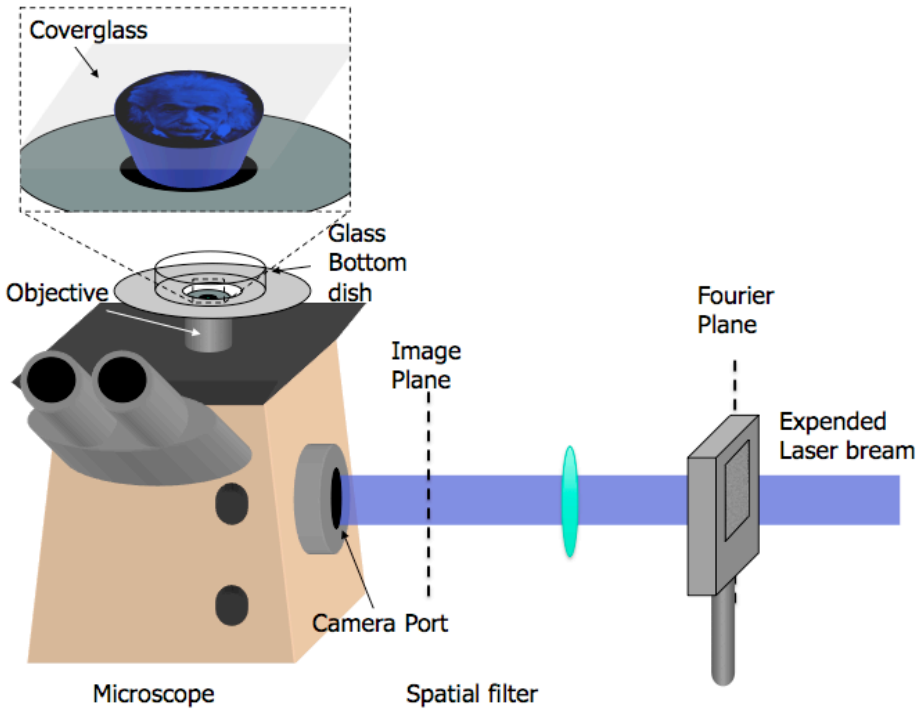


Figure 5.1: Widefield LAPAP using holographic illumination to create desired pattern. The laser is phase-modulated at the Fourier plane (back focal plane) of a lens by a spatial light modulator; this will create the Fourier transform of the phase modulation at the image plane of the microscope. The patterned illumination at the image plane will then be reproduced at a smaller scale at the focal plane of the microscope objective.

## 5.5 Protocols improvements

Several protocols improvement to LAPAP can still be done to make it suitable for a wide rage of applications. One of the main drawbacks of LAPAP is that patterns are made on glass substrates in a multistep procedure before the cells are plated, resulting in the fact that neurons are allowed to grow anywhere on the glass substrate and having axons entering the pattern at any position, or having whole cell already on the pattern at a random position.

A first improvement that could be done is the elaboration of a protocol for patterning that avoids axon growth outside patterns. Another group slightly modified LAPAP by photobleaching high concentration FITC on a glass substrate pre-coated with PEG and then incubating with PDL, which prevented both cell growth and non-desired PDL adsorption on the non-patterned PEG regions [300]. This strategy could be used to fabricate striped patterns of PDL or PLL that would lead to a larger rectangular region where a protein gradient is also fabricated by LAPAP (Fig. 5.2), forcing axonal growth along the stripe to always enter gradients at the same position. One of the disadvantages of this technique would be that on the gradient section, one would have protein concentration growing in one direction, but PEG exposition in the other direction which would repel axons; therefore it would be difficult to outweigh which contributed more to growth cone turning, guidance by the protein or repulsion from PEG. One way to circumvent this problem would be to use only repellant proteins, as axons would have to travel where PEG exposition increases to avoid the repellant. Another way would be to make a constant concentration pre-pattern of BSA over the PEG region where the gradient would lie to avoid repulsion by the PEG in low concentration regions of the gradient.

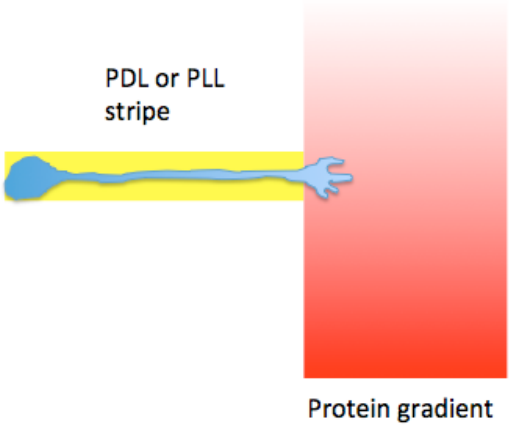


Figure 5.2: Schematic representation of a PDL or PLL stripe pattern (yellow) leading to a protein gradient (red). The surrounding region (white) is coated with PEG, limiting cell adhesion or extension only to the patterned regions.

A particularly interesting improvement to the protocol would be to allow one-step patterning. For example, this could be done by directly conjugating a fluorophore such as FITC to a small peptide. Another option would be to mix a fluorophore in solution with the protein of interest; preliminary experiments with FITC and an antibody (rabbit anti-laminin) demonstrated the feasibility, however improvements on protocol need to be made to obtain patterns with good dynamic range (Annex II). Combining one-step patterning with laser scanning from a confocal microscope or widefield illumination would allow real time patterning near living cells in-between imaging frames. One could then pattern gradients right next to the growth cone of an axon with an orientation perpendicular to the axon orientation (Fig. 5.3) similarly to what is done with the micropipette puffs; but instead of following one cell at the time, several tens of gradients could be produced to follow

multiple cells in parallel. However, this would imply temporarily replacing the growth medium with a solution containing the guidance protein for the duration of the patterning step, which could affect cells sensitivity to the patterned gradients later on. Using a micropipette to locally deliver the guidance molecule that will be adsorbed to the substrate and perfusion of the sample to wash it away quickly could help limit the exposition of cells to the guidance factor.

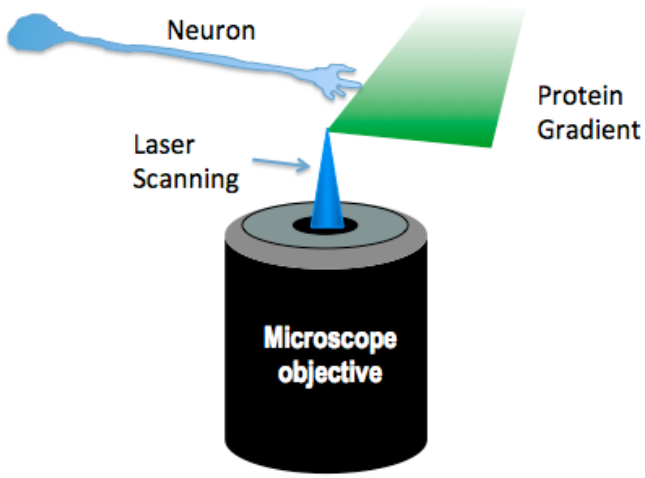


Figure 5.3: One-step protein patterning procedure next to a living neuron done by laser scanning on a confocal microscope. The direction of the gradient could be determined relative to the axon orientation to always have growth cone entering substrate bound gradients at the same position and angle for better consistency in the analysis.

Until now, we only showed that LAPAP was able to pattern a thin layer of protein on a substrate, but it is also able to fabricate relatively thick structures. Usually these kind of structures are fabricated via photopolymerisation; it was recently showed that by mixing

high concentration of methylene blue or flavin adenine dinucleotide (FAD), BSA and/or Avidin, barriers could be fabricated near living cells via two-photon polymerization [306]. The crosslinking of BSA and Avidin is allowed by methylene blue or FAD used as photosensitizers. Using our LAPAP setup, we showed it was possible to produce structures by using only one photon absorption at 473nm, but the laser power required was a least one order of magnitude higher than the one used for standard LAPAP (see Annex III).

## 5.6 3D protein patterning with LAPAP

Despite the fact that living organisms are not two-dimensional, most cell cultures are done on a flat surface for an evident reason: it is more practical. Accordingly, most guidance assays are performed in 2D. Therefore, it would be particularly interesting to use femtosecond lasers with two-photon absorption to produce 3D patterns inside a hydrogel filled with molecules conjugated with a fluorophore to perform LAPAP. We have performed trial experiments showing it was possible to make 3D patterns inside Matrigel$^{TM}$ via one photon adsorption, however the axial resolution was poor. Recent work in our lab performed by Samuel Boutin showed that two-photon absorption LAPAP (2P-LAPAP) was able to produce complex patterns. Instead of using a continuous visible laser as a light source for photobleaching, it uses a pulsed femtosecond IR laser. As it is the case for two-photon microscopy [307], a sufficient photon density to induce two-photon absorption only occurs at the vicinity of the focal volume, therefore providing a very good axial resolution for the patterns created by 2P-LAPAP. 3D patterning requires the control of a 3-axis

motorized stage to create the patterns and using a motorized rotating half-wave plate or a pockell cell in combination of a polarizing beam splitter, the laser intensity can be modulated.

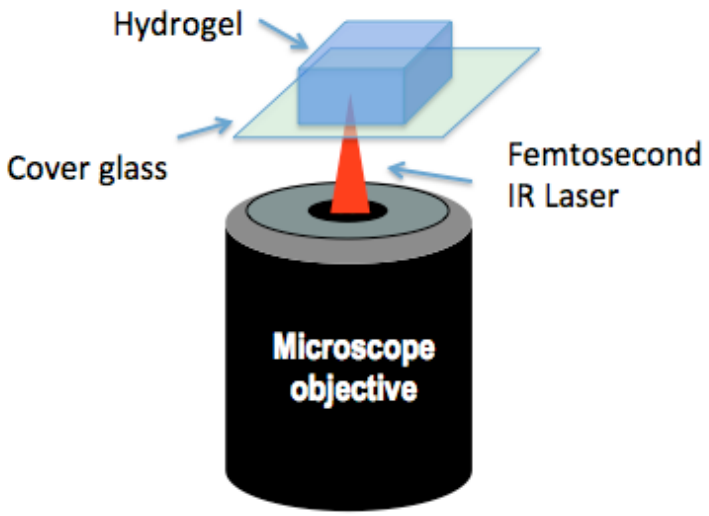


Figure 5.4: Schematic representation of two-photon absorption LAPAP (2P-LAPAP) performed in a hydrogel. A solution of biotin conjugated with a fluorophore is diffusing within the hydrogel and photobleaching is performed via two-photon absorption of a pulsed femtosecond laser. 3-axis motorized stage moves the sample in order to produce the pattern while the laser can be modulated via motorized or electronically controlled optical components.

Samuel Boutin did a miniature version of the earth inside an agarose gel (Fig. 5.5), but patterns could also be fabricated in Matrigel™. One of the main drawbacks of 2P-LAPAP in agarose or Matrigel™ is the procedure to fabricate streptavidin patterns already takes two days. Rinsing steps to remove the unbound Atto 520-biotin takes approximately 6 hours and it is the same for streptavidin-Cy5 used to reveal the pattern.

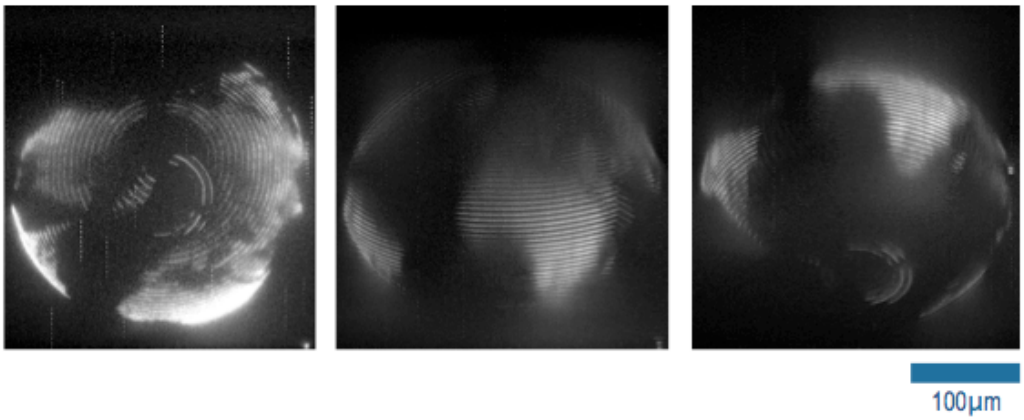


Figure 5.5: 3D pattern of the earth produced by 2P-LAPAP inside agarose. The images shown are 3D representation of an image stack. Despite the hollow configuration of the pattern, the laser scanning took approximately 4 hours.

Moreover, preliminary trials with antibodies showed that their diffusion inside agarose is much slower than streptavidin, most probably limiting the ability to produce functional patterns by binding the final protein via a biotinylated antibody. Monovalent antibodies could be an option to improve diffusion due to their reduced size (50 kDa instead of 150kDa for full-sized antibody) and the fact that their molecular weight is similar to streptavidin (52 kDa). Even using monovalent antibodies, a functional pattern would at least require a few days of incubation and rinsing, therefore increasing chances for contamination for the guidance assay. One-step patterning by using a fluorophore covalently linked to a small peptide could be a clever alternative. Another point to consider would be to control the thickness of the agarose where the pattern is made, until now trial experiments have been performed on agarose gel that is approximately 1mm thick,

reducing this to 100 μm could significantly reduce the fabrication time of functional 3D patterns.

Another aspect of the fabrication to consider is that scanning the focal spot of a laser in 3D is particularly long to make a pattern with intricate details. To choice of the earth replica as a first model (Fig. 5.5) is not random since its hollow design allowed to make it in a reasonable amount of time (4 hours). Fortunately, a new type of microscopy was developed a few years ago to allow full field illumination by two-photon absorption via temporal focusing [308] and was even later improved to allow patterned illumination using a spatial light modulator [305]. Lately, the principles of the technique were used in fast 3D lithographic microfabrication [309]. We believe that using temporal focusing and patterned illumination is one of best solution to speed up the fabrication time of 3D LAPAP patterns.

## 5.7 Determining real bound protein densities

The concentration of proteins in the patterns was always quantified from fluorescence images and basically assumed that the density was proportional to the brightness observed in the image. Despite being a good approximation, it would be particularly interesting to properly quantify the absolute protein numbers in each of the regions. An option would be the use gold-labeled antibodies and scanning electron microscopy (SEM) to directly quantify the bound protein density in each region of a protein pattern. This however would represent a tedious task even for the quantification of small areas. A very recent method based on the analysis of spatial intensity distributions is now

able to unravel the molecular densities from fluorescence images [310]. SpIDA (spatial intensity distributions analysis) fits intensity histograms on the data from regions of fluorescence images to find the density and quantal brightness corresponding to each region. For example, we could calculate the protein density at different location across a gradient.

A specific case where knowing the absolute density could be important, is when concentration is close to saturation. Since full protein patterns use sequential linking of streptavidin, biotinylated secondary antibodies, primary antibodies, between the covalently linked B4F and the full protein, amplification in the absolute protein density between streptavidin and the final protein will occur due to the branching structure created (Fig. 5.6). However, if streptavidin is already close to saturation in one region of the pattern, this amplification will probably be different than the one observed in less dense regions due to steric effects (Fig. 5.6). Indirect proof of this steric effect was observed by fluorescence images in experiments showing how protein concentration can be further amplified using biotinylated anti-streptavidin antibodies (Annex I). For high initial concentration, the amplification ratio measured by fluorescence was significantly smaller. The use of SpIDA could then be particularly interesting to define concentration thresholds for various final proteins as a function of their size. Moreover, the fact that SpIDA is also able to determine oligomerization states could be used in combination with fluorescently tagged antibodies to figure out at which level in the amplification process the steric effect starts playing a significant role for various initial concentrations.

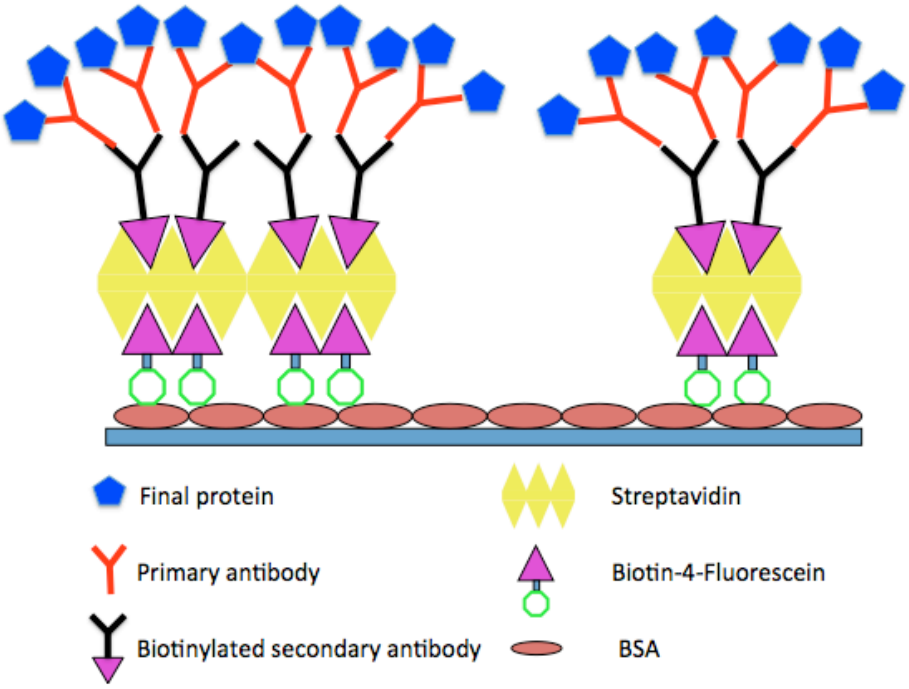


Figure 5.6: Steric effects influence how the density of final protein is amplified by streptavidin, biotinylated secondary antibody and primary antibody. When initially bound streptavidin are close to one another (left part) the amount of final protein per streptavidin should be less. In the left part of the figure, 11 final proteins for 2 streptavidin resulting in a 5.5 amplification factor. When streptavidin is less dense (right part) the more final protein per streptavidin are allowed due to reduction in steric effect, 7 final protein for 1 streptavidin in this illustration leading to an amplification ratio of 7 for this example.

# Conclusion

This thesis presented a novel method, LAPAP, to produce substrate-bound protein patterns using visible light and molecules conjugated to fluorophores for binding biomolecules to a substrate.

We first showed the basis of the method that uses a laser scanning strategy to create patterns with B4F as a first binding molecule. A full characterization of the method was done showing high dynamic range and, as proof functionality, we guided DRG cells on IKVAV peptide gradients. The method was then improved by using antibodies as first binding molecules. This later allowed fabricating multicomponent patterns using antibodies conjugated to different fluorophores by using several lasers having wavelengths corresponding to each fluorophore. Moreover, the optical setup was simplified by introducing widefield illumination by using a spatial light modulator instead of laser scanning. Finally, the method was used in high-content analysis of neurite guidance on laminin-1 gradients as a proof of principle for working with weak guidance cues.

Since the work presented in this thesis is a new technique, our expectation is that other groups find our technology useful. This has already began, our work has already been cited approximately twenty times and various collaborators are using our samples and other groups have reproduced our technique. Furthermore, LAPAP was lately used to create protein patterns on a self-assembled monolayer of methacrylate [311], which is a particularly interesting improvement since thiol-coupled molecules can be bind to the

remaining methacrylate where no protein was bound by LAPAP; for example, thiol-PEG was used since it is resistant to cellular adhesion. Finally, LAPAP has also been used to create alternating PDL and PEG stripe patterns in order to study neurite dynamics while forcing neurons to grow linearly and compared their finding with various model of neurite growth and competition [300].

We expect LAPAP will also be used to decipher the signaling pathways occurring during turning on substrate-bound gradients, in a similar way as micropipette puffs [123] and Dunn chamber [169] were used for soluble gradients. The ability of LAPAP to study guidance on several gradients in parallel will be particularly useful since in the case of weak guidance or reaction of only a small fraction of the neurons, thousands cells should be observed to obtain statistically significant results [284]. Moreover, substrate-bound patterns fabricated using LAPAP could also be combined with soluble gradients obtained by other methods to better mimic the extracellular environment found in vivo.

Obviously, the use of our method is not restricted to axon guidance, and it could also be used to answer more general questions about cellular migration and chemotaxis. For example, locomotion of fish keratocytes on fibronectin is known to be adaptive [312], and LAPAP could be used to understand how the adaptation period varies as a function of fibronectin concentration and distribution. We plan to use LAPAP to study vessel wiring during angiogenesis, since it shares several common mechanisms with axon guidance [146] and we have established a collaboration to achieve this. These are only a few examples, but

we believe that LAPAP can be an important contribution for in vitro experiments where precisely controlling the extracellular environment allows a better understanding of the cellular behavior.

We strongly believe this technique is particularly powerful as it stands now due to its simplicity and precision, however we proposed several improvements that could be done to further improve LAPAP. These improvements are beyond the scope of this thesis, but we hope they could be the seeds leading to subsequent thesis work. We expect LAPAP will allow a larger number of laboratories to use protein patterning and become an important tool for major advances in the field of cell guidance.

# References


1. Feldman, R.P. and J.T. Goodrich, *The Edwin Smith Surgical Papyrus.* Childs Nerv. Syst., 1999. 15(6-7): p. 281-284.

2. Pevsner, J., *Leonardo da Vinci's contributions to neuroscience.* Trends Neurosci., 2002. 25(4): p. 217-220.

3. Tessier-Lavigne, M., *Axon guidance by molecular gradients.* Curr. Opin. Neurobiol., 1992. 2(1): p. 60-65.

4. Dickson, B.J., *Molecular mechanisms of axon guidance.* Science, 2002. 298(5600): p. 1959-1964.

5. Chilton, J.K., *Molecular mechanisms of axon guidance.* Dev. Biol., 2006. 292(1): p. 13-24.

6. Mann, F., W.A. Harris, and C.E. Holt, *New views on retinal axon development: a navigation guide.* Int. J. Dev. Biol., 2004. 48(8-9): p. 957-964.

7. Harrison, R.G., *Observations on the living developing nerve fiber.* The Anatomical Record, 1907. 1(5): p. 116-128.

8. Weiss, P. and A.C. Taylor, *Further experimental evidence against "neurotropism" in nerve regeneration.* J. Exptl. Zool., 1944. 95(2): p. 233-257.

9. Sperry, R.W., *Chemoaffinity in the Orderly Growth of Nerve Fiber Patterns and Connections.* Proc. Natl. Acad. Sci. U. S. A., 1963. 50: p. 703-710.

10. Walter, J., et al., *Recognition of position-specific properties of tectal cell membranes by retinal axons in vitro.* Development, 1987. 101(4): p. 685-696.

11. Walter, J., S. Henke-Fahle, and F. Bonhoeffer, *Avoidance of posterior tectal membranes by temporal retinal axons.* Development, 1987. 101(4): p. 909-913.

12. Walter, J., T.E. Allsopp, and F. Bonhoeffer, *A common denominator of growth cone guidance and collapse?* Trends Neurosci., 1990. 13(11): p. 447-452.

13. Drescher, U., et al., *In vitro guidance of retinal ganglion cell axons by RAGS, a 25 kDa tectal protein related to ligands for Eph receptor tyrosine kinases.* Cell, 1995. 82(3): p. 359-370.

14. Cheng, H.J., et al., *Complementary gradients in expression and binding of ELF-1 and Mek4 in development of the topographic retinotectal projection map.* Cell, 1995. 82(3): p. 371-381.

15. Ciossek, T., et al., *Eph receptor-ligand interactions are necessary for guidance of retinal ganglion cell axons in vitro.* Eur. J. Neurosci., 1998. 10(5): p. 1574-1580.

16. Brown, A., et al., *Topographic mapping from the retina to the midbrain is controlled by relative but not absolute levels of EphA receptor signaling.* Cell, 2000. 102(1): p. 77-88.

17. Feldheim, D.A., et al., *Genetic analysis of ephrin-A2 and ephrin-A5 shows their requirement in multiple aspects of retinocollicular mapping.* Neuron, 2000. 25(3): p. 563-574.

18. Wilkinson, D.G., *Multiple roles of EPH receptors and ephrins in neural development.* Nat. Rev. Neurosci., 2001. 2(3): p. 155-164.

19. Mann, F., et al., *Topographic mapping in dorsoventral axis of the Xenopus retinotectal system depends on signaling through ephrin-B ligands.* Neuron, 2002. 35(3): p. 461-473.

20. Hindges, R., et al., *EphB forward signaling controls directional branch extension and arborization required for dorsal-ventral retinotopic mapping.* Neuron, 2002. 35(3): p. 475-487.

21. McLaughlin, T. and D.D. O'Leary, *Molecular gradients and development of retinotopic maps.* Annu. Rev. Neurosci., 2005. 28: p. 327-355.

22. Williams, S.E., et al., *Ephrin-B2 and EphB1 mediate retinal axon divergence at the optic chiasm.* Neuron, 2003. 39(6): p. 919-935.

23. Henkemeyer, M., et al., *Nuk controls pathfinding of commissural axons in the mammalian central nervous system.* Cell, 1996. 86(1): p. 35-46.

24. Davy, A., et al., *Compartmentalized signaling by GPI-anchored ephrin-A5 requires the Fyn tyrosine kinase to regulate cellular adhesion.* Genes Dev., 1999. 13(23): p. 3125-3135.

25. Knoll, B. and U. Drescher, *Ephrin-As as receptors in topographic projections.* Trends Neurosci., 2002. 25(3): p. 145-149.

26. Knoll, B., et al., *A role for the EphA family in the topographic targeting of vomeronasal axons.* Development, 2001. 128(6): p. 895-906.

27. Raper, J.A., *Semaphorins and their receptors in vertebrates and invertebrates.* Curr. Opin. Neurobiol., 2000. 10(1): p. 88-94.

28. Kolodkin, A.L., et al., *Fasciclin IV: sequence, expression, and function during growth cone guidance in the grasshopper embryo.* Neuron, 1992. 9(5): p. 831-845.

29. Luo, Y., D. Raible, and J.A. Raper, *Collapsin: a protein in brain that induces the collapse and paralysis of neuronal growth cones.* Cell, 1993. 75(2): p. 217-227.

30. Luo, Y., et al., *A family of molecules related to collapsin in the embryonic chick nervous system.* Neuron, 1995. 14(6): p. 1131-1140.

31. Nakamura, F., R.G. Kalb, and S.M. Strittmatter, *Molecular basis of semaphorin-mediated axon guidance.* J. Neurobiol., 2000. 44(2): p. 219-229.

32. He, Z. and M. Tessier-Lavigne, *Neuropilin is a receptor for the axonal chemorepellent Semaphorin III.* Cell, 1997. 90(4): p. 739-751.

33. Kolodkin, A.L., et al., *Neuropilin is a semaphorin III receptor.* Cell, 1997. 90(4): p. 753-762.

34. Chen, H., et al., *Semaphorin-neuropilin interactions underlying sympathetic axon responses to class III semaphorins.* Neuron, 1998. 21(6): p. 1283-1290.

35. Winberg, M.L., et al., *Plexin A is a neuronal semaphorin receptor that controls axon guidance.* Cell, 1998. 95(7): p. 903-916.

36. Winberg, M.L., et al., *The transmembrane protein Off-track associates with Plexins and functions downstream of Semaphorin signaling during axon guidance.* Neuron, 2001. 32(1): p. 53-62.

37. Tamagnone, L., et al., *Plexins are a large family of receptors for transmembrane, secreted, and GPI-anchored semaphorins in vertebrates.* Cell, 1999. 99(1): p. 71-80.

38. Cheng, H.J., et al., *Plexin-A3 mediates semaphorin signaling and regulates the development of hippocampal axonal projections.* Neuron, 2001. 32(2): p. 249-263.

39. Comeau, M.R., et al., *A poxvirus-encoded semaphorin induces cytokine production from monocytes and binds to a novel cellular semaphorin receptor, VESPR.* Immunity, 1998. 8(4): p. 473-482.

40. Swiercz, J.M., et al., *Plexin-B1 directly interacts with PDZ-RhoGEF/LARG to regulate RhoA and growth cone morphology.* Neuron, 2002. 35(1): p. 51-63.

41. Castellani, V., et al., *Analysis of the L1-deficient mouse phenotype reveals cross-talk between Sema3A and L1 signaling pathways in axonal guidance.* Neuron, 2000. 27(2): p. 237-249.

42. Giordano, S., et al., *The semaphorin 4D receptor controls invasive growth by coupling with Met.* Nat. Cell Biol., 2002. 4(9): p. 720-724.

43. Falk, J., et al., *Dual functional activity of semaphorin 3B is required for positioning the anterior commissure.* Neuron, 2005. 48(1): p. 63-75.

44. Pasterkamp, R.J., et al., *Semaphorin 7A promotes axon outgrowth through integrins and MAPKs.* Nature, 2003. 424(6947): p. 398-405.

45. Sakai, J.A. and M.C. Halloran, *Semaphorin 3d guides laterality of retinal ganglion cell projections in zebrafish.* Development, 2006. 133(6): p. 1035-1044.

46. Liu, Y., et al., *Semaphorin3D guides retinal axons along the dorsoventral axis of the tectum.* J. Neurosci., 2004. 24(2): p. 310-318.

47. Zou, Y., et al., *Squeezing axons out of the gray matter: a role for slit and semaphorin proteins from midline and ventral spinal cord.* Cell, 2000. 102(3): p. 363-375.

48. Roche, F.K., B.M. Marsick, and P.C. Letourneau, *Protein synthesis in distal axons is not required for growth cone responses to guidance cues.* J. Neurosci., 2009. 29(3): p. 638-652.

49. Imai, T., et al., *Pre-target axon sorting establishes the neural map topography.* Science, 2009. 325(5940): p. 585-590.

50. Maruyama, T., et al., *Cooperative activity of multiple upper layer proteins for thalamocortical axon growth.* Dev. Neurobiol., 2008. 68(3): p. 317-331.

51. Wong, J.T., S.T. Wong, and T.P. O'Connor, *Ectopic semaphorin-1a functions as an attractive guidance cue for developing peripheral neurons.* Nat. Neurosci., 1999. 2(9): p. 798-803.

52. Polleux, F., T. Morrow, and A. Ghosh, *Semaphorin 3A is a chemoattractant for cortical apical dendrites.* Nature, 2000. 404(6778): p. 567-573.

53. Song, H., et al., *Conversion of neuronal growth cone responses from repulsion to attraction by cyclic nucleotides.* Science, 1998. 281(5382): p. 1515-1518.

54. Hedgecock, E.M., J.G. Culotti, and D.H. Hall, *The unc-5, unc-6, and unc-40 genes guide circumferential migrations of pioneer axons and mesodermal cells on the epidermis in C. elegans.* Neuron, 1990. 4(1): p. 61-85.

55. Ishii, N., et al., *UNC-6, a laminin-related protein, guides cell and pioneer axon migrations in C. elegans.* Neuron, 1992. 9(5): p. 873-881.

56. Tessier-Lavigne, M., et al., *Chemotropic guidance of developing axons in the mammalian central nervous system.* Nature, 1988. 336(6201): p. 775-778.

57. Kennedy, T.E., et al., *Netrins are diffusible chemotropic factors for commissural axons in the embryonic spinal cord.* Cell, 1994. 78(3): p. 425-435.

58. Serafini, T., et al., *The netrins define a family of axon outgrowth-promoting proteins homologous to C. elegans UNC-6.* Cell, 1994. 78(3): p. 409-424.

59. Colamarino, S.A. and M. Tessier-Lavigne, *The role of the floor plate in axon guidance.* Annu. Rev. Neurosci., 1995. 18: p. 497-529.

60. Serafini, T., et al., *Netrin-1 is required for commissural axon guidance in the developing vertebrate nervous system.* Cell, 1996. 87(6): p. 1001-1014.

61. Kennedy, T.E., et al., *Axon guidance by diffusible chemoattractants: a gradient of netrin protein in the developing spinal cord.* J. Neurosci., 2006. 26(34): p. 8866-8874.

62. Schneiders, F.I., et al., *Binding of netrin-4 to laminin short arms regulates basement membrane assembly.* J Biol Chem, 2007. 282(33): p. 23750-23758.

63. Colamarino, S.A. and M. Tessier-Lavigne, *The axonal chemoattractant netrin-1 is also a chemorepellent for trochlear motor axons.* Cell, 1995. 81(4): p. 621-629.

64. Winberg, M.L., K.J. Mitchell, and C.S. Goodman, *Genetic analysis of the mechanisms controlling target selection: complementary and combinatorial functions of netrins, semaphorins, and IgCAMs.* Cell, 1998. 93(4): p. 581-591.

65. Keleman, K. and B.J. Dickson, *Short- and long-range repulsion by the Drosophila Unc5 netrin receptor.* Neuron, 2001. 32(4): p. 605-617.

66. Ming, G.L., et al., *cAMP-dependent growth cone guidance by netrin-1.* Neuron, 1997. 19(6): p. 1225-1235.

67. Hong, K., et al., *Calcium signalling in the guidance of nerve growth by netrin-1.* Nature, 2000. 403(6765): p. 93-98.

68. Culotti, J.G. and D.C. Merz, *DCC and netrins.* Curr. Opin. Cell Biol., 1998. 10(5): p. 609-613.

69. Deiner, M.S., et al., *Netrin-1 and DCC mediate axon guidance locally at the optic disc: loss of function leads to optic nerve hypoplasia.* Neuron, 1997. 19(3): p. 575-589.

70. de la Torre, J.R., et al., *Turning of retinal growth cones in a netrin-1 gradient mediated by the netrin receptor DCC.* Neuron, 1997. 19(6): p. 1211-1224.

71. Hong, K., et al., *A ligand-gated association between cytoplasmic domains of UNC5 and DCC family receptors converts netrin-induced growth cone attraction to repulsion.* Cell, 1999. 97(7): p. 927-941.

72. Corset, V., et al., *Netrin-1-mediated axon outgrowth and cAMP production requires interaction with adenosine A2b receptor.* Nature, 2000. 407(6805): p. 747-750.

73. Stein, E., et al., *Binding of DCC by netrin-1 to mediate axon guidance independent of adenosine A2B receptor activation.* Science, 2001. 291(5510): p. 1976-1982.

74. Erskine, L. and E. Herrera, *The retinal ganglion cell axon's journey: insights into molecular mechanisms of axon guidance.* Dev. Biol., 2007. 308(1): p. 1-14.

75. Hopker, V.H., et al., *Growth-cone attraction to netrin-1 is converted to repulsion by laminin-1.* Nature, 1999. 401(6748): p. 69-73.

76. Ratcliffe, E.M., F. D'Autreaux, and M.D. Gershon, *Laminin terminates the Netrin/DCC mediated attraction of vagal sensory axons.* Dev. Neurobiol., 2008. 68(7): p. 960-971.

77. Wilson, B.D., et al., *Netrins promote developmental and therapeutic angiogenesis.* Science, 2006. 313(5787): p. 640-644.

78. Seeger, M., et al., *Mutations affecting growth cone guidance in Drosophila: genes necessary for guidance toward or away from the midline.* Neuron, 1993. 10(3): p. 409-426.

79. Kidd, T., et al., *Roundabout controls axon crossing of the CNS midline and defines a novel subfamily of evolutionarily conserved guidance receptors.* Cell, 1998. 92(2): p. 205-215.

80. Keleman, K., C. Ribeiro, and B.J. Dickson, *Comm function in commissural axon guidance: cell-autonomous sorting of Robo in vivo.* Nat. Neurosci., 2005. 8(2): p. 156-163.

81. Kidd, T., K.S. Bland, and C.S. Goodman, *Slit is the midline repellent for the robo receptor in Drosophila.* Cell, 1999. 96(6): p. 785-794.

82. Battye, R., A. Stevens, and J.R. Jacobs, *Axon repulsion from the midline of the Drosophila CNS requires slit function.* Development, 1999. 126(11): p. 2475-2481.

83. Brose, K., et al., *Slit proteins bind Robo receptors and have an evolutionarily conserved role in repulsive axon guidance.* Cell, 1999. 96(6): p. 795-806.

84. Sabatier, C., et al., *The divergent Robo family protein rig-1/Robo3 is a negative regulator of slit responsiveness required for midline crossing by commissural axons.* Cell, 2004. 117(2): p. 157-169.

85. Shirasaki, R., R. Katsumata, and F. Murakami, *Change in chemoattractant responsiveness of developing axons at an intermediate target.* Science, 1998. 279(5347): p. 105-107.

86. Stein, E. and M. Tessier-Lavigne, *Hierarchical organization of guidance receptors: silencing of netrin attraction by slit through a Robo/DCC receptor complex.* Science, 2001. 291(5510): p. 1928-1938.

87. Long, H., et al., *Conserved roles for Slit and Robo proteins in midline commissural axon guidance.* Neuron, 2004. 42(2): p. 213-223.

88. Myat, A., et al., *Drosophila Nedd4, a ubiquitin ligase, is recruited by Commissureless to control cell surface levels of the roundabout receptor.* Neuron, 2002. 35(3): p. 447-459.

89. Li, H.S., et al., *Vertebrate slit, a secreted ligand for the transmembrane protein roundabout, is a repellent for olfactory bulb axons.* Cell, 1999. 96(6): p. 807-818.

90. Erskine, L., et al., *Retinal ganglion cell axon guidance in the mouse optic chiasm: expression and function of robos and slits.* J. Neurosci., 2000. 20(13): p. 4975-4982.

91. Plump, A.S., et al., *Slit1 and Slit2 cooperate to prevent premature midline crossing of retinal axons in the mouse visual system.* Neuron, 2002. 33(2): p. 219-232.

92. Niclou, S.P., L. Jia, and J.A. Raper, *Slit2 is a repellent for retinal ganglion cell axons.* J. Neurosci., 2000. 20(13): p. 4962-4974.

93. Ringstedt, T., et al., *Slit inhibition of retinal axon growth and its role in retinal axon pathfinding and innervation patterns in the diencephalon.* J. Neurosci., 2000. 20(13): p. 4983-4991.

94. Thompson, H., et al., *Slits contribute to the guidance of retinal ganglion cell axons in the mammalian optic tract.* Dev. Biol., 2006. 296(2): p. 476-484.

95. Wang, K.H., et al., *Biochemical purification of a mammalian slit protein as a positive regulator of sensory axon elongation and branching.* Cell, 1999. 96(6): p. 771-784.

96. Charron, F. and M. Tessier-Lavigne, *Novel brain wiring functions for classical morphogens: a role as graded positional cues in axon guidance.* Development, 2005. 132(10): p. 2251-2262.

97. Charron, F. and M. Tessier-Lavigne, *The Hedgehog, TGF-beta/BMP and Wnt families of morphogens in axon guidance.* Adv. Exp. Med. Biol., 2007. 621: p. 116-133.

98. Ashe, H.L. and J. Briscoe, *The interpretation of morphogen gradients.* Development, 2006. 133(3): p. 385-394.

99. Gurdon, J.B. and P.Y. Bourillot, *Morphogen gradient interpretation.* Nature, 2001. 413(6858): p. 797-803.

100. Jessell, T.M., *Neuronal specification in the spinal cord: inductive signals and transcriptional codes.* Nat. Rev. Genet., 2000. 1(1): p. 20-29.

101. Briscoe, J. and J. Ericson, *The specification of neuronal identity by graded Sonic Hedgehog signalling.* Semin. Cell Dev. Biol., 1999. 10(3): p. 353-362.

102. Briscoe, J., et al., *Homeobox gene Nkx2.2 and specification of neuronal identity by graded Sonic hedgehog signalling.* Nature, 1999. 398(6728): p. 622-627.

103. Augsburger, A., et al., *BMPs as mediators of roof plate repulsion of commissural neurons.* Neuron, 1999. 24(1): p. 127-141.

104. Butler, S.J. and J. Dodd, *A role for BMP heterodimers in roof plate-mediated repulsion of commissural axons.* Neuron, 2003. 38(3): p. 389-401.

105. Charron, F., et al., *The morphogen sonic hedgehog is an axonal chemoattractant that collaborates with netrin-1 in midline axon guidance.* Cell, 2003. 113(1): p. 11-23.

106. Bourikas, D., et al., *Sonic hedgehog guides commissural axons along the longitudinal axis of the spinal cord.* Nat. Neurosci., 2005. 8(3): p. 297-304.

107. Lyuksyutova, A.I., et al., *Anterior-posterior guidance of commissural axons by Wnt-frizzled signaling.* Science, 2003. 302(5652): p. 1984-1988.

108. McKenna, M.P. and J.A. Raper, *Growth cone behavior on gradients of substratum bound laminin.* Dev. Biol., 1988. 130(1): p. 232-236.

109. Adams, D.N., et al., *Growth cones turn and migrate up an immobilized gradient of the laminin IKVAV peptide.* J. Neurobiol., 2005. 62(1): p. 134-147.

110. Dertinger, S.K., et al., *Gradients of substrate-bound laminin orient axonal specification of neurons.* Proc. Natl. Acad. Sci. U. S. A., 2002. 99(20): p. 12542-12547.

111. Yao, L., et al., *The effect of laminin peptide gradient in enzymatically cross-linked collagen scaffolds on neurite growth.* J. Biomed. Mater. Res. A, 2009. 92(2): p. 484-492.

112. Halfter, W., *The behavior of optic axons on substrate gradients of retinal basal lamina proteins and merosin.* J. Neurosci., 1996. 16(14): p. 4389-4401.

113. Joanne Wang, C., et al., *A microfluidics-based turning assay reveals complex growth cone responses to integrated gradients of substrate-bound ECM molecules and diffusible guidance cues.* Lab Chip, 2008. 8(2): p. 227-237.

114. Paulus, J.D. and M.C. Halloran, *Zebrafish bashful/laminin-alpha 1 mutants exhibit multiple axon guidance defects.* Dev. Dyn., 2006. 235(1): p. 213-224.

115. Gundersen, R.W. and J.N. Barrett, *Neuronal chemotaxis: chick dorsal-root axons turn toward high concentrations of nerve growth factor.* Science, 1979. 206(4422): p. 1079-1080.

116. Gundersen, R.W. and J.N. Barrett, *Characterization of the turning response of dorsal root neurites toward nerve growth factor.* J. Cell Biol., 1980. 87(3 Pt 1): p. 546-554.

117. Yu, L.M., J.H. Wosnick, and M.S. Shoichet, *Miniaturized system of neurotrophin patterning for guided regeneration.* J. Neurosci. Methods, 2008. 171(2): p. 253-263.

118. Mai, J., et al., *Axon initiation and growth cone turning on bound protein gradients.* J. Neurosci., 2009. 29(23): p. 7450-7458.

119. Nishiyama, M., et al., *Membrane potential shifts caused by diffusible guidance signals direct growth-cone turning.* Nat. Neurosci., 2008. 11(7): p. 762-771.

120. Song, H.J., G.L. Ming, and M.M. Poo, *cAMP-induced switching in turning direction of nerve growth cones.* Nature, 1997. 388(6639): p. 275-279.

121. Zheng, J.Q., et al., *Turning of nerve growth cones induced by neurotransmitters.* Nature, 1994. 368(6467): p. 140-144.

122. O'Donnell, M., R.K. Chance, and G.J. Bashaw, *Axon growth and guidance: receptor regulation and signal transduction.* Annu. Rev. Neurosci., 2009. 32: p. 383-412.

123. Nishiyama, M., et al., *Cyclic AMP/GMP-dependent modulation of Ca2+ channels sets the polarity of nerve growth-cone turning.* Nature, 2003. 423(6943): p. 990-995.

124. Wen, Z., et al., *A CaMKII/calcineurin switch controls the direction of Ca(2+)-dependent growth cone guidance.* Neuron, 2004. 43(6): p. 835-846.

125. Shelly, M., et al., *Local and long-range reciprocal regulation of cAMP and cGMP in axon/dendrite formation.* Science, 2010. 327(5965): p. 547-552.

126. Murray, A.J., S.J. Tucker, and D.A. Shewan, *cAMP-dependent axon guidance is distinctly regulated by Epac and protein kinase A.* J. Neurosci., 2009. 29(49): p. 15434-15444.

127. Zheng, J.Q. and M.M. Poo, *Calcium signaling in neuronal motility.* Annu. Rev. Cell Dev. Biol., 2007. 23: p. 375-404.

128. Tojima, T., et al., *Second messengers and membrane trafficking direct and organize growth cone steering.* Nat. Rev. Neurosci., 2011. 12(4): p. 191-203.

129. Dent, E.W., S.L. Gupton, and F.B. Gertler, *The growth cone cytoskeleton in axon outgrowth and guidance.* Cold Spring Harb. Perspect. Biol., 2011. 3(3).

130. Lin, C.H., et al., *Myosin drives retrograde F-actin flow in neuronal growth cones.* Neuron, 1996. 16(4): p. 769-782.

131. Chang, C., et al., *MIG-10/lamellipodin and AGE-1/PI3K promote axon guidance and outgrowth in response to slit and netrin.* Curr. Biol., 2006. 16(9): p. 854-862.

132. Krause, M., et al., *Ena/VASP proteins: regulators of the actin cytoskeleton and cell migration.* Annu. Rev. Cell Dev. Biol., 2003. 19: p. 541-564.

133. Matusek, T., et al., *Formin proteins of the DAAM subfamily play a role during axon growth.* J. Neurosci., 2008. 28(49): p. 13310-13319.

134. Menna, E., et al., *Eps8 regulates axonal filopodia in hippocampal neurons in response to brain-derived neurotrophic factor (BDNF).* PLoS Biol., 2009. 7(6): p. e1000138.

135. Davis, D.A., et al., *Capzb2 interacts with beta-tubulin to regulate growth cone morphology and neurite outgrowth.* PLoS Biol., 2009. 7(10): p. e1000208.

136. De Arcangelis, A., E. Georges-Labouesse, and J.C. Adams, *Expression of fascin-1, the gene encoding the actin-bundling protein fascin-1, during mouse embryogenesis.* Gene Expr. Patterns, 2004. 4(6): p. 637-643.

137. Brown, J.A. and P.C. Bridgman, *Disruption of the cytoskeleton during Semaphorin 3A induced growth cone collapse correlates with differences in actin organization and associated binding proteins.* Dev. Neurobiol., 2009. 69(10): p. 633-646.

138. Marsick, B.M., et al., *Activation of ADF/cofilin mediates attractive growth cone turning toward nerve growth factor and netrin-1.* Dev. Neurobiol., 2010. 70(8): p. 565-588.

139. Hung, R.J., et al., *Mical links semaphorins to F-actin disassembly.* Nature, 2010. 463(7282): p. 823-827.

140. Lee, H., et al., *The microtubule plus end tracking protein Orbit/MAST/CLASP acts downstream of the tyrosine kinase Abl in mediating axon guidance.* Neuron, 2004. 42(6): p. 913-926.

141. Akhmanova, A. and M.O. Steinmetz, *Tracking the ends: a dynamic protein network controls the fate of microtubule tips.* Nat. Rev. Mol. Cell Biol., 2008. 9(4): p. 309-322.

142. Del Rio, J.A., et al., *MAP1B is required for Netrin 1 signaling in neuronal migration and axonal guidance.* Curr. Biol., 2004. 14(10): p. 840-850.

143. Noiges, R., et al., *Microtubule-associated protein 1A (MAP1A) and MAP1B: light chains determine distinct functional properties.* J. Neurosci., 2002. 22(6): p. 2106-2114.

144. Li, Y.H., et al., *Rnd1 regulates axon extension by enhancing the microtubule destabilizing activity of SCG10.* J. Biol. Chem., 2009. 284(1): p. 363-371.

145. Riano, E., et al., *Pleiotropic effects of spastin on neurite growth depending on expression levels.* J. Neurochem., 2009. 108(5): p. 1277-1288.

146. Carmeliet, P. and M. Tessier-Lavigne, *Common mechanisms of nerve and blood vessel wiring.* Nature, 2005. 436(7048): p. 193-200.

147. Gurtner, G.C., et al., *Wound repair and regeneration.* Nature, 2008. 453(7193): p. 314-321.

148. Mackay, C.R., *Chemokines: immunology's high impact factors.* Nat. Immunol., 2001. 2(2): p. 95-101.

149. Keenan, T.M. and A. Folch, *Biomolecular gradients in cell culture systems.* Lab Chip, 2008. 8(1): p. 34-57.

150. Blawas, A.S. and W.M. Reichert, *Protein patterning.* Biomaterials, 1998. 19(7-9): p. 595-609.

151. Postma, M. and P.J. van Haastert, *Mathematics of experimentally generated chemoattractant gradients.* Methods Mol. Biol., 2009. 571: p. 473-488.

152. Zigmond, S.H., *Ability of polymorphonuclear leukocytes to orient in gradients of chemotactic factors.* J. Cell Biol., 1977. 75(2 Pt 1): p. 606-616.

153. Alstergren, P., et al., *Polarization and directed migration of murine neutrophils is dependent on cell surface expression of CD44.* Cell. Immunol., 2004. 231(1-2): p. 146-157.

154. Bultmann, B.D. and H. Gruler, *Analysis of the directed and nondirected movement of human granulocytes: influence of temperature and ECHO 9 virus on N-formylmethionylleucylphenylalanine-induced chemokinesis and chemotaxis.* J. Cell Biol., 1983. 96(6): p. 1708-1716.

155. Bultmann, B.D., et al., *Echo 9 virus-induced order-disorder transition of chemotactic response of human polymorphonuclear leucocytes: phenomenology and molecular biology.* Blood Cells, 1984. 10(1): p. 79-106.

156. Hujanen, E.S., S.T. Seppa, and K. Virtanen, *Polymorphonuclear leukocyte chemotaxis induced by zinc, copper and nickel in vitro.* Biochim. Biophys. Acta, 1995. 1245(2): p. 145-152.

157. Jager, U., H. Gruler, and B. Bultmann, *Morphological changes and membrane potential of human granulocytes under influence of chemotactic peptide and/or echo-virus, type 9.* Klin Wochenschr, 1988. 66(10): p. 434-436.

158. Marasco, W.A., E.L. Becker, and J.M. Oliver, *The ionic basis of chemotaxis. Separate cation requirements for neutrophil orientation and locomotion in a gradient of chemotactic peptide.* Am. J. Pathol., 1980. 98(3): p. 749-768.

159. Vollmer, K.L., et al., *Tumor necrosis factor-alpha decreases neutrophil chemotaxis to N-formyl-1-methionyl-1-leucyl-1-phenylalanine: analysis of single cell movement.* J. Leukoc. Biol., 1992. 52(6): p. 630-636.

160. Yang, L.V., et al., *Gi-independent macrophage chemotaxis to lysophosphatidylcholine via the immunoregulatory GPCR G2A.* Blood, 2005. 105(3): p. 1127-1134.

161. Fuller, K., et al., *Macrophage colony-stimulating factor stimulates survival and chemotactic behavior in isolated osteoclasts.* J. Exp. Med., 1993. 178(5): p. 1733-1744.

162. Fuller, K., J.M. Owens, and T.J. Chambers, *Macrophage inflammatory protein-1 alpha and IL-8 stimulate the motility but suppress the resorption of isolated rat osteoclasts.* J. Immunol., 1995. 154(11): p. 6065-6072.

163. Fabro, G., et al., *Chemotaxis of capacitated rabbit spermatozoa to follicular fluid revealed by a novel directionality-based assay.* Biol. Reprod., 2002. 67(5): p. 1565-1571.

164. Oliveira, R.G., et al., *Increased velocity and induction of chemotactic response in mouse spermatozoa by follicular and oviductal fluids.* J. Reprod. Fertil., 1999. 115(1): p. 23-27.

165. Sun, F., et al., *Lack of species-specificity in mammalian sperm chemotaxis.* Dev. Biol., 2003. 255(2): p. 423-427.

166. Sun, F., et al., *Human sperm chemotaxis: both the oocyte and its surrounding cumulus cells secrete sperm chemoattractants.* Hum. Reprod., 2005. 20(3): p. 761-767.

167. Zicha, D., G.A. Dunn, and A.F. Brown, *A new direct-viewing chemotaxis chamber.* J. Cell Sci., 1991. 99 ( Pt 4): p. 769-775.

168. Webb, S.E., J.W. Pollard, and G.E. Jones, *Direct observation and quantification of macrophage chemoattraction to the growth factor CSF-1.* J. Cell Sci., 1996. 109 ( Pt 4): p. 793-803.

169. Yam, P.T., et al., *Sonic hedgehog guides axons through a noncanonical, Src-family-kinase-dependent signaling pathway.* Neuron, 2009. 62(3): p. 349-362.

170. Maden, M., G. Keen, and G.E. Jones, *Retinoic acid as a chemotactic molecule in neuronal development.* Int. J. Dev. Neurosci., 1998. 16(5): p. 317-322.

171. Zicha, D., G. Dunn, and G. Jones, *Analyzing chemotaxis using the Dunn direct-viewing chamber.* Methods Mol. Biol., 1997. 75: p. 449-457.

172. Lohof, A.M., et al., *Asymmetric modulation of cytosolic cAMP activity induces growth cone turning.* J. Neurosci., 1992. 12(4): p. 1253-1261.

173. Tojima, T., R. Itofusa, and H. Kamiguchi, *The nitric oxide-cGMP pathway controls the directional polarity of growth cone guidance via modulating cytosolic Ca2+ signals.* J. Neurosci., 2009. 29(24): p. 7886-7897.

174. Gomez, T.M., et al., *Filopodial calcium transients promote substrate-dependent growth cone turning.* Science, 2001. 291(5510): p. 1983-1987.

175. Gomez, T.M. and J.Q. Zheng, *The molecular basis for calcium-dependent axon pathfinding.* Nat. Rev. Neurosci., 2006. 7(2): p. 115-125.

176. Yao, J., et al., *An essential role for beta-actin mRNA localization and translation in Ca2+-dependent growth cone guidance.* Nat. Neurosci., 2006. 9(10): p. 1265-1273.

177. Pujic, Z., et al., *Analysis of the growth cone turning assay for studying axon guidance.* J. Neurosci. Methods, 2008. 170(2): p. 220-228.

178. Xiang, Y., et al., *Nerve growth cone guidance mediated by G protein-coupled receptors.* Nat. Neurosci., 2002. 5(9): p. 843-848.

179. Ming, G.L., et al., *Adaptation in the chemotactic guidance of nerve growth cones.* Nature, 2002. 417(6887): p. 411-418.

180. Zheng, J.Q., J.J. Wan, and M.M. Poo, *Essential role of filopodia in chemotropic turning of nerve growth cone induced by a glutamate gradient.* J. Neurosci., 1996. 16(3): p. 1140-1149.

181. Ming, G., et al., *Electrical activity modulates growth cone guidance by diffusible factors.* Neuron, 2001. 29(2): p. 441-452.

182. Bouzigues, C., et al., *Asymmetric redistribution of GABA receptors during GABA gradient sensing by nerve growth cones analyzed by single quantum dot imaging.* Proc. Natl. Acad. Sci. U. S. A., 2007. 104(27): p. 11251-11256.

183. Li, L., B.I. Hutchins, and K. Kalil, *Wnt5a induces simultaneous cortical axon outgrowth and repulsive axon guidance through distinct signaling mechanisms.* J. Neurosci., 2009. 29(18): p. 5873-5883.

184. Servant, G., et al., *Dynamics of a chemoattractant receptor in living neutrophils during chemotaxis.* Mol. Biol. Cell, 1999. 10(4): p. 1163-1178.

185. Servant, G., et al., *Polarization of chemoattractant receptor signaling during neutrophil chemotaxis.* Science, 2000. 287(5455): p. 1037-1040.

186. Wong, K., et al., *Neutrophil polarization: spatiotemporal dynamics of RhoA activity support a self-organizing mechanism.* Proc. Natl. Acad. Sci. U. S. A., 2006. 103(10): p. 3639-3644.

187. Li, N., A. Tourovskaia, and A. Folch, *Biology on a chip: microfabrication for studying the behavior of cultured cells.* Crit. Rev. Biomed. Eng., 2003. 31(5-6): p. 423-488.

188. Whitesides, G.M., et al., *Soft lithography in biology and biochemistry.* Annu. Rev. Biomed. Eng., 2001. 3: p. 335-373.

189. Qin, D., Y. Xia, and G.M. Whitesides, *Soft lithography for micro- and nanoscale patterning.* Nat. Protoc., 2010. 5(3): p. 491-502.

190. Folch, A. and M. Toner, *Microengineering of cellular interactions.* Annu. Rev. Biomed. Eng., 2000. 2: p. 227-256.

191. Takayama, S., et al., *Patterning cells and their environments using multiple laminar fluid flows in capillary networks.* Proc. Natl. Acad. Sci. U. S. A., 1999. 96(10): p. 5545-5548.

192. Delamarche, E., et al., *Patterned delivery of immunoglobulins to surfaces using microfluidic networks.* Science, 1997. 276(5313): p. 779-781.

193. Bernard, A., et al., *Microcontact printing of proteins.* Advanced Materials, 2000. 12(14): p. 1067-1070.

194. Hsu, C.H., C. Chen, and A. Folch, *"Microcanals" for micropipette access to single cells in microfluidic environments.* Lab Chip, 2004. 4(5): p. 420-424.

195. Irimia, D., *Microfluidic technologies for temporal perturbations of chemotaxis.* Annu. Rev. Biomed. Eng., 2010. 12: p. 259-284.

196. Chung, B.G. and J. Choo, *Microfluidic gradient platforms for controlling cellular behavior.* Electrophoresis, 2010. 31(18): p. 3014-3027.

197. Jeon, N.L., et al., *Generation of Solution and Surface Gradients Using Microfluidic Systems.* Langmuir, 2000. 16(22): p. 8311-8316.

198. Li Jeon, N., et al., *Neutrophil chemotaxis in linear and complex gradients of interleukin-8 formed in a microfabricated device.* Nat. Biotechnol., 2002. 20(8): p. 826-830.

199. Irimia, D., et al., *Microfluidic system for measuring neutrophil migratory responses to fast switches of chemical gradients.* Lab Chip, 2006. 6(2): p. 191-198.

200. Dertinger, S.K.W., et al., *Generation of Gradients Having Complex Shapes Using Microfluidic Networks.* Anal. Chem., 2001. 73(6): p. 1240-1246.

201. Wang, S.J., et al., *Differential effects of EGF gradient profiles on MDA-MB-231 breast cancer cell chemotaxis.* Exp. Cell Res., 2004. 300(1): p. 180-189.

202. Chung, B.G., et al., *Human neural stem cell growth and differentiation in a gradient-generating microfluidic device.* Lab Chip, 2005. 5(4): p. 401-406.

203. Englert, D.L., M.D. Manson, and A. Jayaraman, *Flow-based microfluidic device for quantifying bacterial chemotaxis in stable, competing gradients.* Appl. Environ. Microbiol., 2009. 75(13): p. 4557-4564.

204. Kamholz, A.E., et al., *Quantitative analysis of molecular interaction in a microfluidic channel: the T-sensor.* Anal. Chem., 1999. 71(23): p. 5340-5347.

205. Hatch, A., et al., *A rapid diffusion immunoassay in a T-sensor.* Nat. Biotechnol., 2001. 19(5): p. 461-465.

206. Mao, H., P.S. Cremer, and M.D. Manson, *A sensitive, versatile microfluidic assay for bacterial chemotaxis.* Proc. Natl. Acad. Sci. U. S. A., 2003. 100(9): p. 5449-5454.

207. Lanning, L.M., R.M. Ford, and T. Long, *Bacterial chemotaxis transverse to axial flow in a microfluidic channel.* Biotechnol. Bioeng., 2008. 100(4): p. 653-663.

208. Barkefors, I., et al., *Endothelial cell migration in stable gradients of vascular endothelial growth factor A and fibroblast growth factor 2: effects on chemotaxis and chemokinesis.* J. Biol. Chem., 2008. 283(20): p. 13905-13912.

209. Irimia, D., D.A. Geba, and M. Toner, *Universal microfluidic gradient generator.* Anal. Chem., 2006. 78(10): p. 3472-3477.

210. Campbell, K. and A. Groisman, *Generation of complex concentration profiles in microchannels in a logarithmically small number of steps.* Lab Chip, 2007. 7(2): p. 264-272.

211. Abhyankar, V.V., et al., *Characterization of a membrane-based gradient generator for use in cell-signaling studies.* Lab Chip, 2006. 6(3): p. 389-393.

212. Kim, T., M. Pinelis, and M.M. Maharbiz, *Generating steep, shear-free gradients of small molecules for cell culture.* Biomed Microdevices, 2009. 11(1): p. 65-73.

213. Paliwal, S., et al., *MAPK-mediated bimodal gene expression and adaptive gradient sensing in yeast.* Nature, 2007. 446(7131): p. 46-51.

214. Li, C.W., R. Chen, and M. Yang, *Generation of linear and non-linear concentration gradients along microfluidic channel by microtunnel controlled stepwise addition of sample solution.* Lab Chip, 2007. 7(10): p. 1371-1373.

215. Mosadegh, B., et al., *Generation of stable complex gradients across two-dimensional surfaces and three-dimensional gels.* Langmuir, 2007. 23(22): p. 10910-10912.

216. Saadi, W., et al., *Generation of stable concentration gradients in 2D and 3D environments using a microfluidic ladder chamber.* Biomedical Microdevices, 2007. 9(5): p. 627-635.

217. Haessler, U., et al., *An agarose-based microfluidic platform with a gradient buffer for 3D chemotaxis studies.* Biomed. Microdevices, 2009. 11(4): p. 827-835.

218. Haessler, U., et al., *Dendritic cell chemotaxis in 3D under defined chemokine gradients reveals differential response to ligands CCL21 and CCL19.* Proc. Natl. Acad. Sci. U. S. A., 2011. 108(14): p. 5614-5619.

219. Diao, J., et al., *A three-channel microfluidic device for generating static linear gradients and its application to the quantitative analysis of bacterial chemotaxis.* Lab Chip, 2006. 6(3): p. 381-388.

220. Wu, H., B. Huang, and R.N. Zare, *Generation of complex, static solution gradients in microfluidic channels.* Journal of the American Chemical Society, 2006. 128(13): p. 4194-4195.

221. Keenan, T.M., C.H. Hsu, and A. Folch, *Microfluidic "jets" for generating steady-state gradients of soluble molecules on open surfaces.* Applied Physics Letters, 2006. 89(11): p. -.

222. Keenan, T.M., et al., *A new method for studying gradient-induced neutrophil desensitization based on an open microfluidic chamber.* Lab Chip, 2010. 10(1): p. 116-122.

223. Frevert, C.W., et al., *Measurement of cell migration in response to an evolving radial chemokine gradient triggered by a microvalve.* Lab Chip, 2006. 6(7): p. 849-856.

224. Juncker, D., H. Schmid, and E. Delamarche, *Multipurpose microfluidic probe.* Nat. Mater., 2005. 4(8): p. 622-628.

225. Delamarche, E., et al., *Microfluidic networks for chemical patterning of substrate: Design and application to bioassays.* Journal of the American Chemical Society, 1998. 120(3): p. 500-508.

226. Fosser, K.A. and R.G. Nuzzo, *Fabrication of patterned multicomponent protein gradients and gradient arrays using microfluidic depletion.* Anal. Chem., 2003. 75(21): p. 5775-5782.

227. Quist, A.P., E. Pavlovic, and S. Oscarsson, *Recent advances in microcontact printing.* Anal. Bioanal. Chem., 2005. 381(3): p. 591-600.

228. Falconnet, D., et al., *Surface engineering approaches to micropattern surfaces for cell-based assays.* Biomaterials, 2006. 27(16): p. 3044-3063.

229. Branch, D.W., et al., *Microstamp patterns of biomolecules for high-resolution neuronal networks.* Med. Biol. Eng. Comput., 1998. 36(1): p. 135-141.

230. von Philipsborn, A.C., et al., *Microcontact printing of axon guidance molecules for generation of graded patterns.* Nat. Protoc., 2006. 1(3): p. 1322-1328.

231. Thery, M., *Micropatterning as a tool to decipher cell morphogenesis and functions.* Journal of Cell Science, 2010. 123(24): p. 4201-4213.

232. Csucs, G., K. Quirin, and G. Danuser, *Locomotion of fish epidermal keratocytes on spatially selective adhesion patterns.* Cell Motil. Cytoskeleton, 2007. 64(11): p. 856-867.

233. Lauer, L., C. Klein, and A. Offenhausser, *Spot compliant neuronal networks by structure optimized micro-contact printing.* Biomaterials, 2001. 22(13): p. 1925-1932.

234. von Philipsborn, A.C., et al., *Growth cone navigation in substrate-bound ephrin gradients.* Development, 2006. 133(13): p. 2487-2495.

235. Foxman, E.F., J.J. Campbell, and E.C. Butcher, *Multistep navigation and the combinatorial control of leukocyte chemotaxis.* J. Cell Biol., 1997. 139(5): p. 1349-1360.

236. Foxman, E.F., E.J. Kunkel, and E.C. Butcher, *Integrating conflicting chemotactic signals. The role of memory in leukocyte navigation.* J. Cell Biol., 1999. 147(3): p. 577-588.

237. Rosoff, W.J., et al., *A new chemotaxis assay shows the extreme sensitivity of axons to molecular gradients.* Nat. Neurosci., 2004. 7(6): p. 678-682.

238. Rosoff, W.J., et al., *Generating controlled molecular gradients in 3D gels.* Biotechnol. Bioeng., 2005. 91(6): p. 754-759.

239. Lee, S.H., J.J. Moon, and J.L. West, *Three-dimensional micropatterning of bioactive hydrogels via two-photon laser scanning photolithography for guided 3D cell migration.* Biomaterials, 2008. 29(20): p. 2962-2968.

240. Seidlits, S.K., C.E. Schmidt, and J.B. Shear, *High-Resolution Patterning of Hydrogels in Three Dimensions using Direct-Write Photofabrication for Cell Guidance.* Advanced Functional Materials, 2009. 19(22): p. 3543-3551.

241. Kleinfeld, D., K.H. Kahler, and P.E. Hockberger, *Controlled outgrowth of dissociated neurons on patterned substrates.* J. Neurosci., 1988. 8(11): p. 4098-4120.

242. Healy, K.E., et al., *Kinetics of bone cell organization and mineralization on materials with patterned surface chemistry.* Biomaterials, 1996. 17(2): p. 195-208.

243. Britland, S., et al., *Micropatterned substratum adhesiveness: a model for morphogenetic cues controlling cell behavior.* Exp. Cell Res., 1992. 198(1): p. 124-129.

244. Lom, B., K.E. Healy, and P.E. Hockberger, *A versatile technique for patterning biomolecules onto glass coverslips.* J. Neurosci. Methods, 1993. 50(3): p. 385-397.

245. Britland, S., et al., *Micropatterning proteins and synthetic peptides on solid supports: a novel application for microelectronics fabrication technology.* Biotechnol. Prog., 1992. 8(2): p. 155-160.

246. Doh, J. and D.J. Irvine, *Photogenerated polyelectrolyte bilayers from an aqueous-processible photoresist for multicomponent protein patterning.* Journal of the American Chemical Society, 2004. 126(30): p. 9170-9171.

247. Doh, J. and D.J. Irvine, *Immunological synapse arrays: patterned protein surfaces that modulate immunological synapse structure formation in T cells.* Proc. Natl. Acad. Sci. U. S. A., 2006. 103(15): p. 5700-5705.

248. Kim, M., et al., *Addressable micropatterning of multiple proteins and cells by microscope projection photolithography based on a protein friendly photoresist.* Langmuir, 2010. 26(14): p. 12112-12118.

249. Sigrist, H., et al., *Surface Immobilization of Biomolecules by Light.* Optical Engineering, 1995. 34(8): p. 2339-2348.

250. Das, M. and C.F. Fox, *Chemical Cross-Linking in Biology.* Annual Review of Biophysics and Bioengineering, 1979. 8: p. 165-193.

251. Morgan, H., D.J. Pritchard, and J.M. Cooper, *Photo-patterning of sensor surfaces with biomolecular structures: characterisation using AFM and fluorescence microscopy.* Biosens. Bioelectron., 1995. 10(9-10): p. 841-846.

252. Clemence, J.F., et al., *Photoimmobilization of a bioactive laminin fragment and pattern-guided selective neuronal cell attachment.* Bioconjug. Chem., 1995. 6(4): p. 411-417.

253. Pritchard, D.J., H. Morgan, and J.M. Cooper, *Patterning and regeneration of surfaces with antibodies.* Anal. Chem., 1995. 67(19): p. 3605-3607.

254. Pirrung, M.C. and C.Y. Huang, *A general method for the spatially defined immobilization of biomolecules on glass surfaces using "caged" biotin.* Bioconjug. Chem., 1996. 7(3): p. 317-321.

255. Fodor, S.P., et al., *Light-directed, spatially addressable parallel chemical synthesis.* Science, 1991. 251(4995): p. 767-773.

256. Blawas, A.S., et al., *Step-and-repeat photopatterning of protein features using caged/biotin-BSA: Characterization and resolution.* Langmuir, 1998. 14(15): p. 4243-4250.

257. Sundarababu, G., H. Gao, and H. Sigrist, *Photochemical linkage of antibodies to silicon chips.* Photochem. Photobiol., 1995. 61(6): p. 540-544.

258. Gao, H., et al., *Immunosensing with photo-immobilized immunoreagents on planar optical wave guides.* Biosens. Bioelectron., 1995. 10(3-4): p. 317-328.

259. Dillmore, W.S., M.N. Yousaf, and M. Mrksich, *A photochemical method for patterning the immobilization of ligands and cells to self-assembled monolayers.* Langmuir, 2004. 20(17): p. 7223-7231.

260. Dulcey, C.S., et al., *Deep UV photochemistry of chemisorbed monolayers: patterned coplanar molecular assemblies.* Science, 1991. 252(5005): p. 551-554.

261. Spargo, B.J., et al., *Spatially controlled adhesion, spreading, and differentiation of endothelial cells on self-assembled molecular monolayers.* Proc. Natl. Acad. Sci. U. S. A., 1994. 91(23): p. 11070-11074.

262. Bhatia, S.K., et al., *Use of thiol-terminal silanes and heterobifunctional crosslinkers for immobilization of antibodies on silica surfaces.* Anal. Biochem., 1989. 178(2): p. 408-413.

263. Azioune, A., et al., *Protein micropatterns: A direct printing protocol using deep UVs.* Methods Cell Biol., 2010. 97: p. 133-146.

264. Azioune, A., et al., *Simple and rapid process for single cell micro-patterning.* Lab Chip, 2009. 9(11): p. 1640-1642.

265. Welle, A., et al., *Photo-chemically patterned polymer surfaces for controlled PC-12 adhesion and neurite guidance.* Journal of Neuroscience Methods, 2005. 142(2): p. 243-250.

266. Welle, A. and E. Gottwald, *UV-based patterning of polymeric substrates for cell culture applications.* Biomedical Microdevices, 2002. 4(1): p. 33-41.

267. Mitchell, S.A., et al., *Orientation and confinement of cells on chemically patterned polystyrene surfaces.* Colloids and Surfaces B-Biointerfaces, 2005. 46(2): p. 108-116.

268. Mitchell, S.A., et al., *Cellular attachment and spatial control of cells using micro-patterned ultra-violet/ozone treatment in serum enriched media.* Biomaterials, 2004. 25(18): p. 4079-4086.

269. Huang, Y.M., et al., *Neutravidin micropatterning by deep UV irradiation.* Lab Chip, 2008. 8(10): p. 1745-1747.

270. Heinze, K.G., et al., *Beyond photobleaching, laser illumination unbinds fluorescent proteins.* J. Phys. Chem. B, 2009. 113(15): p. 5225-5233.

271. Holden, M.A. and P.S. Cremer, *Light activated patterning of dye-labeled molecules on surfaces.* J. Am. Chem. Soc., 2003. 125(27): p. 8074-8075.

272. Tessier-Lavigne, M. and C.S. Goodman, *The molecular biology of axon guidance.* Science, 1996. 274(5290): p. 1123-1133.

273. Parent, C.A. and P.N. Devreotes, *A cell's sense of direction.* Science, 1999. 284(5415): p. 765-770.

274. Baier, H. and F. Bonhoeffer, *Axon guidance by gradients of a target-derived component.* Science, 1992. 255(5043): p. 472-475.

275. Chung, B.G., F. Lin, and N.L. Jeon, *A microfluidic multi-injector for gradient generation.* Lab Chip, 2006. 6(6): p. 764-768.

276. Arnold, M., et al., *Induction of cell polarization and migration by a gradient of nanoscale variations in adhesive ligand spacing.* Nano Lett., 2008. 8(7): p. 2063-2069.

277. Costantino, S., et al., *Fabrication of protein gradients for cell culture using a miniature squeegee.* J. Biochem. Biophys. Methods, 2008. 70(6): p. 1192-1195.

278. Buxboim, A., et al., *A single-step photolithographic interface for cell-free gene expression and active biochips.* Small, 2007. 3(3): p. 500-510.

279. Gros, J., O. Serralbo, and C. Marcelle, *WNT11 acts as a directional cue to organize the elongation of early muscle fibres.* Nature, 2009. 457(7229): p. 589-593.

280. Horner, P.J. and F.H. Gage, *Regenerating the damaged central nervous system.* Nature, 2000. 407(6807): p. 963-970.

281. Olson, L., *Regeneration in the adult central nervous system: experimental repair strategies.* Nat. Med., 1997. 3(12): p. 1329-1335.

282. Belisle, J.M., et al., *Patterning protein concentration using laser-assisted adsorption by photobleaching, LAPAP.* Lab Chip, 2008. 8(12): p. 2164-2167.

283. Lang, S., et al., *Growth cone response to ephrin gradients produced by microfluidic networks.* Anal. Bioanal. Chem., 2008. 390(3): p. 809-816.

284. Aletti, G. and P. Causin, *Mathematical characterisation of the transduction chain in growth cone pathfinding.* IET Syst. Biol., 2008. 2(3): p. 150-161.

285. Dragunow, M., *Opinion - High-content analysis in neuroscience.* Nat. Rev. Neurosci., 2008. 9(10): p. 779-788.

286. Perlman, Z.E., et al., *Multidimensional drug profiling by automated microscopy.* Science, 2004. 306(5699): p. 1194-1198.

287. Lang, P., et al., *Cellular imaging in drug discovery.* Nat. Rev. Drug Discov., 2006. 5(4): p. 343-356.

288. Neumann, B., et al., *High-throughput RNAi screening by time-lapse imaging of live human cells.* Nat. Methods, 2006. 3(5): p. 385-390.

289. Echeverri, C.J. and N. Perrimon, *High-throughput RNAi screening in cultured cells: a user's guide.* Nat. Rev. Genet., 2006. 7(5): p. 373-384.

290. Hu, M., et al., *High content screen microscopy analysis of A beta 1-42-induced neurite outgrowth reduction in rat primary cortical neurons: neuroprotective effects of alpha 7 neuronal nicotinic acetylcholine receptor ligands.* Brain Res., 2007. 1151: p. 227-235.

291. Vallotton, P., et al., *Automated analysis of neurite branching in cultured cortical neurons using HCA-Vision.* Cytometry A, 2007. 71A(10): p. 889-895.

292. Wang, D.D., et al., *HCA-Vision: Automated Neurite Outgrowth Analysis.* J. Biomol. Screen., 2010. 15(9): p. 1165-1170.

293. Belisle, J.M., D. Kunik, and S. Costantino, *Rapid multicomponent optical protein patterning.* Lab Chip, 2009. 9(24): p. 3580 - 3585.

294. Gupton, S.L. and F.B. Gertler, *Integrin signaling switches the cytoskeletal and exocytic machinery that drives neuritogenesis.* Dev. Cell, 2010. 18(5): p. 725-736.

295. Lieven, C.J., et al., *Induction of axon and dendrite formation during early RGC-5 cell differentiation.* Exp. Eye Res., 2007. 85(5): p. 678-683.

296. Gonzalez, R.C., R.E. Woods, and S.L. Eddins, *Digital Image processing using MATLAB®*. 2004, Upper Saddle River, N. J.: Pearson Prentice Hall. xiv, 609 p.

297. Keenan, T.M., et al., *Automated identification of axonal growth cones in time-lapse image sequences.* J. Neurosci. Methods, 2006. 151(2): p. 232-238.

298. Costantino, S., et al., *Semi-automated quantification of filopodial dynamics.* J. Neurosci. Methods, 2008. 171(1): p. 165-173.

299. Okamoto, K., et al., *The role of CaMKII as an F-actin-bundling protein crucial for maintenance of dendritic spine structure.* Proc. Natl. Acad. Sci. U. S. A., 2007. 104(15): p. 6418-6423.

300. Wissner-Gross, Z.D., et al., *Large-scale analysis of neurite growth dynamics on micropatterned substrates.* Integr. Biol., 2011. 3(1): p. 65-74.

301. Pologruto, T.A., B.L. Sabatini, and K. Svoboda, *ScanImage: flexible software for operating laser scanning microscopes.* Biomed. Eng. Online, 2003. 2: p. 13.

302. Lutz, C., et al., *Holographic photolysis of caged neurotransmitters.* Nat. Methods, 2008. 5(9): p. 821-827.

303. Therrien, O.D., et al., *Wide-field multiphoton imaging of cellular dynamics in thick tissue by temporal focusing and patterned illumination.* Biomed. Opt. Express, 2011. 2(3): p. 696-704.

304. Wyrowski, F. and O. Bryngdahl, *Iterative Fourier-Transform Algorithm Applied to Computer Holography.* Journal of the Optical Society of America a-Optics Image Science and Vision, 1988. 5(7): p. 1058-1065.

305. Papagiakoumou, E., et al., *Patterned two-photon illumination by spatiotemporal shaping of ultrashort pulses.* Opt. Express, 2008. 16(26): p. 22039-22047.

306. Kaehr, B., et al., *Guiding neuronal development with in situ microfabrication.* Proc. Natl. Acad. Sci. U. S. A., 2004. 101(46): p. 16104-16108.

307. Denk, W., J.H. Strickler, and W.W. Webb, *Two-photon laser scanning fluorescence microscopy.* Science, 1990. 248(4951): p. 73-76.

308. Oron, D., E. Tal, and Y. Silberberg, *Scanningless depth-resolved microscopy.* Opt. Express, 2005. 13(5): p. 1468-1476.

309. Kim, D. and P.T. So, *High-throughput three-dimensional lithographic microfabrication.* Opt. Lett., 2010. 35(10): p. 1602-1604.

310. Godin, A.G., et al., *Revealing protein oligomerization and densities in situ using spatial intensity distribution analysis.* Proc. Natl. Acad. Sci. U. S. A., 2011. 108(17): p. 7010-7015.

311. Scrimgeour, J., et al., *Photobleaching-activated micropatterning on self-assembled monolayers.* J. Phys. Condens. Matter, 2010. 22(19): p. 194103.

312. Liu, H.W., et al., *Locomotion guidance by extracellular matrix is adaptive and can be restored by a transient change in Ca2+ level.* PLoS One, 2009. 4(10): p. e7330.

313. Mortimer, D., et al., *Growth cone chemotaxis.* Trends Neurosci., 2008. 31(2): p. 90-98.

314. McFarlane, S., *Attraction vs. repulsion: the growth cone decides.* Biochem. Cell Biol., 2000. 78(5): p. 563-568.

315. Sick, S., et al., *WNT and DKK determine hair follicle spacing through a reaction-diffusion mechanism.* Science, 2006. 314(5804): p. 1447-1450.

316. Boyden, S., *The chemotactic effect of mixtures of antibody and antigen on polymorphonuclear leucocytes.* J. Exp. Med., 1962. 115: p. 453-466.

317. Hosokawa, K. and M. Maeda, *Spatial distribution of laminar flow-assisted dendritic amplification.* Lab Chip, 2009. 9(3): p. 464-468.

# Annex I: Conference proceedings

This conference proceeding describes in detail how it is possible to amplify the amount of protein that is bound by LAPAP. The strategy described here using altering incubation of streptavidin and a biotinylated antibody against streptavidin to create tree-like structures to amplify the final amount of protein that can bind to the top layer of streptavidin via a biotinylated antibody. Here we show how that the measured amplification ratio for low concentration patterns are particularly influenced by the background in the image. However, increasing the concentration limits decrease the amplification, most probably due to steric effects.

# Density Amplification in Laser-Assisted Protein Adsorption by Photobleaching

Jonathan M. Bélisle[ab] and Santiago Costantino*[abc]
[a]Maisonneuve-Rosemont Hospital, University of Montreal, QC, Canada H1T2M4;
[b]Institute of Biomedical Engineering, University of Montreal, QC, Canada H3C3J7;
[c]Department of Ophthalmology, University of Montreal, QC, Canada H3C3J7

## ABSTRACT

Spatial distributions of proteins are crucial for development, growth and normal life of organism. Position of cells in a morphogen gradient determines their differentiation in a specific manner. Neutrophils are the initial responders to bacterial infection or other inflammatory stimuli and have the ability to migrate rapidly up shallow gradients of attractants in vivo. Moreover, for the correct wiring of the nervous system, axonal growth cones detect concentration changes of specific proteins called guidance cues to navigate and reach their targets. Guidance cues can either be chemoattractive or chemorepulsive, and the same protein can act successively as both depending on the time point in development or the simultaneous presence of other molecules. A prerequisite to understand chemotaxis in a precise manner is the availability of a method able to reproduce *in vitro* the spatial distributions of proteins found *in vivo*. We recently introduced LAPAP (*Laser-assisted protein adsoption by photobleaching*), an optical method to produce substrate-bound protein patterns with micron resolution. Here, we present how the amount of protein present on the pattern can be increased by one order of magnitude.

**Keywords:** Protein patterning, photobleaching, density amplification

## 1. INTRODUCTION

Distributions of protein are required for many processes occurring in living organisms. A particularly important process is axonal guidance which is needed to correctly wire the nervous system [4, 5, 272]. The growth cone is located at the tip the axon and extends and retracts filopodia to read information from molecular cues in order to guide the axon in the appropriate direction [313, 314]. Understanding axonal guidance is crucial for repairing central nervous system damaged nerves in order to guide axons back to their original target [280, 281]. Many other processes in development and normal life rely on distributions of proteins : morphogenesis [98, 99] , angiogenesis[77], epidermal patterns[315], wound healing[147] and immune response [148].

Several methods have been developed to study cellular response to graded distribution of proteins *in vitro* [149, 150]. Traditional methods rely on diffusion to produce protein gradients such as the Boyden [316], Dunn [171] and Zigmond [152] chambers as well as biological hydrogels [34]. Micropipette generated gradients [115, 121] are produced in a more active manner since the volume of the puff, its frequency and the distance of the micropipette tip from the studied cells allows to modulate the produced gradient. New methods based on microfluidics have allowed producing user-defined protein patterns [197, 224]. Another one, based on microcontact printing, generated gradients from a macroscopic perspective by designing stamps with increasing spot size in one direction [234].

Recently, we introduced LAPAP [282], an optical protein patterning method which uses a low power laser to photobleach biotin-4-fluorescein (B4F) and adsorb it to a glass substrate. On-demand protein patterns can be obtained by scanning the laser beam while varying the laser intensity and the scanning velocity to modulate the amount of B4F adsorbed. Streptavidin is then incubated on the B4F pattern due to its strong affinity with biotin. The functionalization of the pattern can be done by then using biotinylated molecules or biotinylated antibodies and their antigen. The spatial resolution obtained with LAPAP is close to 1µm and the amount of bound protein can be modulated by three orders of magnitude. Using lasers of different wavelength and a mixture of antibodies conjugated with different dyes, it is also possible to produce two components protein patterns [293].

In order to speed up the photobleaching step, the method was improved by illuminating the whole field at once instead of scanning the laser beam, this method is called Widefield LAPAP [293]. Finally, using subsequent illumination of FITC conjugated antibodies against different targets; we were able to produce three component patterns.

To increase protein density that can be patterned, we present here an assay where the amount of streptavidin available to bind biotinylated antibodies is amplified [317].

## 2. MATERIALS AND METHODS

### 2.1 Experimental setup

The LAPAP setup (Fig. 1) used to produce protein patterns includes a 473 nm diode pumped solid state (DPSS) laser (Laserglow, ON, Canada). This laser can deliver up to 50mW, but intensities ranging from 0.1µW to 160µW are normally used. A 60x 1.2 NA water immersion objective (Olympus, Japan) is used to focus the laser beam at the interface of the coverglass and the solution of B4F. A xyz motorized translation stage (Thorlabs, NJ) is used to move the sample with respect to the focal spot of the laser. The laser power as well as the position of the sample is controlled by a home-made Labview (National Instrument, TX) program.

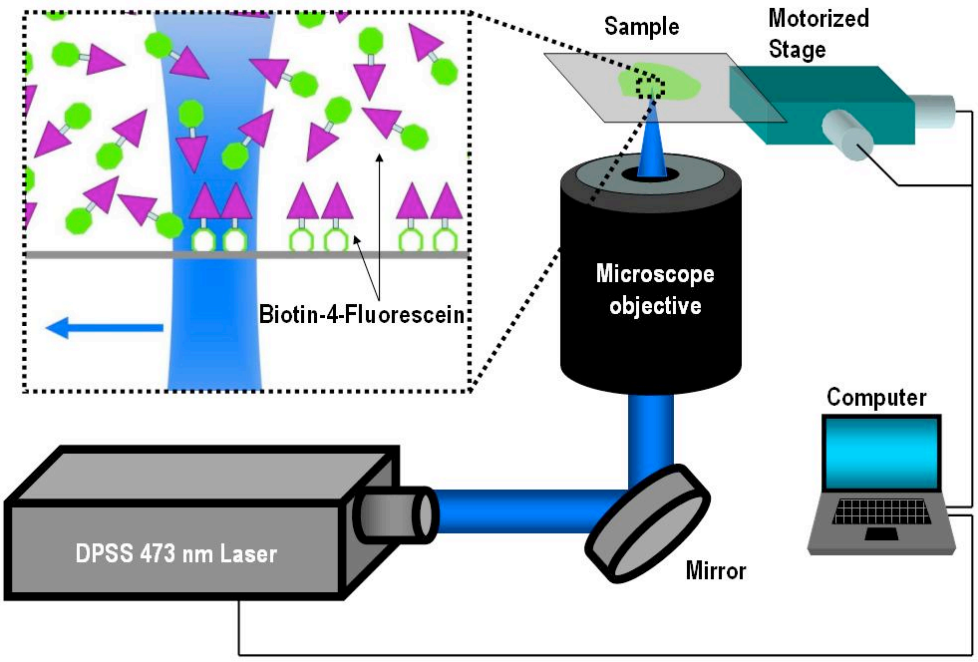


Figure I.1: LAPAP setup includes a 473nm diode pumped solid state (DPSS) laser which is focused by a microscope objective on the top surface of a coverglass where a drop of biotin-4-fluorescein

(B4F) is placed. The photobleaching of fluorescein binds B4F to the glass surface and a pattern can be created by scanning the laser across the surface while changing its intensity or velocity.

### 2.2 Patterning procedure

Protein patterns were produced on the coverglass of a 14mm glass-bottom-dish (MatTek Corporation, MA) on which a 3% bovine serum albumin (BSA) solution was incubated for 20 minutes in order to reduce the non-specific adsorption during the patterning step. The dish was then rinsed several times with PBS and positioned on the LAPAP setup (Fig. 1). A drop of B4F at 50 µg/mL in 3% BSA was placed on the glass bottom dish and the photobleaching step was performed. A total of 15 squares of 10µm were patterned with a combination of 3 laser scanning velocities (2, 8 and 32µm/s) and 5 laser powers (1.3 to 153.5µW) in order to characterize density amplification. The dish was then rinsed several times with PBS to completely remove the unbound B4F. For the standard patterns, 5µg/mL of streptavidin-Cy5 in 3% BSA was then incubated on the patterns for 30minutes. For density-amplified patterns, three consecutive 30 minutes incubation steps of streptavidin, biotinylated rabbit anti-streptavidin and streptavidin-Cy5 all at 5µg/mL in BSA 3% were performed. Figure 2 shows a schematic representation of the molecular structures obtained for both standard and amplification procedures. Graded patterns of proteins were also obtained with standard and amplified LAPAP.

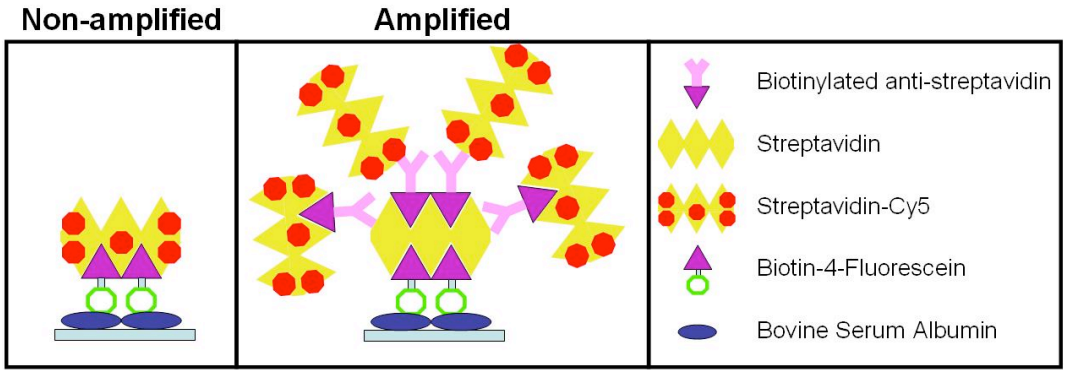


Figure I.2. Schematic representation of standard and density amplified patterns obtained by LAPAP.

### 2.3 Image analysis

Images of standard and amplified patterns were acquired on an IX71 microscope (Olympus, Japan) equipped with a Retiga 2000R CCD (QImaging, Canada). To compare standard and amplified patterns, the gain and the exposure time of the CCD remained unchanged for all the image acquisitions. The images were analyzed using ImageJ (http://rsbweb.nih.gov/ij/index.html) in order to measure the mean and standard deviation of the Cy5 fluorescence intensity in each of 15 patterned squares for both patterning procedures. No image modification or contrast adjustment were performed.

## 3. RESULTS AND DISCUSSION

### 3.1 Gradients

The gradients that were patterned (Fig. 3) show a clear amplification of the amount of Streptavidin-Cy5. For images acquired with the same parameters, the fluorescence from Cy5 is more intense from amplified patterns (Fig. 3b) compared to the intensity of non-amplified patterns (Fig. 3a).

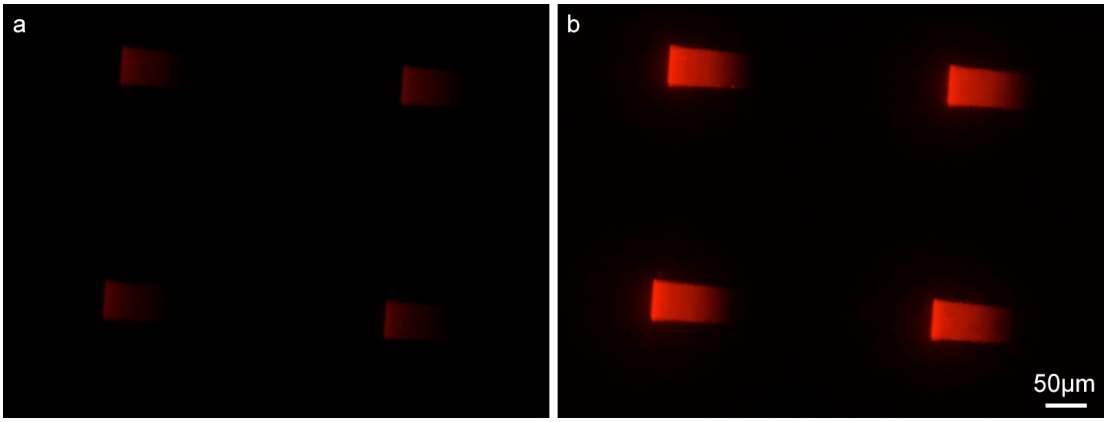


Figure I.3. Streptavidin-Cy5 gradients obtained with (a) standard and (b) density amplification LAPAP. The camera gain and exposure time are the same for both images and no contrast adjustment was performed.

### 3.2 Characterization

We show Strepatavidin-Cy5 fluorescence variation as a function of laser power for three different scanning velocities both for non-amplified and amplified patterns in Fig.4. Figure 4a shows that protein densities that before were only possible to achieve with very low scanning velocity (2µm/s) and maximum laser intensity (153.5µW) can now be easily achieved and surpassed at fast scanning velocity (32µm/s) by amplifying the patterns. It must be noted that a saturation of the amount of bound protein was observed previously in a detailed characterization of LAPAP for a laser power of approximately 160µW [282].

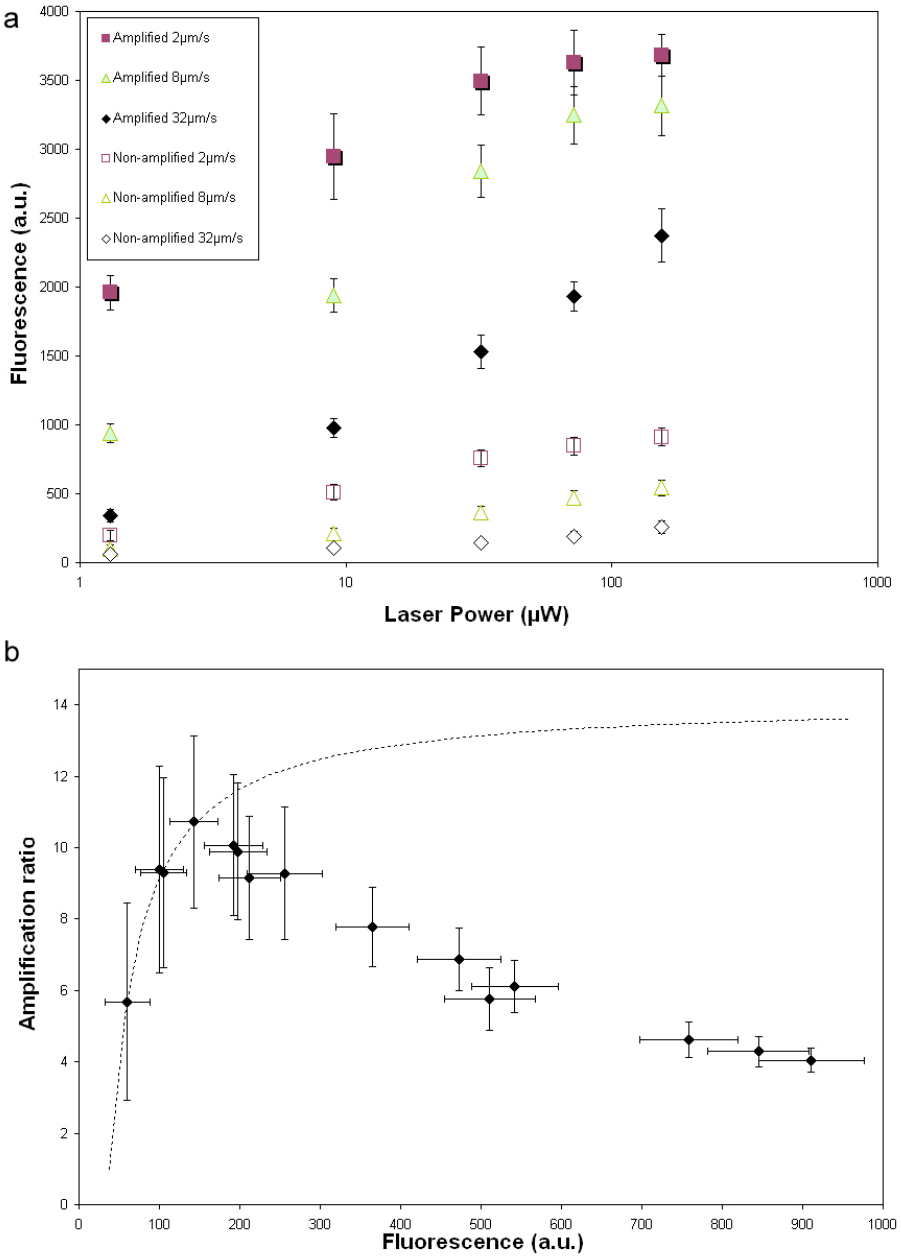


Figure I.4. Amplification characterization. (a) Streptavidin-Cy5 density measured by the Cy5 fluorescence as a function of laser power at three different laser scanning velocities (2, 8 and 32µm/s) for both amplified and non-amplified patterns. (b) Amplification rate as a function of the non-amplified streptavidin-Cy5 amount measured by fluorescence.

Concentration gains were obtained based on fluorescence of streptavidin-Cy5. When plotted the fluorescence ratio amplified vs. non-amplified streptavidin-Cy5 density (Fig. 4b). The result shows how our ability to increase the density decreases for large concentrations. This can be explained by the fact that access to bound

streptavidin becomes limited when the concentration is high. On the other end, the amplification ratio seems also to decrease for low amount of bound streptavidin (below a fluorescence value of 150). We believe this is due to the background noise of the measured fluorescence signal. A simple model explaining this would be that the measured amplification ratio ($K_{meas}$) is function of the fluorescence due to streptavidin-Cy5 ($C_{Strep}$), the fluorescence due to background noise (BG) and the real amplification ratio ($K_{real}$).

$$K_{meas} = \frac{K_{real} C_{strep} + BG}{C_{strep} + BG} \quad (1)$$

For low values of $C_{Strep}$, BG is a dominant term in Equation 1 and for a value of $C_{Strep}$ that tends to zero, $K_{meas}$ tends 1. For higher values of $C_{Strep}$, BG can be neglected and $K_{meas}$ tends to $K_{real}$. For our experiment, BG was estimated by acquiring an image while no sample was on the microscope. We measured the mean fluorescence intensity of the image acquired and this yielded a BG value of 38. Based on this value, we evaluated $K_{real}$ for the first four data point of Figure 4b and obtain an average value of 14.1with a 0.3 standard deviation. The dashed line in Figure 4b represents ratio obtained from Equation 1 using these estimations of $K_{real}$ and BG.

## 4. CONCLUSION

We have shown that amplification offers the possibility to reach higher protein concentration in patterns produced by LAPAP by only adding two incubation steps after the photobleaching procedure. Moreover, we showed that measured gains can reach a factor 10 depending of the initial protein amount.

## 5. ACKNOWLEDGEMENTS

This work is supported by the Natural Sciences and Engineering Research Council of Canada (NSERC), *Fonds québécois de la recherche sur la nature et les technologies* (FQRNT), *Fondation de l'Hôpital Maisonneuve-Rosemont*.

# Annex II: One step patterning

This annex briefly describes a procedure to produce patterns, in a single step, by mixing a fluorophores and the protein of interest. A solution of FITC at 66 µg/mL mixed with rabbit anti-laminin at 166 µg/mL in BSA 1% is placed on a glass bottom dish. A 473nm DPSS is then scanned to directly produce the rabbit anti-laminin pattern. An Alexa594 conjugated goat anti-rabbit antibody later confirms the patterning of the rabbit anti-laminin via fluorescence microscopy.

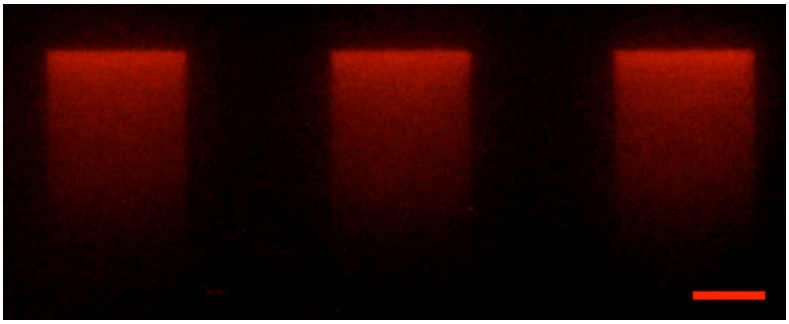

Figure II.1: One step patterning of rabbit anti-laminin mixed with FITC as a photosensitizer. Scale bar = 100µm.

# Annex III: BSA structure fabrication

This annex describes a procedure to create solid structure out of BSA by LAPAP by using a photosensitizer to polymerize BSA. Using our LAPAP setup, it is possible to produce structure by using one photon absorption at 671nm and laser power in the range of 1-5 mW with scanning velocities of 5 μm/s using a 60X 1.2 NA water immersion objective. A solution of 320 mg/mL BSA and 2 mg/ml of methylene blue was exposed to a laser power of 2.2 mW to produce these line structures. RGC5 cells were then plated at a density of 1000 cell/cm$^2$ and cultured overnight (see Figure III.1).

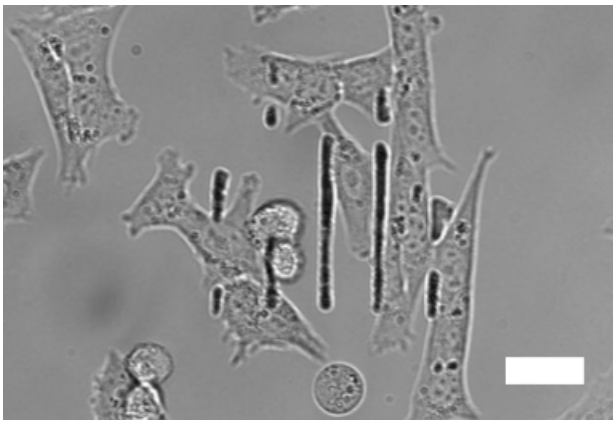

Figure III.1: Thick BSA structures fabricated with our LAPAP setup and RCG-5 cells growing along them (scale bar = 30μm).

It is also possible to fabricate structures with rose bengal as a photosensitizer and a 532nm laser or fluorescein and a 473nm laser, but very small increase in laser power led to drastic structure size increases.

# Annex IV: Sonic Hedgehog and netrin-1 patterns

This annex describes how to obtain Netrin-1 and Sonic Hedgehog patterns. For Sonic Hedgehog, let's start from stripes patterns of streptavidin obtained by LAPAP. Then, biotinylated goat anti-human Fc (5 μg/mL in BSA 3%) is incubated on the pattern for 30 minutes. A fusion protein made with human Fc and Sonic Hedgehog (5 μg/mL in BSA 3%) is then incubated for 30 minutes to obtain functional pattern. The pattern was later revealed by subsequent 30 minutes incubation of mouse anti-Sonic Hedgehog and Cy5 goat anti-mouse (both at 5 μg/mL in BSA 3%). The control is a pattern where human Fc Hedgehog incubation step was skipped to verify for non-specific binding of revealing antibodies. For the netrin-1 pattern, let's also start from streptavidin. First, two subsequent incubations of biotinylated goat anti-mouse Fc and mouse anti-myc9e10 (both at 5 μg/mL in BSA 3%) for 30 minutes are necessary. Then, netrin-1 fused with myc9e10 tag (5 μg/mL in BSA 10%) is incubated on the pattern for 2 hours. We later confirm the presence of netrin-1 via consecutive binding of rabbit anti-netrin-1 and Cy5 goat anti-rabbit (5 μg/mL in BSA 3%, 30 minutes each). For both Sonic Hedgehog and netrin-1, we see a limited amount of non-specific binding of the protein outside the patterns (Fig. IV.1). For netrin-1, it is necessary to dilute it in a high concentration of BSA to decrease this non-specific binding. Also, one of the revealing antibodies for netrin-1 binds to the stripe patterns even in the absence of netrin-1, but only in a small fraction if we compare it to the fluorescence obtained from the netrin-1 pattern.

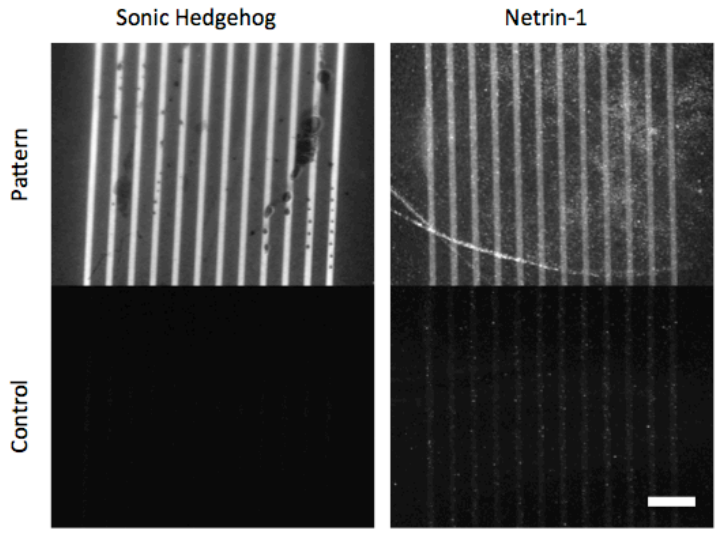


Figure IV.1: Sonic Hedgehog and netrin-1 stripe patterns revealed by immunostaining.